Australian Government
Department of Defence
Defence Science and
Technology Organisation

The Visible Signature Modelling and Evaluation ToolBox

Joanne B. Culpepper and Rodney A.J. Borg

Maritime Platforms Division

Defence Science and Technology Organisation

DSTO–TR–2212

ABSTRACT

A new software suite, the Visible Signature ToolBox (VST), has been developed to model and evaluate the visible signatures of maritime platforms. The VST is a collection of commercial, off-the-shelf software and DSTO developed programs and procedures. The software can logically be divided into image generation and probability of detection (POD) modelling codes. CAMOGEN (CAMOuflage GENeration) and CAMEO-SIM (CAMouflage Electro-Optic SIMulation) provide the image generation, whereas ORACLE provides the POD analysis capability. The ocean modelling is supplied by HYDROLIGHT. All of these stand-alone programs are integrated through DSTO developed software and procedures, to produce a software suite. The VST can be utilised to model and assess visible signatures of maritime platforms. A number of examples are presented to demonstrate the capabilities of the VST. In one example, the visible signature of a submarine is examined under various conditions. In another example, visible imagery of a ship is presented for different times of day and various observer perspectives. A demonstration of how a change in surface colour affects the visible signature of the ship is also shown. The final example is the creation and initial assessement of a disruptive pattern for a watercraft on a river.

Published by

Defence Science and Technology Organisation
506 Lorimer St,
Fishermans Bend, Victoria 3207, Australia

Telephone: *(03) 9626 7000*
Facsimile: *(03) 9626 7999*

AR No. AR–014–321
December, 2008

APPROVED FOR PUBLIC RELEASE

The Visible Signature Modelling and Evaluation ToolBox

EXECUTIVE SUMMARY

Naval platforms are used in a variety of roles including surveillance and deployment operations. Performance of any operation exposes the platform to the risk of detection and engagement by a plethora of battlefield sensors. Electro-optic sensors are becoming more prevalent and technological advances continue to improve the performance of sensors in this domain. It is becoming increasingly important to understand and manage the visible signature of naval platforms in response to the changing threat. Naval platform susceptibility due to the visible signature varies depending on the environmental conditions, location and time of day. To determine an optimum visible signature reduction strategy, signature modelling across all areas of operation is required. To assist in this analysis a new software suite, the Visible Signature ToolBox (VST), has been developed to model and evaluate the visible signatures of maritime platforms. This report describes the components of the VST, usage of the VST and potential applications.

The VST is a collection of commercial, off-the-shelf software and DSTO developed programs and procedures. The software can logically be divided into image generation and probability of detection (POD) modelling codes. CAMOGEN (CAMOuflage GENeration) and CAMEO-SIM (CAMouflage Electro-Optic SIMulation) provide the image generation, whereas ORACLE provides the POD analysis capability. The ocean modelling is supplied by HYDROLIGHT. There are also a number of commercial software support codes that perform various functions such as generating wireframe models for input into the signature modelling software. All of these stand-alone programs are glued together through DSTO developed software and procedures, to produce an integrated software suite. The VST can be utilised to model and assess visible signatures of maritime platforms. ORACLE has the ability to quantify the visible signature in terms of POD. CAMEO-SIM can generate synthetic imagery of platforms in operational environments. The visible signature may then be quantified using human observer trials.

A number of examples are presented to demonstrate the capabilities of the VST. These examples include an examination of submarine POD, synthetic image generation of an Anzac Class Frigate and generation of a pixellated camouflage scheme for a watercraft on a river. The report will also describe the known limitations of the VST and areas that require further work to enhance the capability of the VST.

Authors

Joanne B. Culpepper
Maritime Platforms Division

Joanne Culpepper graduated from Monash University with a B.AppSci. in Physics in 2000. She joined the Experimental Particle Physics Group at the University of Melbourne in 2000. After completing a Post Graduate Diploma in Physics she commenced a Master of Science in Particle Physics in 2001. Following her Masters she undertook a Summer Scholarship at the Swinburne University in the area of AstroParticle Physics in early 2006, conducting a feasibility study into the detection of lunar neutrino signals by means of a radio telescope array. In mid 2006 she joined the Martime Platforms Division at DSTO. She is currently working in the area of Signature Management on visible signature modelling of naval platforms.

Rodney A. J. Borg
Maritime Platforms Division

Rodney Borg joined the then Materials Research Laboratory (MRL) of DSTO in 1988 and worked on various experimental and theoretical projects related to high explosives. In 1996 he joined Kodak Australasia where he worked on photographic emulsion research, coating technologies and manufacturing improvement projects. In late 2005, he returned to DSTO and joined Maritime Platforms Division. He is currently working in the Signature Management area on IR and visible signature modelling of naval platforms.

Contents

Figures

Tables

Glossary

Airlight Spectrum The airlight spectrum describes the amount of scattered light into and out of the viewing path of an observer. Physically it is the path radiance and is used in the determination of the attenuation of light by the atmosphere in ORACLE.

Apparent Optical Property An apparent optical property is a property that depends both on the inherent optical properties of a medium, such as a water body, and the directional structure of the ambient light field. It also must exhibit regular features and stability so that it can be used as a descriptor of the water body.

Beam Attenuation Coefficient The beam attenuation coefficient is defined in terms of the radiant power lost from a single, narrow, collimated beam of photons. It is a measure of how much an incident collimated beam of photons is lost by absorption and scattering through a medium.

Bi-directional Reflectance Distribution Function The bi-directional reflectance distribution function is defined as the ratio of the reflected radiance from a surface exiting along a given outgoing direction to the incident plane irradiance of a collimated beam in a given direction. It is a measure of how light is reflected at an opaque surface.

Bioluminescence Bioluminescence is the light produced by organisms as a result of conversion of chemical energy into radiant energy.

Chlorophyll Chlorophyll are chemical compounds that occur in plants which enable radiant energy to be converted to chemical energy in the process of photosynthesis.

Coloured Dissolved Organic Matter Coloured dissolved organic matter is comprised of high molecular weight organic compounds, typically humic and fulvic acids, formed from the decomposition of plant tissue.

Diffuse Attenuation Coefficients (K-functions) The diffuse attenuation coefficients are a collection of apparent optical properties that are defined as ratios, and as such require no absolute radiometric measurements. They provide a measure of the decrease, with respect to depth, of a diffuse or uncollimated light field. As an apparent optical property they depend on the structure of the ambient light field. They are strongly correlated with phytoplankton chlorophyll concentration and therefore provide a connection between the biology and optics of a body of water.

Effective Source Function The effective source function is the combination of the inelastic and true sources of emission terms of the radiative transfer equation for a water body. It is considered to be a known quantity even though it may include contributions to wavelength λ by inelastic scatter from other wavelengths $\lambda' \neq \lambda$.

Elastic Scatter Elastic scatter is a scattering process where the energy of the incident particles or radiation is conserved. In this process only the direction of propagation is altered.

Filter Spectrum The filter spectrum corresponds to the wavelength-dependent transmission of light through a medium. This can either be the transmission through the atmosphere or a combination of the atmosphere and an optical device.

Fovea The fovea is the area of the retina that contains the visual receptors (rods and cones). It covers a circular portion of the visual field subtending between 10 and 20 *mrad* diameter.

Foveal Detection Probability The foveal detection probability is the probability of detecting a target in a given scenario using the area of central vision, known as the fovea. It corresponds to a retinal eccentricity of 0°.

Fractional Perimeter The fractional perimeter is the parameter that describes the visual search task in ORACLE. It is defined as the fraction of the perimeter of the target that is needed to be resolved for the observer to successfully accomplish the visual task. A fractional perimeter of 1.0 denotes that the observer must distinguish the entire perimeter of the target and corresponds to the visual task of pure energy detection.

Fulvic Substance A fulvic substance is a high molecular weight organic compound containing fulvic acid resulting from plant decay, especially phytoplankton.

Hard-shell Approximation The hard-shell approximation is a method of treating the visual lobe area. In this approximation the retinal eccentricity at which the probability of target detection reaches a specified value is determined. In the ORACLE model this probability is 50%. It is then assumed that targets within this eccentricity are detected and those outside are not. Thus there is a clearly defined boundary for the visual lobe.

Histogram Matching Histogram matching is the process of equalising or comparing the frequency of occurrence. In image processing, histogram matching is performed on the frequency, or count, of pixels with a particular RGB or greyscale value.

Hue Hue is one of the descriptors of colour. It is the attribute of visual perception for which an area (of colour) appears to be similar to one of the perceived colours: red, yellow, green and blue, or some combination of them.

Humic Substance A humic substance is a high molecular weight organic compound containing humic acid resulting from plant decay, especially terrestrial plants. If the humic substance is water-soluble soil then it gives water a yellow colour.

Illuminance Illuminance is a measure of the intensity of the incident light, weighted by the luminosity function so as to correlate with human perception of brightness. It is defined as the total luminous flux incident on a surface per unit area.

Illuminance Gradient on the Retina The illuminance gradient on the retina is the change in illuminance as function of the retinal position. It is the rate of change in total luminous flux per unit area with respect to retinal position.

Inelastic Scatter Inelastic scatter is a scattering process where the kinetic energy of the incident particle or radiation is not conserved. In this process the energy of the

incident particle or radiation is lost or gained and may or may not be accompanied with a change in the direction of propagation.

Inherent Optical Property An inherent optical property is a property that depends only on the medium. As such it is independent of the ambient light field within the medium.

Lambertian Reflecting Surface A Lambertian reflecting surface is a surface that reflects radiance equally in all directions over the observable hemisphere.

Luminance Luminance describes the amount of light that passes through or is emitted from a particular area, and falls within a given solid angle. It is a measure of the density of luminous intensity in a given direction. Luminance is an indicator of how bright an object will be when viewed by a human observer. That is, it indicates how much luminous power will be perceived by an eye looking at an object that is emitting and reflecting light.

Meteorological Visibility Meteorological visibility is a measure of the distance at which an object, or light, can be clearly discerned. Meteorological visibility is a property of the air and refers to the transparency of air: in the dark the meteorological visibility is the same as in daylight for the same air.

Modulation Transfer Function The modulation transfer function describes how much a piece of optical equipment blurs the image of an object. It is defined as the ratio of the image amplitude to the object amplitude as a function of sinusoidal frequency variation in the object.

Non-Lambertian Reflector A non-Lambertian reflector is a reflector where the reflected radiance varies with direction over the observable hemisphere.

Octree An octree is a tree data structure where each internal node has up to eight children. Octrees are most often used to partition a 3 dimensional space by recursively sub-dividing it into eight octants.

Particle Phase Function The particle phase function describes the angular distribution of scattered radiation resulting from radiation incident on a particle. It is the ratio of the volume scattering function to the scattering coefficient.

Point Spread Function The point spread function describes the response of an imaging system to a point source. It is the spatial domain version of the modulation transfer function. Thus the degree of the spreading (blurring) of an object is a measure of the quality of the imaging system.

Principal Component Analysis Principal component analysis is a technique used to reduce multidimensional data sets to a lower dimension for analysis.

Probability of Detection The probability of detection is the probability that an observer will detect a target in a given scene.

Retinal Eccentricity Retinal eccentricity is the angle from a fixation point to the central point of the retina.

Single Glimpse Probability The single glimpse probability is the probability of seeing a target in a given scenario in a single glimpse.

Soft-Shell Lobe A soft-shell lobe is a visual lobe area based on the probability of detecting a target with distance. It requires the determination of the probability of target detection at various eccentricities, providing a map of probability of detection at each eccentricity.

Software Suite A software suite is a collection of computer programs, typically application software and programming software, of related functionality. Seamless data sharing between programs and a common GUI are usual features of a software suite.

Steerable Pyramid A steerable pyramid is a steerable, multi-scale oriented image transform useful in image analysis and synthesis. It has non-aliased sub-bands, which offer advantages over orthogonal wavelet image transforms.

Sky-to-Ground Luminance Ratio The sky-to-ground luminance ratio is a ratio of the intrinsic and apparent luminance of the background. It is used for the calculation of atmospheric attenuation in slant path viewing.

Target Intrinsic Contrast The target intrinsic contrast is the measure of the intrinsic contrast of the target against its immediate background. It is a direct measure of the luminance contrast. A target intrinsic contrast of -0.9 denotes that the target is much lighter than its immediate background.

Veiling Glare Veiling glare is diffuse stray light at the image plane of an optical system that results in reduced contrast or resolution.

Visual Lobe A visual lobe describes the peripheral sensitivity for particular target and background characteristics. It represents the target acquisition or detection probability as a function of eccentricity from the fovea. In other words, it is the area around the fixation point within which information can be extracted about the given scenario in a single glimpse.

Visual Search Visual search is a type of perceptual task. It involves actively scanning the visual environment for a particular target (an object or feature) amongst other objects or features, known as distractors.

Volume Scattering Function The volume scattering function is the ratio of the scattered intensity to the incident irradiance per unit volume of the medium (e.g. water). It can also be interpreted as the differential scattering cross section per unit volume.

Abbreviations

2D Two Dimensional

3D Three Dimensional

AOP Apparent Optical Property

ASCII American Standard Code for Information Interchange

ASD Analytical Spectral Devices

BRDF Bi-directional Reflectance Distribution Function

CAMEO-SIM CAMouflage Electro-Optic SIMulation

CAMOGEN CAMOuflage GENeration

CDOM Coloured Dissolved Organic Matter

CIE Commission Internationale de l'Éclairage

COTS Commercial, Off-The-Shelf

DP Disruptive Pattern

DSTO Defence Science and Technology Organisation

EO Electro-Optic

FFG Guided missile frigate (specifically RAN Adelaide Class)

FFH Frigate class ships with Helicopter as principal weapon (specifically RAN Anzac Class)

FOV Field-Of-View

FPI Floating-Point Image

GAM Gorden and Morel

GMT Greenwich Mean Time

GPS Global Positioning System

GTV Georgia Tech Vision

GUI Graphical User Interface

HM Histogram Matching

ID Identification

IR Infrared

IOP Inherent Optical Property

MODTRAN MODerate resolution of atmospheric TRANsmission

MPD Maritime Platforms Division

MRL Materials Research Laboratory

MTF Modulation Transfer Function

NATO North Atlantic Treaty Organization

NTCS Naval Threat/Countermeasures Simulator

NURBS Non-Uniform, Rational B-Spline

PAW Physics Analysis Workstation

PCA Principal Component Analysis

POD Probability Of Detection

PPF Particle Phase Function

PSF Point Spread Function

PSM Prieur-Sathyendranath-Morel

RAN Royal Australian Navy

RHIB Rigid Hull Inflatable Boat

RTE Radiative Transfer Equation

SP Steerable Pyramid

USAF United States Air-Force

UV Ultra-Violet

VISEO VISual and Electro-Optical

VSF Volume Scattering Function

VST Visible Signature ToolBox

XYZ CIE tristimulus values

Units

cd Candela. It is a measure of the luminous intensity in a given direction.

mrad Milli Radian

nm Nanometer

ppm Parts Per Million

sq° Square Degree. It is a unit of solid angle equivalent to $\left(\frac{1}{\pi}\right)^2$ steradian.

sr Steradian

W Watt

1 Introduction

Naval platforms are used in a variety of roles including surveillance and deployment operations. Performance of any operation exposes the platform to the risk of detection and engagement by a plethora of battlefield sensors. Electro-optic sensors are becoming more prevalent and technological advances continue to improve the performance of sensors in this domain. These factors, in particular changes in operations and the emergence of imaging seekers, have resulted in the need for a visible signature modelling capability for naval platforms, both blue water and littoral. This capability should include the ability to model complex visual scenes and to evaluate susceptibility to imaging sensors including human observers. The latter is particularly important in littoral environments. To enable the modelling of submerged platforms the system should include a through-water capability.

Maritime Platforms Division (MPD) of the Defence Science and Technology Organisation (DSTO) has been modelling the infrared (IR) signatures of naval platforms using the Naval Threat Countermeasure Simulator (NTCS), also known as ShipIR [1–3]. This NATO-standard code allows modelling of surface naval platform IR contrast signatures in blue water scenarios. However, NTCS has a limited capability for modelling visible band seekers; restricted to those that behave in the same fashion as non-imaging IR seekers. It has no capability for modelling naval platforms in a littoral environment, that is in shallow water with nearby land masses. A survey of alternative Commercial, off-the-shelf (COTS) software available indicated that there is no single code capable of meeting all of the new requirements. Therefore it was decided to obtain several codes and incorporate them into what has been called the Visible Signature ToolBox (VST).

This report describes the VST developed in response to the above requirements. The individual codes comprising the VST are described including their functions and interactions with other codes in the toolbox. Some examples of the use of the VST will be presented to demonstrate how the VST can be used to support RAN. Future enhancements to the toolbox will also be discussed, particularly in the context of the known limitations of the VST.

2 The Visible Signature ToolBox

The VST is composed of a number of software components. These can be divided into four categories: DSTO developed software and procedures, signature modelling, ocean modelling and commercial support software. This is illustrated in the flow chart of the VST presented in Figure 1. At the heart of the VST is the signature modelling software. This can be broken down into two types dependent on the signature model employed, either image generation or probability of detection (POD). The image generation modelling is provided by CAMOGEN (CAMOuflage GENeration) and CAMEO-SIM (CAMouflage Electro-Optic SIMulation), and the POD modelling by ORACLE. The ocean modelling is provided by HYDROLIGHT. The commercial support software has a number of different functionalities. Rhinoceros provides the wireframe models required as input into CAMOGEN and CAMEO-SIM. RadThermIR permits the thermal modelling of complex

man-made structures. MODTRAN (MODerate resolution of atmospheric TRANsmission) provides the modelling of the atmosphere for a complete model of the background. Finally, the DSTO software and procedures are the glue that holds the VST together. They permit the necessary interactions between the components so that the visible signatures of platforms in various environments can be modelled. In other words, they are the software and procedures that turn the stand-alone programs into the VST software suite by enabling the transfer of data from one program to another.

In Figure 1 these DSTO developed procedures are represented by red connections between the components. The black lines denote interactions between components which have built-in interfaces supplied by one of the commercially obtained modelling softwares. The dashed black and red connections indicate proposed extensions to the VST, which at present are not implemented. In the following sections all of the components of the VST will be described in detail.

2.1 HYDROLIGHT

HYDROLIGHT 4.2 was developed by Curtis D. Mobley and is marketed by Sequoia Scientific Inc. in the US. It was designed to model radiative transfer through water in the visible waveband. HYDROLIGHT is a numerical radiative transfer model that evaluates radiance distributions and properties of natural bodies of water. As such it is used widely in oceanography for modelling ocean colour and properties and for remote sensing applications [4–8]. The following section provides an overview of the physical model employed by HYDROLIGHT. The basis of the model can be found in the book *Light and Water Radiative Transfer Through Natural Waters* [9].

2.1.1 General Description

Radiance distributions leaving or within a body of water are modelled by solving a time-independent radiative transfer equation (RTE). In the ocean this equation is defined by the spectral radiance $L(z, \theta, \phi, \lambda)$. It is dependent on the depth z, direction (θ, ϕ) and wavelength λ. From the spectral radiance all other parameters of interest, such as the diffuse attenuation functions, irradiances and reflectances, can be calculated. HYDROLIGHT derives the spectral radiance by solving the RTE numerically using specified boundary conditions. The general form of the RTE for a water body is given by:

$$\mu \frac{dL(z,\hat{\xi},\lambda)}{dz} = -c(z,\lambda)L(z,\hat{\xi},\lambda) + \int_{\Xi} L(z,\hat{\xi}',\lambda)\beta(z,\hat{\xi}' \rightarrow \hat{\xi},\lambda)\, d\Omega(\hat{\xi}') + S(z,\hat{\xi},\lambda), \quad (1)$$

where $L(z,\hat{\xi},\lambda)$ is the radiance with a direction given by the unity vector $\hat{\xi}$ at wavelength λ and depth z; μ is the cosine of the angle between $\hat{\xi}$ and the z plane, $c(z,\lambda)$ is the beam attenuation coefficient at depth z, $L(z,\hat{\xi}'.\lambda)$ is spectral radiance generated by elastic scatter, $\beta(z,\hat{\xi}' \rightarrow \hat{\xi},\lambda)$ is the volume scattering function (VSF) for scattering from the direction ξ' to ξ, $d\Omega(\hat{\xi}')$ is the solid angle centred on $\hat{\xi}$ and $S(z,\hat{\xi},\lambda)$ is the effective source function. This function is the summation of the inelastic scatter and true sources of emission (bioluminescence) and is defined as:

$$S(z,\hat{\xi},\lambda) = L_*^I(z,\hat{\xi},\lambda) + L_*^S(z,\hat{\xi},\lambda), \quad (2)$$

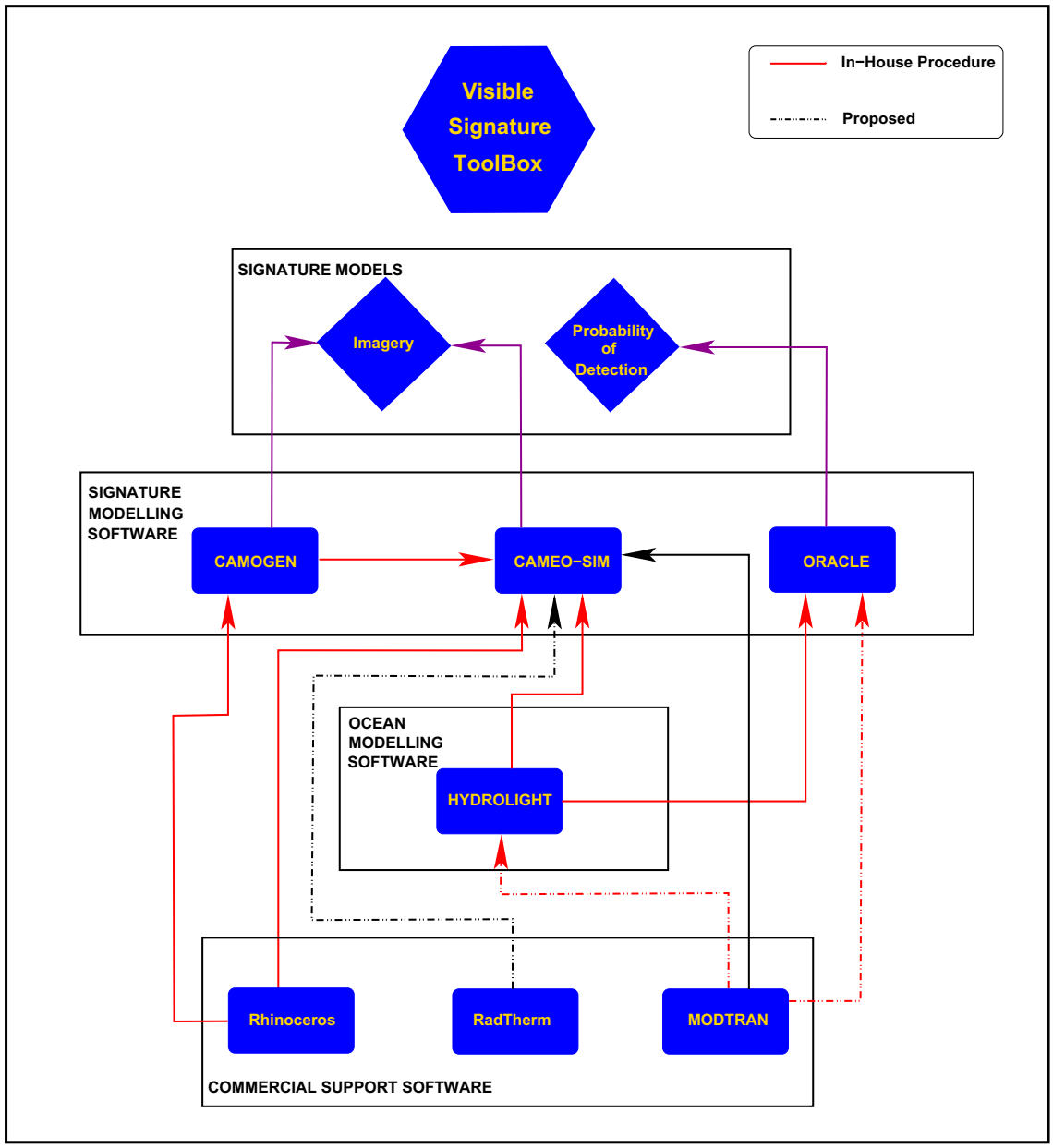

Figure 1: *The Visible Signature ToolBox flow chart.*

where L_*^I refers to inelastic scatter and L_*^S to true sources of emission. This situation is depicted in Figure 2 and illustrates the complexity of the radiance calculations at each depth. That is, there are contributions from elastic scatter, inelastic scatter, internal sources and reflectance from the bottom surface. Not shown is the absorption of radiance. However, this is of critical importance as it defines the amount of the transmitted radiance through the media.

Table 1 lists the common inherent optical properties (IOPs) of water. It is these properties that govern the transmission, reflection and scattering of light in water. Equation 1 contains two IOPs, $\beta(z, \hat{\xi}' \rightarrow \hat{\xi}, \lambda)$ and $c(z, \lambda)$. Although $c(z, \lambda)$ is an IOP it is not gener-

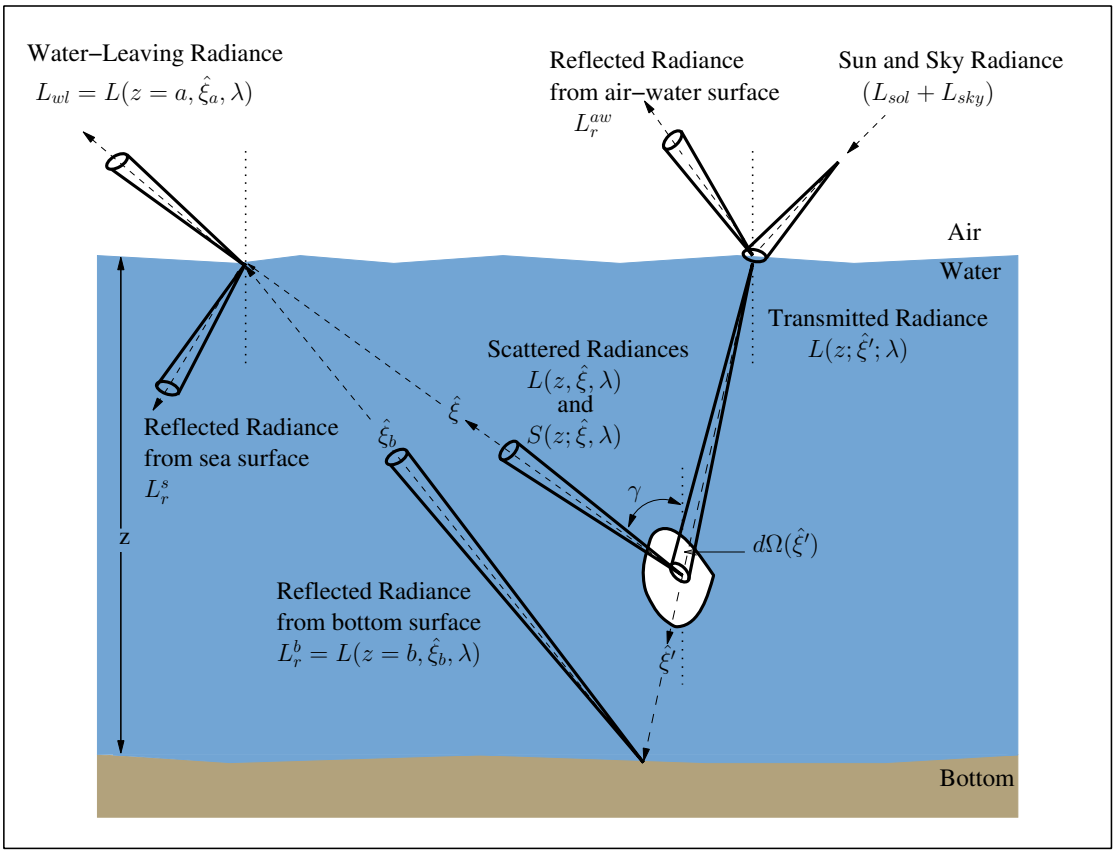

Figure 2: *Schematic representation of the HYDROLIGHT radiance calculations.*

ally used in ocean optics calculations. It is more common to use the spectral absorption and scattering coefficients $a(z, \lambda)$ and $b(z, \lambda)$ as these quantities can be easily measured and $c(z, \lambda)$ can be expressed in terms of $a(z, \lambda)$ and $b(z, \lambda)$. This relationship is:

$$c(z, \lambda) = a(z, \lambda) + b(z, \lambda). \tag{3}$$

Using the definition of $c(z, \lambda)$ given in Equation 3 the general form of the RTE (Eq. 1) can be rewritten as:

$$\begin{aligned} \mu \frac{dL(z, \hat{\xi}, \lambda)}{dz} &= -[a(z, \lambda) + b(z, \lambda)] L(z, \hat{\xi}, \lambda) \\ &\quad + \int_{\Xi} L(z, \hat{\xi}', \lambda) \beta(z, \hat{\xi}' \rightarrow \hat{\xi}, \lambda) \, d\Omega(\hat{\xi}') + S(z, \hat{\xi}, \lambda). \end{aligned} \tag{4}$$

This definition has two consequences. Firstly, if two water bodies possess the same volume scattering function, spectral absorption and scattering coefficients then they will have the same spectral radiance. Secondly, the key quantity required by HYDROLIGHT is the spectral radiance.

From the definition of the general form of the RTE given in Equation 4, it can be seen that of critical significance are the spectral absorption and scattering coefficients and the

Table 1: *Inherent Optical Properties.*

Quantity	Symbol
index of refraction	n
absorption coefficient	a
volume scattering function	β
scattering phase function	$\tilde{\beta}$
scattering coefficient	b
beam attenuation coefficient	c
single-scattering albedo	$\tilde{\omega}$ or ω_0

volume scattering function, as it is these variables that operate on the irradiance terms of the RTE. In ocean optics it is common practice to use these parameters to describe the IOPs of water. It is generally accepted that the key contributors to these properties for a water body are the following components: pure sea water, Chlorophyll-bearing particles, Coloured Dissolved Organic Matter (CDOM) and minerals. The effect on the IOPs of water can be specified, as is the case in HYDROLIGHT, as the summation of all the contributing optical components [10]:

$$\begin{aligned} a(z,\lambda) &= a_w(\lambda) + C(z)a_c^*(\lambda) + Y(z)a_y^*(\lambda) + M(z)a_m^*(\lambda) \text{ and} \\ b(z,\lambda) &= b_w(\lambda) + C(z)b_c^*(\lambda) + Y(z)b_y^*(\lambda) + M(z)b_m^*(\lambda), \end{aligned} \tag{5}$$

where $a_w(\lambda)$ and $b_w(\lambda)$ are the spectral absorption and scattering coefficients of pure sea water, $a_c^*(\lambda)$, $a_y^*(\lambda)$, $a_m^*(\lambda)$, $b_c^*(\lambda)$, $b_y^*(\lambda)$ and $b_m^*(\lambda)$ are the specific spectral absorption and scattering coefficients of the Chlorophyll-bearing particles, CDOM and minerals, respectively and $C(z)$, $Y(z)$ and $M(z)$ represent the concentration profiles for the Chlorophyll-bearing particles, CDOM and minerals.

The boundary conditions required for solving the RTE in the water body are the bottom water layer and the sea-air interface. The bottom water layer or seabed is modelled in HYDROLIGHT in one of two ways - either as an infinite or a finite depth. That is, it simulates deep water and finite-depth water bodies. These two situations are modelled in completely different fashions. In the case of an infinitely deep seabed it is assumed that the water below the maximum depth is homogeneous and possesses the same IOPs as computed at the maximum depth. HYDROLIGHT calculates the bi-directional reflectance distribution function (BRDF) of the infinitely deep, homogeneous layer below the maximum depth. It then uses this BRDF as the bottom layer boundary condition. Beyond the maximum depth the water is a non-Lambertian reflector. For finite-depth water an opaque Lambertian reflecting surface is positioned at the maximum depth. The radiance reflectance properties are then computed by combining the irradiance reflectance of the Lambertian surface with a Lambertian BRDF. The wind-blown sea surface is described statistically by a Gaussian distribution and is modelled using Monte Carlo methods. The wave slope is usually described by capillary waves [11].

In order to simulate the reflected radiance emanating from the sea surface the atmospheric conditions must also be modelled. This is achieved in HYDROLIGHT using two

routines that return information regarding modelled and measured sky radiances. These routines combine together to compute the sky radiance distribution in all directions. The first models the sky irradiance using the Gregg and Carder RADTRAN model for cloudless maritime environments [12]. This separates the sky downwelling plane irradiance into two components: direct and diffuse. Together they form the spectral plane irradiance E_d adjacent to the sea surface and establish the magnitude of the sky radiance. The second routine determines the angular pattern of the sky radiance using the Harrison and Coombes clear sky model [13]. Once the angular pattern is determined it is integrated to yield a sky radiance. If this irradiance equals the irradiance computed by the first routine then nothing is changed. If not, the angular pattern radiance is forced to equal the earlier computed downwelling plane irradiance.

2.1.2 Inputs and Usage

A brief overview of the HYDROLIGHT inputs and usage will be provided in this section. For a more extensive description consult the HYDROLIGHT 4.2 documentation [10, 14]. HYDROLIGHT is written in Fortran95 and is generally controlled by a Graphical User Interface (GUI) but can also be run in batch mode. To run in batch mode an input file containing all the necessary variables can either be created manually or the GUI can be used to generate the file. In both cases the HYDROLIGHT run consists of firstly compiling the program and then running it. This method is chosen as there are a number of input choices that are subroutines and re-compiling the program is the best method for including these. Another feature resulting from the re-compilation before every run is that the user can create their own subroutines.

Due to the large number, the input variables will not be discussed individually. However they can be categorised into:

- IOPs
- scattering properties
- waveband
- air-water surface boundary conditions
- sky conditions
- bottom layer boundary conditions
- depths
- output options

The input parameters corresponding to these categories are summarised in Table 2. This demonstrates the large number of variables required to describe a body of water in a particular environment.

Table 2: *HYDROLIGHT Input Parameters.*

IOPS	The water model Pure sea water absorption and scattering coefficients Chlorophyll absorption and scattering parameters CDOM absorption and scattering parameters Minerals absorption and scattering parameters
Scattering Sources	Bioluminescence Chlorophyll fluorescence CDOM fluorescence Raman scattering
Wavelength	Single or Multiple wavelengths Wavelength bands of an ocean sensor
Air-Water Surface Boundary Conditions	Wind speed (m/s) Sky model
Sky Conditions	Sun position Cloud cover Atmospheric conditions
Bottom Layer Boundary Conditions	Infinite or Finite depth Bottom reflectance (%)
Depths	Output depths Type of output depths
Output Options	Amount of information printed to print-out file Choice of the output text files generated

2.1.3 Outputs

HYDROLIGHT generates five output text files; print-out, radiance, digital, single wavelength and multiple wavelength files. Contained in these files are a number of parameters that describe the optical properties and radiative transfer entering, leaving and within the water body. These can be classified into:

- diffuse attenuation coefficients (K-functions)
- apparent optical properties (AOPs)
- irradiances
- IOPs
- remote sensing variables

See Table 3 for the full list of output variables.

For the purposes of modelling visible signatures using ORACLE, the most important output from HYDROLIGHT is the spectral upwelling radiance just above the sea surface, $L_u(z = a, \theta, \phi, \lambda)$. This is the sum of the water-leaving radiance and the sun and sky radiance reflected from the sea surface. It is defined to be:

$$L_u(z = a, \theta, \phi, \lambda) = L_r(z = a, \theta, \phi, \lambda) + L_{wl}(z = a, \theta, \phi, \lambda), \tag{6}$$

where $L_r(z = a, \theta, \phi, \lambda)$ is the sun and sky radiance reflected by the sea surface and $L_{wl}(z = a, \theta, \phi, \lambda)$ is the water-leaving radiance. Since this radiance can be utilised as input into ORACLE a new subroutine was written in HYDROLIGHT to generate a data file in the format required for input into ORACLE.

Table 3: *HYDROLIGHT Output Variables.*

K-functions	Diffuse attenuation coefficient of downward irradiance K_d
	Diffuse attenuation coefficient of upward irradiance K_u
	Diffuse attenuation coefficient of total scalar irradiance K_0
	Diffuse attenuation coefficient of total irradiance K_{net}
	Diffuse attenuation coefficient of radiance K_{Lu}
AOPs	Spectral upwelling radiance to downward plane irradiance ratio $\frac{Lu}{E_d}$
	Spectral irradiance reflectance $R = \frac{E_u}{E_d}$
	Spectral downwelling average cosine μ_{ud}
	Spectral upwelling average cosine μ_u
	Total spectral average cosine μ
IOPs	Spectral absorption coefficient $a(\lambda)$
	Spectral scattering coefficient $b(\lambda)$
	Spectral beam attenuation coefficient $c(\lambda)$
	Single scattering albedo ω_0
	Spectral backscattering coefficient $bb(\lambda)$
	Backscattering ratio $\frac{bb(\lambda)}{b(\lambda)}$
Irradiances	Spectral downward (downwelling) plane irradiance E_d
	Spectral upward (upwelling) plane irradiance E_u
	Total spectral scalar irradiance E_0
	Spectral upward (upwelling) radiance L_u
	Ratio of spectral upward (upwelling) radiance to downward (downwelling) plane irradiance $\frac{L_u}{E_d}$
Remote Sensing	Remote sensing reflectance $R_{rs} = \frac{L_{wl}}{E_d}$
	Water-leaving radiance L_{wl}

2.2 ORACLE

The ORACLE software is developed and marketed by the Advanced Technology Centre of BAE Systems in the UK [15, 16]. It is designed to model human visual search and detection performance in the waveband 380 nm to 780 nm. The human vision model has the ability to predict, evaluate and assess the performance of both the unaided and aided eye in the task of target acquisition and identification. That is, it will predict either the probability of detecting a target or the time required to acquire a target once the target and environmental conditions are described through various inputs. The response of the human visual system is based upon physiological evidence. It is calculated as a function of length of the target perimeter and the strength of each part of the contrast edge that defines the perimeter. The two fundamental target characteristics that govern acquisition are therefore size and contrast. ORACLE uses knowledge of visual performance with increasing angle between the observer's direction and the target position to specify search within any defined field-of-view (FOV). The calibration of the model is accomplished using data derived from laboratory studies and field trials. In the following section, a brief overview of visual search and the ORACLE model is given. A detailed description of the model can be found elsewhere [15, 16].

2.2.1 General Description

Visual search of complex natural scenes is generally modelled as a number of random and independent fixations or glimpses. Thus the cumulative detection probability ϕ_t after time t is defined as:

$$\phi_t = 1 - (1 - P_g)^n \,, \tag{7}$$

where P_g is the single glimpse probability and n is the number of glimpses. For a more complete description of ϕ_t the difficulty in acquiring a target within the defined FOV must be incorporated. In the ORACLE vision model this is accomplished by weighting Equation 7 with the foveal detection probability P_f. Equation 7 is therefore redefined to be:

$$\phi_t = P_f \left[1 - (1 - P_g)^n\right] , \tag{8}$$

the single glimpse probability is given as:

$$P_g = \left(\frac{\theta}{\theta_f} - \frac{\theta^2}{4\theta_f^2}\right) , \tag{9}$$

where θ is the visual angle at which the detection probability of a single glimpse is 50% and θ_f is the angular size of the FOV. This method of calculating the single glimpse probability uses the hard-shell approximation and is therefore referred to as the Hard-Shell Search Model. It evaluates the common area between the retinal eccentricity associated with a 50% detection probability and the search FOV.

ORACLE computes the foveal probability in a given scenario by taking into consideration a number of key parameters. These are:

- the adaptation level of the visual system

- the pupil size
- the modulation transfer function (MTF) and point spread function (PSF) of the eye
- the illuminance gradient on the retina
- the nature of the visual task (detection or identification)
- the number of retinal receptors on the target

There are two types of visual lobes that are used to describe the single glimpse detection probability in human visual search: hard-shell and soft-shell . For the hard-shell lobe, the POD within the lobe boundary is assumed to be a specific value and outside the lobe it is 0. In the soft-shell lobe a number of probability functions can be used, and represents the variability in the performance of individuals over a long period of time. This soft-shell lobe concept is quite important since the hard-shell approximation has been found to be inadequate for all the visual lobes measured [15]. In particular the hard-shell approximation is inadequate for lobes originating from large targets, such as submarines, as they tend to produce flatter lobes. ORACLE addresses this issue by dividing the lobe into nine subsets of the population. Individually each subset has a hard-shell lobe. It is the collection of hard-shell lobes that approximates the soft-shell lobe. The hard-shell accumulator is used to summate the performance probabilities for each subset of the population which is then averaged after each glimpse. This method provides a slower probability increase for flatter lobes than do accumulators based on hard-shell lobes.

2.2.2 Inputs and Usage

Extensive descriptions of the inputs of ORACLE can be found in the ORACLE Online Help Documentation [17], however a brief overview will be provided in this section. The user interface of ORACLE has a hierarchical structure. At the top level the user has five choices, either one of the four Optical Pre-processors or the Direct Input.

The four Optical Pre-processors are the Optical and Naked Eye, Spectral or Colour, Thermal Imaging and Image Intensifier. These correspond to distinct types of visual modelling and consequently have different inputs. However, the inputs can be classified into five main categories: target, background, search, optical system and file input variables. As an example of the required variables for a pre-processor, the input parameters for the Spectral Pre-processor are listed in Table 4. This example was chosen as the Spectral Pre-processor not only models colour, but also allows the input of target and background spectra from a data file. The contents of these files are the spectral radiance as a function of wavelength. As such it may be used in combination with the HYDROLIGHT software (Section 2.1.3) to model submarines.

The Direct Input permits operation of the ORACLE visual performance model without the use of one of the Pre-processors. The input variables in this case are divided into four main classes: task, sight/display, file input and target variables. The input parameters corresponding to these categories are given in Table 5. This illustrates the variety of inputs necessary to define the target, the display and the type of visual task. It also demonstrates that ORACLE defines the target to be a two-dimensional (2D) object specified by its height

Table 4: *ORACLE Spectral or Colour Pre-processor Input Parameters.*

Target Variables	Target Height (m)
	Target Width (m)
	Range (m)
	Crossing Velocity (m/s)
	Closing Velocity (m/s)
	Intrinsic Target Contrast
Background Variables	Surrounding Luminance (cd/m^2)
	Meteorological Visibility (km)
	Sky-to-Ground Luminance Ratio
Search Variables	Number of Glimpses
Optical System Variables	FOV Type
	FOV Diameter
	FOV Height
	FOV Width
	Veiling Glare
	Magnification
	MTF Frequency Increments
	Number of MTF Values
File Input Variables	Background Spectrum
	Target Spectrum
	Airlight Spectrum
	Filter Spectrum
	MTF Data File

and width. As a result the target can be either a square or a rectangle. Another feature of the Direct Input interface is the iterative run facility for some of the parameters. This is accomplished by defining the starting, ending and increment values for the input variable of interest.

2.2.2.1 HYDROLIGHT Generated Input

Shown in Figure 3 is a plot of the spectral radiance distribution for a Case 1 water type. Case 1 water is defined as water whose optical properties are primarily determined by the phytoplankton, co-varying CDOM and detritus. In this example, the ABCASE1 subroutine from HYDROLIGHT was used. This is based on a reformulation of the "Gordon-Morel" water model by Morel and Maritorena [18]. The key parameters to this model are the pure sea water absorption and scattering coefficients and the Chloro-

Table 5: *ORACLE Direct Input Parameters.*

Target Variables at the Eye	Target Height ($mrad$) Target Width ($mrad$) Luminance Contrast Background Luminance (cd/m^2) RG Colour Contrast BY Colour Contrast Target Crossing Velocity ($mrad/s$)
Task Variables	Fractional Perimeter Confidence Level Vision Type Glimpse Time (s) Number of Glimpses Search Area ($sq°$) Slew Rate ($°/s$)
Sight/Display Variables	FOV Type: Circular or Rectangular FOV Dimensions: FOV Diameter (°) FOV Height (°) FOV Width (°) Actual Sample Width ($mrad$) Fixed Pattern Noise (standard deviation) Luminance Fluctuation (cd/m^2) Display Pixel Area ($mrad^2$) Display Integration Time (s) MTF Frequency Increments ($cycles/mrad$) Number of MTF Samples
File Input Variables	Task Data File Sensor Data File MTF Data File Number of Data Sets

phyll concentration. These inputs along with the other parameters input are summarised in Table 6.

From Table 6 it can be seen that two different types of output depths were employed: infinite and finite. In Figure 3 the infinite and finite depth waters correspond to the background and target respectively. They are referred to in this manner as the spectral upwelling radiance from these HYDROLIGHT runs are input into ORACLE as background and target spectra. For the target depths, the reflectance of the bottom layer was set to 4.0% to simulate the reflectance of a black submarine.

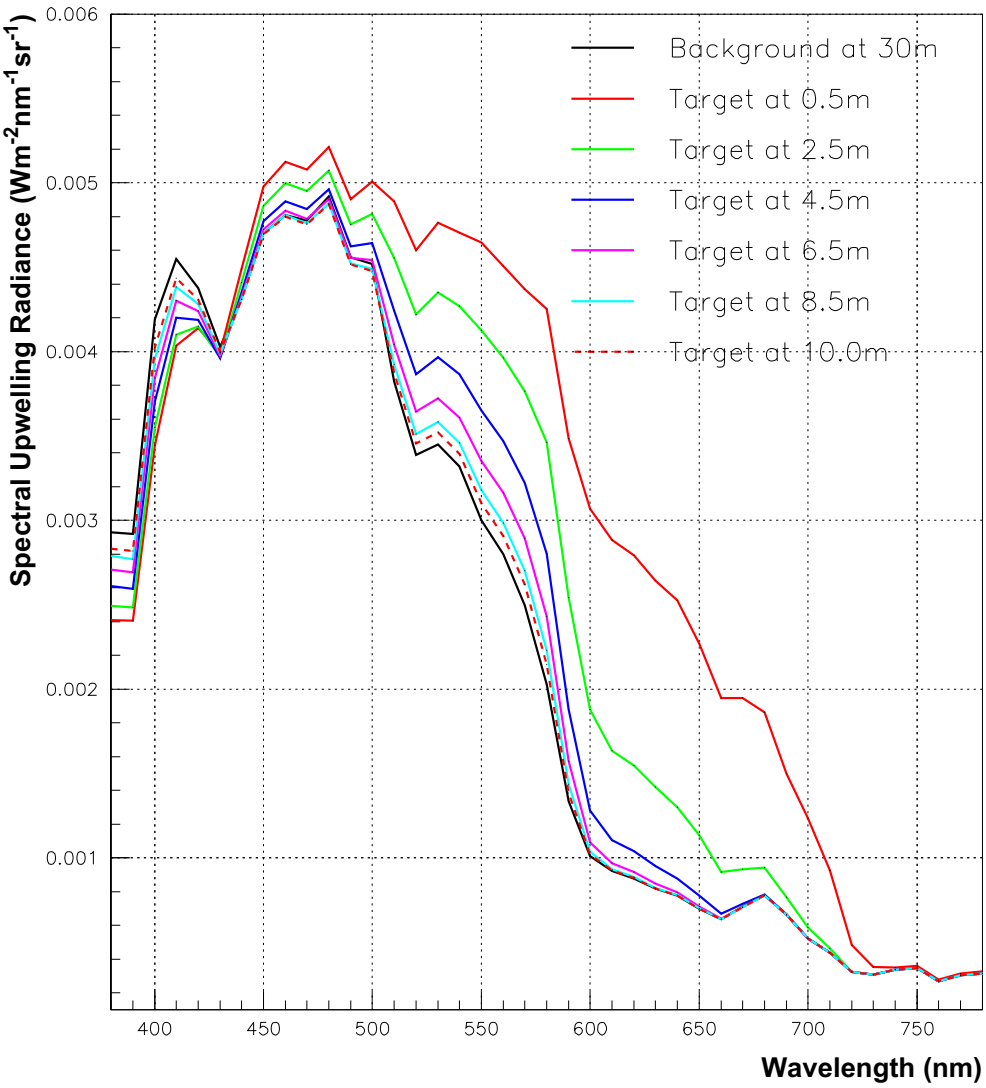

Figure 3: *The spectral upwelling radiance for a Case 1 water type at various depths.*

Table 6: *HYDROLIGHT Input Parameters for the Case 1 Water HYDROLIGHT Data Runs.*

HYDROLIGHT Parameters	**Source of Data**	**Parameter Value**
Water Model	HYDROLIGHT documentation [10, 14]	ABCASE1
Pure sea water absorption coefficient	Pope & Fry [19]	Wavelength dependent
Pure sea water scattering coefficient	Smith & Baker [20]	Wavelength dependent
Chlorophyll concentration profile	HYDROLIGHT documentation [10, 14]	Wavelength dependent
Chlorophyll phase function	Petzold's average particle [21]	Angle dependent
Chlorophyll fluorescence	HYDROLIGHT documentation [10, 14]	
Raman Scattering	HYDROLIGHT documentation [10, 14]	
Wavelength (nm)		$380 - 780$
Bandwidth (nm)		10
Water depth for background (m)		30
Water depth for targets (m)		$0 - 10$
Sun position		Location: $37^\circ\ 52'$ S $145^\circ\ 08'$ E Date: 12th July 2006 Time: $2:00\ am\ GMT$
Wind speed (m/s)	HYDROLIGHT example [10, 14]	0
Cloud cover		0
Sky model	Gregg & Carder [12]	Semi-Empirical RADTRAN
Sky conditions	Harrison & Coombes [13]	Semi-Empirical normalised radiance pattern
Bottom reflectance	HYDROLIGHT documentation [10, 14]	Infinitely deep at 30 m Finite depth $R = 4.0\%$

2.2.3 Outputs

ORACLE produces output via two methods. Firstly, it displays an input summary, visual lobe results, search results and the MTF of the display in the GUI. This is illustrated in Figures 4 - 7 for an ORACLE data run that iterates the glimpse time from 0.11 s to 0.66 s in 0.11 s increments. All of the data on the left-hand side of the GUI is accessible through use of a copy and paste facility. The lobe results data contains the acquisition probability (probability of detection) and the eccentricity for each glimpse. The range of the eccentricity values are from 0° to a maximum equal to the diameter of the search FOV, which was 20° in this example. This can be seen in Figure 5 in a line plot of acquisition probability as a function of eccentricity for glimpse 1. In the context of the ORACLE model the term eccentricity refers to retinal eccentricity, which is the angle the target/FOV makes with the visual axis of the optical system. By increasing the eccentricity the target is moving from the area of central vision to that of the periphery. This is not the same as changing the viewer angle in programs where the viewing angle changes between the target and the observer, but the target remains in the central area of vision. Figure 6 depicts the search results. The data included here is best illustrated on the right-hand side with a plot of cumulative acquisition probability as a function of the glimpse number. This contains the data relating to the visual search task. The final output is shown in Figure 7. It consists of the MTF frequency increments and the response of the optical system. In this example the response across the frequency range was 1. This can be changed via the input of a data file containing the MTF response of a particular sight or sensor.

Input Variables | Input Summary | Lobe Results | Search Results | MTF

VARIABLES USED DURING CURRENT RUN

DATA FILE NAMES

C:\ORACLE_COMPILED_V1.71\generic\taskdata.dat	
C:\ORACLE_COMPILED_V1.71\generic\sensdata.dat	
Glimpse No.	1
TASK DATA	
Fractional perimeter	1.0000
Glimpse Time (s)	0.6600
confidence level	1.7500
Search Area	200.0000
Slewing rate	0.0000
Number of Glimpses	10
TARGET DATA	
Target Height	2.0000
Target Width	6.7500
Target Luminance Contrast	0.0456
Background Luminance (cd/m²)	1000.0000
Colour Contrast RG	0.0001
Colour Contrast BY	0.0000
Target Crossing Velocity	0.0000
SIGHT DATA	
Search Field (1=Circ. 2=Rect.)	1
Circular Field of View Diameter (°)	20.0000
Rectangular Field of View Height (°)	20.0000
Rectangular Field of View Width (°)	20.0000

Figure 4: *The input summary from the GUI.*

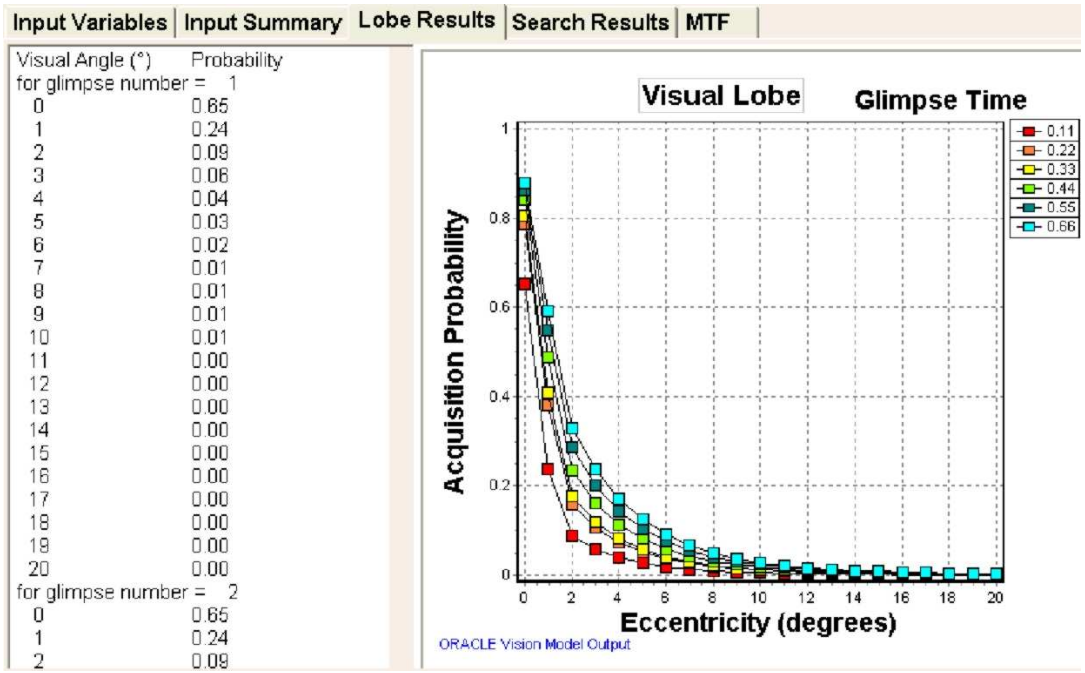

Figure 5: *The lobe results from the GUI for an iterative run.*

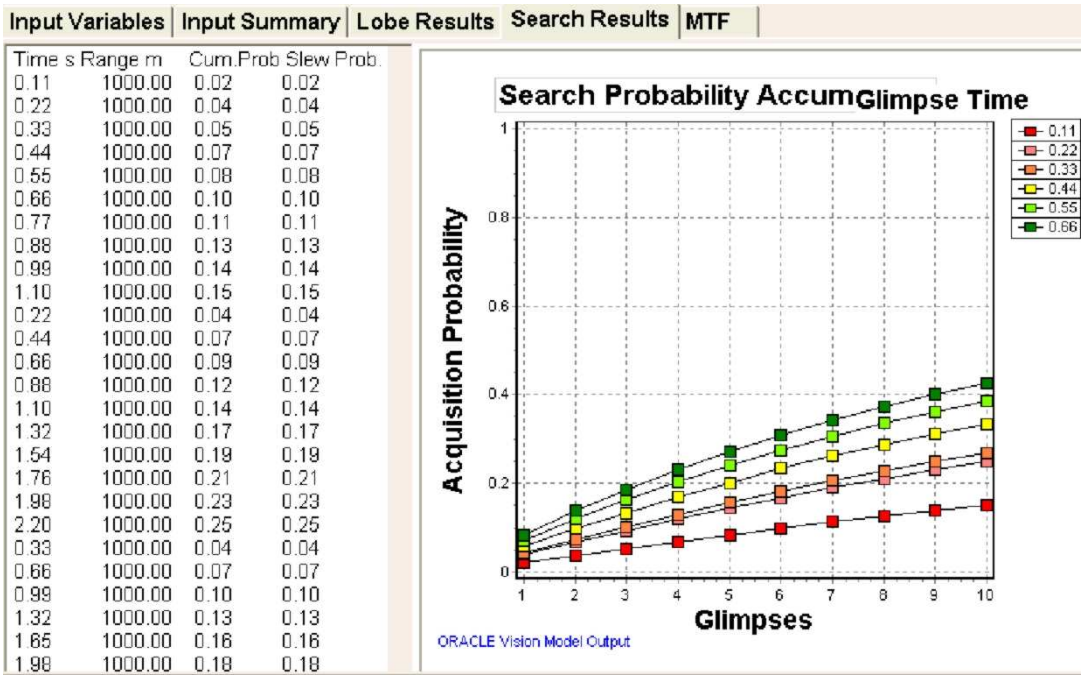

Figure 6: *The search results from the GUI for an iterative run.*

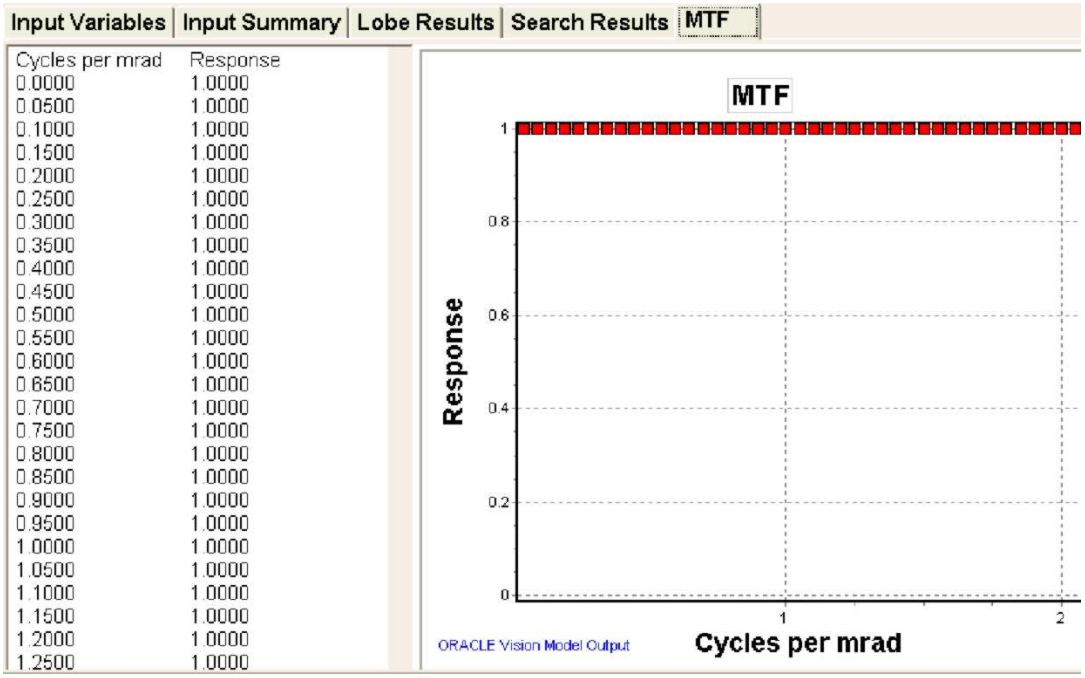

Figure 7: *The MTF from the GUI.*

The second output method is to an ASCII data file. All of the above mentioned results along with the summary of the input variables are found in this output file. This file can then be utilised by a data analysis package such as a spreadsheet program or PAW (Physics Analysis Workstation) [22].

2.2.4 Examples

Depicted in Figure 8 are plots of the POD as a function of depth and range using the ORACLE Spectral Pre-processor and the Foveal and Search algorithms respectively. These represent a culmination of 200 ORACLE data runs in which both the input target spectrum and the range were varied. The simulated depths refer to the target spectra data files that were generated by HYDROLIGHT. These generated data files contain the spectral upwelling radiance as a function of wavelength for an object with a reflectance of 4% placed at depths ranging from 0.5 m to 10.0 m in 0.5 m increments. The background spectra data file was also generated by HYDROLIGHT. In this case the water was assumed to be homogeneous below a maximum depth of 30 m. In this example, the target height and width were chosen to approximate the dimensions of a generic submarine. The atmospheric conditions were that of a clear sky and the target was defined to be slightly darker than the background. There were no airlight, filter or MTF data files included in these data runs. As a consequence, both the path radiance and transmission through the atmosphere were neglected. The inputs mentioned above and all the other inputs required to model the visual search task are summarised in Table 7.

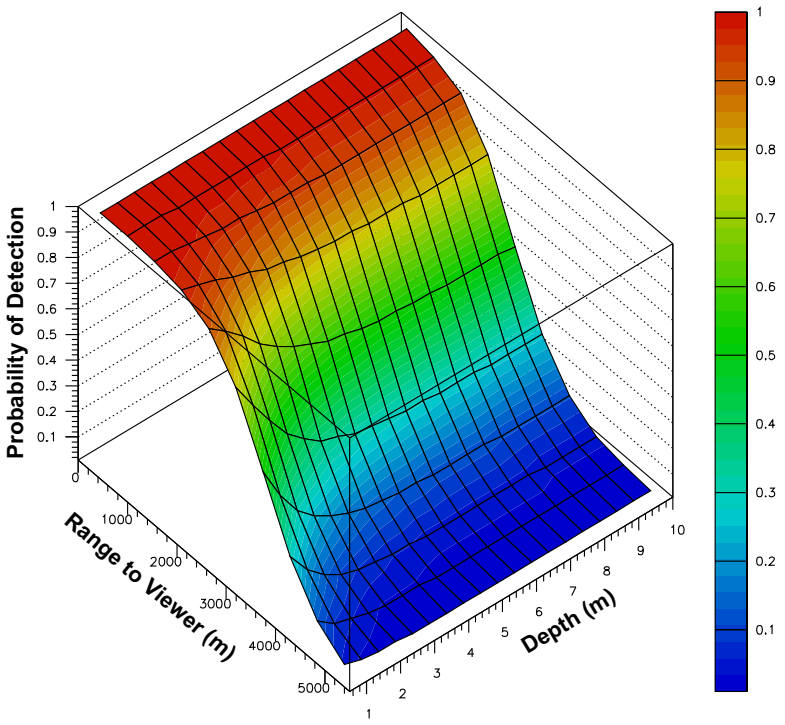

(i) The Foveal algorithm.

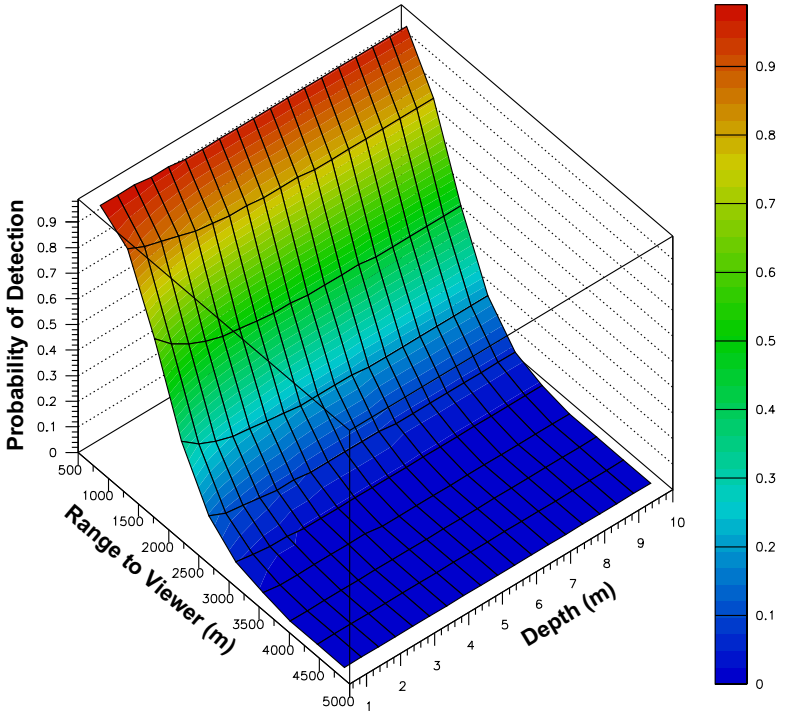

(ii) The Search algorithm.

Figure 8: *POD as a function of depth and range for Case 1 Water, glimpse 1 and a retinal eccentricity of* 0°.

Table 7: *ORACLE Input Parameters for the ORACLE data runs of Case 1 Water.*

Target Height (m)	3.59
Target Width (m)	38.9
Range (m)	500 - 5000
Crossing Velocity (m/s)	0.0
Closing Velocity (m/s)	0.00
Intrinsic Target Contrast	-0.100
Surrounding Luminance (cd/m^2)	10000.00
Meteorological Visibility (km)	15.0
Sky-to-Ground Luminance Ratio	4.0
Number of Glimpses	10
FOV Type	Circular
FOV Diameter $(^\circ)$	20.0
Veiling Glare	0.00
Magnification	1.0
MTF Frequency Increments	0.05
Number of MTF Values	41
Background Spectrum	HYDROLIGHT generated data file
Target Spectrum	HYDROLIGHT generated data files
Airlight Spectrum	None
Filter Spectrum	None
MTF Data File	None

2.3 CAMOGEN

CAMOGEN is developed and marketed by Insys Limited in the UK. It was originally created in 2001/2002 and is designed to generate optimised camouflage schemes. It uses a technique based on human vision to create camouflage schemes for use in the visible part of the spectrum (400 nm to 700 nm). CAMOGEN uses images of real scenes to create disruptive patterns (DPs) suitable for those scenes. CAMOGEN performs colour calibration and provides output in CIE (The Commission Internationale de l'Éclairage) tristimulus colour space (XYZ). Initial assessments of the DP can also be performed using CAMOGEN by inserting targets with the DP applied into the original images used to create the DP. CAMOGEN has a number of options for exporting the DP including bitmaps and spectral data. A detailed description of the algorithms used in CAMOGEN can be found elsewhere [23].

2.3.1 General Description

Briefly, the camouflage generation process includes:

- determining an optimal subset of colours from a large set taken from input textures
- creating a spatial pattern
- assigning the optimal colours to the spatial pattern

CAMOGEN makes use of an image decomposition process known as Steerable Pyramids (SPs). In this process, a number of sub-images are produced from an input image using a series of linear filters. These images, or sub-bands, contain spatial information ranging from high to low frequency with orientation dependencies. There are theories in human perception research that suggest textures that produce similar responses in a bank of linear filters will be difficult to discriminate. The SP approach is primarily based on these theories.

CAMOGEN utilises the synthesis of a greyscale texture as the basis of producing a full colour texture. Greyscale texture synthesis takes a greyscale input image and a uniform white-noise texture. The white-noise texture is modified to reproduce certain characteristics of the input image. This is achieved in CAMOGEN via an iterative histogram matching technique. First, the white-noise texture is histogram-matched to the input image. An SP is produced for the resultant synthetic texture and the input image. The sub-band images of the synthetic texture are then histogram-matched to the corresponding sub-band images of the input texture. The modified SP for the synthetic texture is then collapsed to produce the refined synthetic texture. The process is then repeated for a number of iterations. The result is a synthetic texture with similar spatial characteristics, and an identical histogram, to the input image.

CAMOGEN can also produce a synthetic texture from a number of input images. First a synthetic texture is created for each input image as described above. The resultant synthetic textures are combined by using the sub-bands of the SP from each of the textures. User-supplied factors are used to weight the sub-bands from separate textures prior to the

combination. CAMOGEN uses two different methods to combine the sub-bands. The first is a simple addition of the weighted sub-bands. This produces an homogenous texture based on all of the input images. The second method, known as regional bias addition, preserves large-scale spatial features characteristic of a single image in certain areas of the synthesised texture. The size and shape of these areas are determined by random sampling.

CAMOGEN can use one of two techniques to extend the greyscale texture synthesis method to a full colour texture synthesis. The XYZ device-independent colour space is used by CAMOGEN for all colour operations during the synthesis process. One of the methods, known as principal component analysis (PCA), splits the three-colour channel input image into separate greyscale images. It is necessary to decorrelate the colour channels of the image due to spatial cross-correlation between the three colour channels. PCA is used to decorrelate the channels and transform them to a new colour-coordinate system with less spatial cross-correlation. After this transformation, a synthetic greyscale texture is created for each of the colour channels. The three textures can then be recombined and the inverse decorrelation is applied to produce a synthetic texture in XYZ colour space. With multiple input images, CAMOGEN applies a common decorrelation to all images. The common decorrelation matrix is calculated from all images using an octree data structure. Once the decorrelation matrix is determined it is applied to all input images. The input images are then split into three colour channels and the corresponding colour channel from each of the images is used to produce a greyscale synthetic texture. The three synthetic textures, one from each colour channel, are combined and the reverse decorrelation is applied to produce the final full colour (in XYZ colour space) synthesised texture.

The other technique used by CAMOGEN for full colour synthesis is called histogram matching (HM). The input images are converted to greyscale and then used to create a synthetic texture. Colour is introduced to this newly created texture by histogram matching with a histogram containing the desired colours. The histogram of the desired colours is generated by colour-quantisation of the input images. The colours for each image are placed in an octree and normalised by the number of pixels. These octrees are combined by addition using user-supplied weighting factors. The number of colours in the resultant single octree is reduced down to the user-requested number of colours by minimising the mean square error of the colour choice. The reduced set of colours are used to generate the histogram that will be used to reintroduce colour to the synthesised texture.

The PCA method is claimed to be most suitable for input images that have a common dominant shade of colour. There is a danger that the PCA method will create colours that are not characteristic of any of the input images if there is an absence of this commonality. The HM technique will always produce colours that originate from the input images but may remove spatial boundaries defined by colour in the original input images. This could lead to the introduction of spatial features not characteristic of the input images.

2.3.2 Inputs and Usage

CAMOGEN employs a GUI to facilitate the creation and selection of various inputs/options and to perform various tasks. The CAMOGEN application comes with a built-in help facility describing these inputs/options and also provides some guidance on creating a DP. A brief explanation of the various inputs/options, including a description of the tasks needed to generate a DP, will be summarised in this section.

The following are the basic inputs required by CAMOGEN:

- image files in tif or bmp format
- absolute XYZ values in cd/m^2
- width and height, or range information for regions/items in the images

The image files are used to create patch and composite files. Image files are usually acquired by a digital camera during a field trial. The original version of CAMOGEN was designed to work with a specific digital camera but it can now use images from any camera provided the camera can produce an image file in tif or bmp format. It is also recommended that any special effects the camera may add (for example, enhancing the blue of the sky) are disabled to maintain colour integrity throughout the DP generation process. Absolute XYZ values are used to calibrate the patch files prior to creating a DP. The values are required for objects present in one of the image files used as input to CAMOGEN. Typically, a colour chart is used for this purpose. The absolute XYZ values are measured during the field trial, at the same time the images are acquired, to ensure the lighting conditions are identical for both the image and measured XYZ values. The XYZ values can be measured using either a colorimeter or spectroradiometer to record the spectral radiance from the object of interest. These spectral radiance values can then be converted to XYZ values using the CIE colour matching functions and a standard procedure [24]. Alternatively, some colorimeters provide the absolute XYZ values in cd/m^2 directly. Width and height, or range information is required to obtain the correct spatial dimensions within CAMOGEN. Markers of known dimension can be placed in the scene and included in the acquired images to provide a reference for width and height estimates. Alternatively a range finder can be used to measure the range to specific objects in the scene. It should be noted that the use of range information within CAMOGEN has, on occasion, caused execution problems so it is recommended that width and height data be used in preference to range.

There are various options available through the GUI when building a texture project and creating a DP. For each texture project the user can create a number of categories and assign weighting factors for each category. Categories are used to group patches that will receive the same weighting. Generally, this grouping is based on a physical characteristic of the patches. For example, patches containing grass may be placed into a grass category while patches depicting soil would be placed in a soil category. Patches from the calibrated images can be added to a texture project and must be associated with one of the categories that are present in the texture project. When creating DPs, the user can select the method for colour assignment (PCA or HM) and the number of colours required in the DP. The user can also select the method used to combine sub-bands (Simple or Regional bias).

When Regional bias is chosen, the degree of bias can be selected by entering a number from 0 to 4. The physical size of the DP can be chosen and the number of pixels in the X and Y directions can also be set. These allow control over the repeat unit size and effective resolution of the DP. The remaining two options are iterations and seed. The seed is a random number seed and iterations controls the number of iterations used in the synthesis process.

2.3.3 Outputs

The DP created by CAMOGEN can be displayed on the screen and printed. CAMOGEN also has facilities to output the texture in a variety of formats. The different output files are:

- Text output file: This file contains the normalised XYZ values of the generated colours of the DP and a pixel map. The pixel map contains a colour ID number for each pixel in the DP. The actual colour is determined from the normalised XYZ values that are specified in the file. This file is an ASCII text file.
- Bitmap file: This is a bitmap graphic file of the DP created by CAMOGEN.
- Greyscale image: This is a bitmap graphic file of the greyscaled DP created by CAMOGEN.
- Separation files: CAMOGEN creates separate bitmap graphic files for each colour in the DP. Each separation file displays black where the colour is present in the DP and displays the actual colour elsewhere. In addition to these graphics files, CAMOGEN also creates a file that contains spectral reflectance data for each colour in the DP. This spectral reflectance data is an approximation.
- XYZ file: CAMOGEN can also produce a binary XYZ file for the DP.

2.3.4 Examples

Examples of the type of DP that CAMOGEN can generate are shown in Figure 9. These examples are all 1 m by 1 m physical samples with 256 pixels along each length (pixel size = 3.9 mm). In all examples, histogram matching was used to perform the colour synthesis and the difference between selecting 3, 4 and 5 colours is demonstrated.

(i) Three colours. (ii) Four colours. (iii) Five colours.

Figure 9: *Sample DP generated by CAMOGEN.*

2.4 CAMEO-SIM

CAMEO-SIM is developed and marketed by Insys Limited in the UK. It was designed to produce physically accurate synthetic imagery in all electro-optic (EO) wavebands from 300 nm to 25 μm. The original application of this package was for target vehicles in various operational scenarios. It was also designed to provide a complete audit trail from output imagery back to all input parameters. Varying levels of rendering fidelity are provided to enable a trade-off between computational resources and image quality as well as producing imagery that is fit for a particular purpose. Further details on the operation and uses of CAMEO-SIM can be found elsewhere [25–30].

2.4.1 General Description

CAMEO-SIM renders scenes by solving from first principles, on a ray-by-ray basis, the RTE:

$$I(\chi,\chi') = \tau(\chi,\chi')[E(\chi,\chi') + \int \rho''(\chi,\chi',\chi'')I(\chi',\chi'')dx] + I_{path}(\chi,\chi'), \qquad (10)$$

where $I(\chi,\chi')$ is the spectral radiance, $\tau(\chi,\chi')$ is the atmospheric transmittance, $E(\chi,\chi')$ is the thermal emission, $\rho''(\chi,\chi',\chi'')I(\chi',\chi'')$ is the direct and indirect illumination and $I_{path}(\chi,\chi')$ is the path radiance. The result of this process is a radiance map in $Wm^{-2}sr^{-1}$. The fidelity of the solution to Equation 10 varies from a simple, local solution to a bi-directional, fully recursive, multi-scattering, anti-aliased solution with minimal approximations. The form of this RTE differs from that shown in Equation 1 since this is a general RTE whereas Equation 1 is specifically formulated for through water applications.

2.4.2 Inputs and Usage

Detailed descriptions of the inputs and usage of the CAMEO-SIM system can be found elsewhere [31, 32], however a brief overview will be provided here. Projects are created to produce imagery; related projects are usually grouped into a database. The parameters and selections that control the imagery produced for a project are summarised in Table 8. Each project is built using the following basic entities: terrain, ocean, atmosphere, players, observers and rendering scheme. The selected terrain will have a geometry describing its physical dimensions with a texture or materials applied to the surface. CAMEO-SIM uses a proprietary graphics file format known as Compiled Graphics Format (CGF) to specify the geometry. CAMEO-SIM provides tools to convert objects created using third-party software into CGF files. Table 9 lists the formats that CAMEO-SIM is able to convert to CGF format. Both the thermal and optical properties of materials (whether those materials are applied to terrains or players) can be specified and Table 10 summarizes the properties that can be defined. Both the surface properties and IOPs of an ocean can be specified. The parameters controlling the appearance of the water surface are shown in Table 11. Ocean components are used to define the IOPs of the interior of the water body. Table 12 shows the parameters used to define the ocean components. The terminology shown in Table 12 is that used in the CAMEO-SIM GUI. Strictly speaking, the term referred to as "Absorption Coefficient" with units of m^2/mg is more correctly referred to as "Specific Absorption Coefficient". Similarly the "Scattering Coefficient" should be referred to as the "Specific Scattering Coefficient". The "Scattering Density" with units of sr^{-1} is more correctly called the "Scattering Phase Function". Both the spectral (Table 13) and thermal (Table 14) atmospheres can be defined for a particular project. MODTRAN is used to provide radiation propagation data for the spectral atmosphere. Players that represent objects in the scene can be defined and controlled. A player will have a geometry with textures and materials much like a terrain. However, the player needs to be positioned in the scene with the desired orientation and motion information if required. A plume can also be defined for a player and events can be set to trigger changes in the player. The observer, which must be a player in the scene, provides the viewpoint for the rendered imagery. The FOV and resolution of the observer can be selected and the spectral response of the observer sensor is required. CAMEO-SIM also provides tools for managing databases, materials, textures, geometries and plumes. Imagery tools are also available and an optional module allows rendering across a cluster for performance improvements.

Table 8: *CAMEO-SIM Input Parameters: Project.*

Terrain	Terrain selection
Ocean	Select ocean Tide
Atmosphere	Select spectral atmosphere Sun/moon position/motion Select thermal atmosphere
Players	Add players (i.e. objects) Set player position Set player orientation Set player motion Plume assignment Events for player
Observer	Select player as observer Resolution ($pixels$) FOV (°) Fish-eye mode Sensor response
Rendering	In-band/Multispectral/Colour imagery Start time (s) End time (s) Frame rate (Hz) Rendering scheme (speed versus quality) Processing options

Table 9: *CAMEO-SIM Geometry Conversion Options.*

Third-party software	Format	File suffix
MultiGen II	OpenFlight	FLT
3D Studio Max	3D Studio	3DS
3D Studio Max	ASCII Export	ASE
Several	NIRATAM	PLY
Fluent	Case file	CAS
Wavefront	Wavefront Object	OBJ
RadThermIR	Thermoanalytics TDF	TDF
Lightwave	Lightwave Object File	LWO

Table 10: *CAMEO-SIM Input: Material Properties.*

Surface Optical	**Scatter Model**	Diffuse BRDF Cook and Torrance Sandford Robertson Ashikhmin and Shirley Cloud
	Optical Properties (required values depend on scatter model)	Spectral reflectivity Bidirectional reflectance peaks Mean facet slope Spectral emissivity Fresnel coefficient Specular lobe width Specular reflectivity Shininess exponent
Thermal	**Surface**	Solar absorptivity Thermal emissivity Characteristic length (m)
	Interior	Density (kg/L) Specific heat capacity ($kJkg^{-1}K^{-1}$) Conductivity ($Wm^{-1}K^{-1}$) Depth (m) Minimum temperature ($^{\circ}C$) Maximum temperature ($^{\circ}C$)

Table 11: *CAMEO-SIM Input Parameters: Oceans.*

Shape	Spectrum function: Frequency (Hz) versus spectral power (m^2/Hz) Azimuthal wave direction Directionality Mean water depth (m) Random seed
Tiling	Tesselated or smooth Curved Earth Tile size (m) Cells per tile Twist angle ($^\circ$) Tile repeat factors
Materials	Material type for: Water Whitecaps Ocean floor
Surface	Temperature (K) Surface roughness Whitecaps
Interior	Select ocean components Ocean component concentration (mg/m^3) versus depth (m)
Fidelity	List of sample depths (m) List of floor depths (m) List of solar elevations ($^\circ$) List of wavelengths (μm) No. of sampling rays

Table 12: *CAMEO-SIM Input Parameters: Ocean components.*

Absorption	Absorption coefficient (m^2/mg) vs wavelength (μm)
	Absorption exponent
Scatter	Scattering coefficient (m^2/mg) versus wavelength (μm)
	Scatter exponent
	Scattering density (sr^{-1}) versus phase angle ($^\circ$)

Table 13: *CAMEO-SIM Input Parameters: Spectral Atmosphere.*

General	Day, Month and Year
	Latitude and Longitude
	Wavelength range (μm)
	Atmospheric CO_2 (ppm)
Geometry	List of line-of-sight ranges (km)
	List of line-of-sight elevations ($^\circ$)
	List of observer altitudes (km)
	List of target altitudes (km)
	List of solar elevations ($^\circ$)
	List of solar observer angles ($^\circ$)
	Ground altitude (km)
	Maximum altitude (km)
MODTRAN Parameters	Season and seasonal model
	Surface albedo and material
	Cloud type and rain rate (mm/hr)
	Haze type and Air Mass Characteristic
	Visibility (km)
	Wind speed (m/s)
	Volcanic extinction model and distribution
	Scattering type
Generation	Speed
	MODTRAN or LOWTRAN
	Minimum observer height (m)
	Maximum generated size (Mb)
	Update interval (s)

2.4.3 Outputs

CAMEO-SIM produces imagery as the only output. This imagery is produced in a proprietary format known as Floating-Point Image (FPI) format. Imagery can be a

Table 14: *CAMEO-SIM Input Parameters: Thermal Atmosphere.*

General	Day, Month and Year
	Latitude and Longitude
	Time of day
	Spectral history
Geometry	List of altitudes (km)
	List of slopes ($^\circ$)
	List of azimuths ($^\circ$)
	Time step (hr)
Weather	Sky radiance (W/m^2) versus altitude (km)
	Direct solar radiation (W/m^2) versus altitude (km)
	Scattered solar radiation (W/m^2) versus altitude (km)
	Wind speed (m/s)
	Precipitation rate (mm/hr)
	Air temperature ($^\circ C$)
	Relative humidity (%)
	Rain temperature difference ($^\circ C$)
Ground	Material type
	Bedrock temperature ($^\circ C$)
Generation	Update interval (s)

single, static image or a sequence of images comprising an animation. CAMEO-SIM can produce different types of imagery as shown in Table 15. Colour imagery can be used to produce imagery for human observers or subsequent analysis software that works with colour imagery. Inband and multispectral imagery is useful for generating imagery that corresponds to a particular sensor system. This could be used to challenge different image processing algorithms that would be linked to that particular sensor. The range and incidence imagery provides spatial visualization that, in the case of range, provides a 3D (three dimensional) like impression. The temperature imagery is useful for assessing the thermal qualities of the scene. The player imagery is useful in subsequent image analysis since it facilitates the selection of parts of the scene that contain a particular player. Once these regions are selected, they can be analysed to determine properties related to a specific player (e.g. the average radiance of a player).

In addition to the FPI format, CAMEO-SIM may export imagery in other image file formats as shown in Table 16.

Table 15: *CAMEO-SIM Output: Imagery types.*

Imagery	Description
Inband	Image depicting total radiation for all sensor wavebands.
Multispectral	An image for each sensor waveband.
Colour	Three images containing CIE XYZ tristimulus values for colour imagery.
Range	Image depicting range from observer to object at each pixel.
Incidence	Image depicting incidence angle on the object at each pixel.
Temperature	Image depicting physical temperature of object at each pixel.
Apparent temperature	Image depicting temperature of object as perceived by sensor.
Players	Image depicting percentage of each player present at each pixel.

Table 16: *CAMEO-SIM Output: Export file format.*

Suffix	Format
bmp	Microsoft Windows bitmap image file
fits	Flexible Image Transport System
gif	CompuServe graphics interchange format
jpeg	Joint Photographic Experts Group JFIF format
pgm	Portable graymap format (grayscale)
png	Portable Network Graphics
ppm	Portable pixmap format (colour)
ps	Adobe PostScript file
sgi	Irix RGB image file
tga	Truevision Targa image file
tiff	Tagged Image File Format
xpm	X Windows system pixmap file (colour)

2.4.4 Examples

Figure 10 demonstrates the type of imagery that can be generated from CAMEO-SIM. In this particular example, the scene was rendered in the visible part of the spectrum and colour imagery was produced. The second example (Figure 11) is of a jeep rendered in an IR waveband (3 μm to 5 μm).

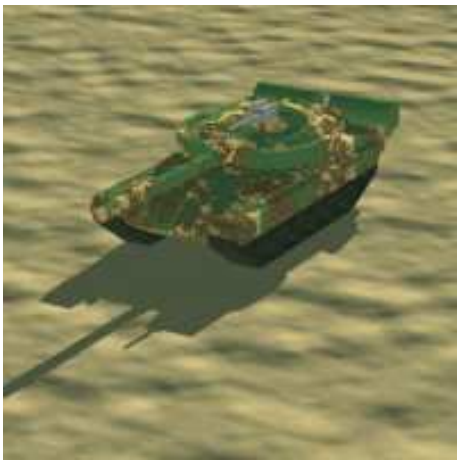

Figure 10: *CAMEO-SIM rendered image of a tank on a bumpy surface.*

Figure 11: *CAMEO-SIM rendered image of a jeep in an infrared waveband.*

2.5 Support Software Codes

2.5.1 Rhinoceros

Rhinoceros, usually referred to as Rhino, is a commercial 3D modelling package available from Robert McNeel & Associates. Rhino uses NURBS (non-uniform rational B-splines) to accurately model any shape and can create a mesh at any resolution. Rhino runs on Windows and can import and export files in a wide variety of standard graphics formats including AutoCAD drawing exchange format (DXF), AutoCAD drawing database (DWG), Initial Graphics Exchange Specification (IGES), Standard for the Exchange of Product Data (STEP), Autodesk 3D Studio 3D scene (3DS), Wavefront object (OBJ) and 3D Systems stereolithography (STL). Rhino is used to manipulate 3D wireframe models of naval platforms and export them in a format suitable for use in other modelling codes such as NTCS and CAMEO-SIM. An example wireframe model from Rhino is shown in

Figure 12. Rhino has also been used to create 2D views of targets for CAMOGEN.

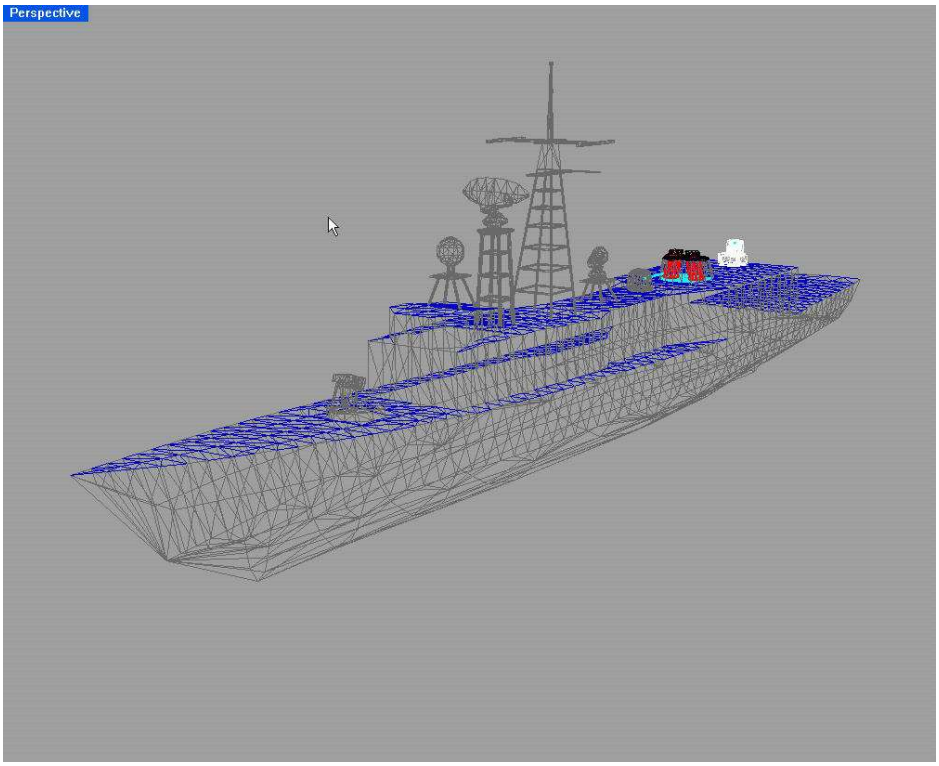

Figure 12: *Rhino wireframe model of an RAN FFG.*

2.5.2 MODTRAN

MODTRAN (MODerate resolution of atmospheric TRANsmission) is a program used to model atmospheric propagation of radiation. MODTRAN is licensed by the USAF but distribution is handled by Ontar Corporation. MODTRAN operates over a broad spectral band from the far IR (about 100 cm^{-1}) through the visible and up to the UV (50,000 cm^{-1}) at a resolution of 1 cm^{-1} and calculates the transmittance of radiation and path radiance for a particular scenario chosen by the user. Details of the usage of MODTRAN can be found in the User's Manual [33]. In the context of the VST, MODTRAN is called by CAMEO-SIM to create spectral atmospheres. CAMEO-SIM handles the creation of the necessary input files for MODTRAN as well as analysing and using the output files.

2.5.2.1 General Description

MODTRAN calculates atmospheric transmittance, atmospheric background radiance, single scattered solar and lunar radiance, direct solar irradiance, and multiple scattered solar and thermal radiance. The model includes the effects of molecular absorption (both line and continuum), molecular scattering, aerosol absorption and scattering, and hy-

drometeor absorption and scattering. The calculation of the atmospheric slant path and attenuation along the path include the effects of refraction and curvature of the Earth.

2.5.2.2 Inputs and Usage

A summary of the input parameters that CAMEO-SIM requires for MODTRAN are shown in Table 13. MODTRAN requires information on atmospheric composition, aerosols, clouds and rain. The atmospheric composition provides the molecular composition as a function of height to allow the calculation of molecular effects and it may be entered in one of two ways:

- selection of an in-built reference atmosphere or
- explicit input of pressure, temperature, density and molecular mixing ratios as a function of altitude

CAMEO-SIM allows the selection of one of the six in-built MODTRAN reference atmospheres (Table 17). Alternatively, the pressure, temperature and relative humidity profiles as a function of altitude can be entered.

Table 17: *MODTRAN Input: Reference atmospheres.*

Atmosphere Name	**Latitude**	**Time of the Year**
Tropical	15° N	Annual average
Midlatitude summer	45° N	July
Midlatitude winter	45° N	January
Subarctic summer	60° N	July
Subarctic winter	60° N	January
1976 US standard	na	na

The aerosol input to MODTRAN can also be entered in one of two ways:

- selection of altitude and seasonal-dependent aerosol profiles and aerosol extinction coefficients or
- explicit aerosol profiles and aerosol extinction coefficients via a NOVAM file

CAMEO-SIM allows the setting of a season (one of spring, summer, autumn, winter), a haze model (for aerosols up to 2 km), a volcanic model (for stratospheric aerosols; 10 km to 30 km), the air mass character (only for Navy maritime haze model), visibility and wind speed (only for Navy maritime and desert haze models). The haze models available are shown in Table 18 and the volcanic models are shown in Table 19.

Table 18: *MODTRAN Input: Haze models.*

Model Name
None (no cloud)
None (cloud)
Maritime
Navy maritime
Rural (5 km visibility)
Rural (23 km visibility)
Advection fog
Radiative fog
Tropospheric
Desert
Urban

Table 19: *MODTRAN Input: Volcanic models.*

Extinction Model	**Vertical Distribution**
Background	Background
	Moderate
	High
Aged	Moderate
	High
Fresh	Moderate
	High
	Extreme

The surface reflectance (albedo) of the ground can be specified. BRDF or Lambertian reflectance can be modelled. There are seven BRDF models available:

- Symmetric Walthall
- Symmetric Sinusoidal-Walthall
- Hapke
- Rahman
- Roujean
- Ross-Li

- Pinty-Verstraete

The cloud type is chosen from a list of standard types available within MODTRAN (Table 20). The rain rate is either determined from the cloud model chosen (Table 20) or it can be set explicitly.

Table 20: *MODTRAN Input: Cloud models including rain.*

Cloud Model	Rain Rate (mm/hr)
None	0.0
Cirrus	0.0
Cirrus sub-visual	0.0
Cumulus	0.0
Cumulus heavy rain	25.0
Cumulus extreme rain	75.0
Nimbostratus	0.0
Nimbostratus light rain	2.0
Nimbostratus moderate rain	12.5
Stratus	0.0
Stratus drizzle	2.0
Altostratus	0.0
Stratocumulus	0.0

In addition to the preceding physical parameters, MODTRAN also allows the selection of different types of computational options for handling scattering. CAMEO-SIM allows the selection of Mie or Henyey-Greenstein scattering. In the case of Henyey-Greenstein scattering, further sub-choices of forward, symmetric or reverse are available. CAMEO-SIM also allows the choice of multiple scattering using the Isaac or DISORT algorithms.

2.5.2.3 Outputs

MODTRAN produces output files that contain atmospheric transmittance, atmospheric background radiance, single scattered solar and lunar radiance, direct solar irradiance, and multiple scattered solar and thermal radiance. CAMEO-SIM reads the data from these files and uses the information to render scenes.

2.6 ToolBox Software Codes and DSTO Developed Techniques

2.6.1 CAMEO-SIM Ocean Model Data

To generate the interior of a water body in CAMEO-SIM a number of IOPs are required to be specified. These are listed in Table 12 in Section 2.4.2. These components can be either generated from or are the inputs into HYDROLIGHT. Consequently, software has been written to retrieve the IOPs from HYDROLIGHT and put them in a format that CAMEO-SIM can utilise.

HYDROLIGHT models the IOPs within a water body using a variety of methods, depending on which water model is used in the simulation. The generic water models distributed in HYDROLIGHT are:

- ABCASE1 - A Case 1 Water Model
- ABCASE2 - A Case 2 Water Model
- ABCASE1H - The Haltrin Water Model
- ABOTHER - A User-Defined Water Model

However, with the exception of the ABOTHER water model they are similar and vary only in the number of components used, and in some instances the actual components and way the IOPs are calculated within HYDROLIGHT (Table 21). Since the ABOTHER routine has not been utilised to date, this discussion will be restricted to the calculation of the IOPs for the other three water models.

2.6.1.1 Absorption Coefficient Data

In CAMEO-SIM the absorption coefficient, $a_i(\lambda)$, of the ith water component is modelled by:

$$a_i(\lambda) = a_i^*(\lambda) X_i^{\alpha_i}, \tag{11}$$

where α_i is an exponent, $a_i^*(\lambda)$ is the specific absorption coefficient and X_i is the concentration profile of the ith component respectively. In this section is a discussion of the methods used to obtain the specific absorption coefficient and the exponent data for the various ocean components in the HYDROLIGHT water models. The concentration profile is discussed in Section 2.6.1.3.

Pure Water

The three generic water models in HYDROLIGHT use the same method for determining the absorption coefficient of the pure water component. This is generally achieved by a user-defined data file containing either values of $a(\lambda)$ or $a^*(\lambda)$ and the exponent is set to 1.0. The values of $a(\lambda)$ and $a^*(\lambda)$ are interchangeable as long as the exponent is 1.0. Since the data is input into HYDROLIGHT using a user-defined input file a new subroutine, which will be referred to as the HYDROLIGHT CAMEO-SIM output subroutine,

Table 21: *HYDROLIGHT Generic Water Models.*

Water Model	Number of Components	Components
ABCASE1	2-3	Pure Water Chlorophyll CDOM
ABCASE2	4	Pure Water Chlorophyll CDOM Minerals
ABCASE1H	4	Pure Water Chlorophyll[1] CDOM[2] Minerals[3]
ABOTHER	User-Defined	User-Defined

was written to output the data to file. The DSTO developed software processes this file to produce the output in the format required for input into CAMEO-SIM. The value of the exponent is hard-coded into the DSTO software, so that once the water component is chosen the value of the exponent is known.

Chlorophyll

In HYDROLIGHT, the chlorophyll absorption is determined using one of the following absorption models:

- a general model of absorption
- the Prieur-Sathyendranath-Morel (PSM) model [34, 35]
- the Haltrin model [36]

Which of these is utilised depends on which HYDROLIGHT water model is requested - if the ABCASE1 water model is selected then chlorophyll absorption is modelled using the PSM model; when the ABCASE2 water is selected then the user has the choice of a general model for absorption or the PSM model; if the ABCASE1H is chosen then the Haltrin model is employed. However all of these models are of the same general form as that given in Equation 11, differing only in the value of the exponent α and in the case of the ABCASE2 water model the values of the specific absorption coefficient $a_c^*(\lambda)$; when using the ABCASE2 water model the user can input a data file containing the $a_c^*(\lambda)$ values.

[1]Modelled as large scattering particles.
[2]Separated into fulvic and humic parts.
[3]Modelled as small scattering particles.

For all the water models the $a_c^*(\lambda)$ values are output from HYDROLIGHT into a data file using the HYDROLIGHT CAMEO-SIM output subroutine. This in turn can be fed into the DSTO software for processing. The other parameter required by CAMEO-SIM is the exponent α. Since the value of α can be found in the literature for all the water models utilised [34–37] it is generated by the DSTO software once the HYDROLIGHT water model, and in the case of the ABCASE2 water model the absorption model, is chosen. This is accomplished through a user interface to the DSTO software.

CDOM or Yellow Substance

The CDOM is the least understood of all the constituents of water bodies. In Oceanography, the absorption is generally modelled using one of two methods: a general absorption model defined as:

$$a_y(z,\lambda) = a_y^*(\lambda) X_y^{\alpha=1}, \tag{12}$$

or a decaying exponential function of the form [38]:

$$a_y(z,\lambda) = a_y(z,\lambda_0) exp\left[-\gamma\left(\lambda-\lambda_0\right)\right], \tag{13}$$

where λ_0 is a reference wavelength, γ is a coefficient, $a_y^*(\lambda)$ is the specific absorption coefficient of the CDOM and $a_y(z,\lambda)$ and $a_y(z,\lambda_0)$ are the absorption coefficients of the CDOM at depth z and wavelength λ and λ_0 respectively. Although HYDROLIGHT offers both these options through the GUI, the literature suggests that it is common practice to use the decaying exponent method [7, 8, 39–41].

The absorption of the CDOM is often determined as a function of the chlorophyll absorption [18, 42–44]. If this covariance method is used then Equation 13 becomes:

$$a_y(z,\lambda) = F a_c(z,\lambda_0) X_c^{\alpha} exp\left[-\gamma(\lambda-440)\right], \tag{14}$$

where X_c is the chlorophyll concentration and F is a coefficient. If the PSM model parameters [34, 42] are used this simplifies to:

$$a_y(z,\lambda) = 0.012 a_c(z,\lambda_0) X_c^{0.65} exp\left[-0.014(\lambda-440)\right], \tag{15}$$

where $a_c(z,440)$ is the absorption coefficient of the chlorophyll component at depth z and a wavelength of 440 nm, which is normalised to 1.0. This leads to the following definition of the specific absorption coefficient:

$$a_y^*(\lambda) = 0.012 exp\left[-0.014(\lambda-440)\right]. \tag{16}$$

When the ABCASE1 water model is employed the CDOM absorption is always modelled using the PSM form of the covariance method given in Equation 15. Since HYDROLIGHT calculates $a^*(\lambda)$ using Equation 16, but never outputs it to file, it is output to file using the HYDROLIGHT CAMEO-SIM output routine. The value of the exponent α can be found in the literature [34, 35, 37] and is also given in Equation 15. As a result once the ABCASE1 water model is chosen through the user interface of the DSTO software, α is set to 0.65.

In the ABCASE2 water model, the user can choose any of the above three methods (Equations 12, 13 and 14[1]) for calculating the absorption of the CDOM component.

[1]Equation 15 is the same form as Equation 14 with $F = 0.012$, $\alpha = 0.65$ and $\gamma = 0.014$

Therefore a number of procedures are required to obtain the specific absorption coefficient. For the case where the covariance model is utilised, the same procedure as that performed for the ABCASE1 water is used. When the decaying exponent method is selected in HYDROLIGHT, there is a complication due to the fact that there is one variable calculated and two unknowns required for input into the CAMEO-SIM ocean model. To solve this either the specific absorption coefficient or the concentration profile must be set to 1.0. Since HYDROLIGHT outputs the CDOM concentration as an absorption coefficient (units of m^{-1}) it was decided to set the specific absorption coefficient to 1.0 and the output of the calculation of Equation 13 to be the concentration profile. To date, the decaying exponent method has not been used in generating an ocean and it remains to be seen whether this method is a reasonable approximation of the CDOM component. Finally, when the general method is employed, HYDROLIGHT either uses an input file containing values of $a_y^*(\lambda)$ or calculates them using the decaying exponent relation. In both cases, the resulting values for the concentration profile and $a_y^*(\lambda)$ are output to a data file using the HYDROLIGHT CAMEO-SIM output subroutine. This in turn is processed by the DSTO software. The choice of which of the models to use in the processing is achieved using the user interface. Once the absorption model is selected the DSTO software either generates the appropriate value for the exponent α or the user is prompted to enter a value. The determination of α is done this way as HYDROLIGHT does not calculate these, they are either found in the literature [34, 35, 37] or are input by the user through the GUI in HYDROLIGHT. The value for α is therefore always known *a priori*.

The modelling of the CDOM in the ABCASE1H or Haltrin water model [36] varies significantly from the other two water models. In this model the CDOM is broken into two parts: the fulvic and humic. In HYDROLIGHT the absorption coefficients of these two components are summed together to yield the total absorption coefficient of the CDOM, which is written to one of the standard output data files. However, for the purpose of entry into CAMEO-SIM the two components remain separate. To achieve this the HYDROLIGHT subroutine responsible for calculating the absorption coefficient for the ABCASE1H was altered to calculate the specific absorption coefficients for the fulvic and humic components using the relations:

$$a_f^*(\lambda) = 35.959 exp\left[-0.0189\lambda\right], \tag{17}$$

and

$$a_h^*(\lambda) = 18.828 exp\left[-0.01105\lambda\right]. \tag{18}$$

The data is then output to a file created using the CAMEO-SIM output subroutine developed in HYDROLIGHT. This data file is then input into the DSTO software. The value of α for both the fulvic and humic parts is set to 1.0 in the DSTO software, once the ABCASE1H water model is selected. It is done in this manner as the absorption coefficients for the two components have the following functional forms [36]:

$$a_f(\lambda) = a_f^0 C_f exp\left[-k_f\lambda)\right], \tag{19}$$

and

$$a_h(\lambda) = a_h^0 C_h exp\left[-k_h\lambda)\right], \tag{20}$$

where k_f and k_h are proportionality constants for the fulvic and humic components respectively.

2.6.1.2 Scattering Coefficient Data

The scattering coefficient, $b_i(\lambda)$, of the ith component in CAMEO-SIM is modelled by:

$$b_i(\lambda) = b_i^*(\lambda) X_i^{\alpha_i}, \tag{21}$$

where α_i is an exponent, $b_i^*(\lambda)$ is the specific absorption coefficient and X_i is the concentration profile of the ith component respectively. As was the case for the absorption coefficient, the determination of the scattering coefficient is accomplished by specifying the spectral specific scattering coefficient $b_i^*(\lambda)$, exponent α and the concentration profile X_i. This section contains the details of the methods employed to obtain the specific scattering coefficient and the exponent data for the various ocean components in the HYDROLIGHT water models. The reader should refer to Section 2.6.1.3 for a discussion on the concentration profile data.

Pure Water

The same method for determining the scattering coefficients of the pure water component of a water body is utilised by the three generic water models in HYDROLIGHT. That is, the user defines a data file which contains values of $b_w(\lambda)$ or $b_w^*(\lambda)$. As was the case for the water absorption data, the HYDROLIGHT CAMEO-SIM output subroutine sends this data to an output file for processing by the DSTO software.

Chlorophyll and Minerals

The scattering coefficients of the chlorophyll and minerals are determined in HYDROLIGHT by employing one of the following models:

- a general model
- a power law [45]
- a linear relation [46]
- the Haltrin model [36]

The particular model used depends on which of the HYDROLIGHT water models is utilised.

When the ABCASE1 water model is requested then the power law method is used with the Gordon and Morel (GAM) model parameters [35, 37]. If the ABCASE2 water is used the user has a choice of the first three models above. However, for both waters the value of $b_i^*(\lambda)$ is either read-in from a data file or calculated in HYDROLIGHT. Therefore the HYDROLIGHT CAMEO-SIM output subroutine sends the appropriate data to file. The value of the exponent α is a standard value for the GAM model so the user does not have to enter this value. However, when using the power law with different parameters (non-default) and the linear relation, the DSTO software prompts the user to enter the appropriate values.

The ABCASE1H water model determines the scattering coefficients for the chlorophyll and minerals in a different manner to that described above. In this model the chlorophyll

is modelled as large scattering particles and the minerals as small scattering particles. Although the standard version of HYDROLIGHT calculates the scattering coefficients of the small and large scattering particles it does not separate the calculation of the specific scattering coefficient. As a result, the subroutine responsible for these calculations was altered to calculate the specific scattering coefficients for the large (chlorophyll) and small (mineral) particles using the relations:

$$b_l^*(\lambda) = 0.341074 \left[\frac{400}{\lambda}\right]^{0.3} \tag{22}$$

and

$$b_s^*(\lambda) = 1.151302 \left[\frac{400}{\lambda}\right]^{1.7}. \tag{23}$$

This data is then output to a file created using the HYDROLIGHT CAMEO-SIM output subroutine, which is later processed by the DSTO software.

2.6.1.3 Concentration Profile Data

For the ABCASE1 and ABCASE2 water models, HYDROLIGHT supplies two standard methods for the determination of the concentration profile: input via a user-defined file or calculation by a subroutine. The particular subroutine employed is selected through the GUI and is at present dependent on the component. That is, for chlorophyll the chlzfunc subroutine calculates the concentration profile as a gaussian with a constant background [47], whereas for the CDOM the acdom subroutine calculates the concentration as an exponential. In either case, the results of the calculation can be output to file using the HYDROLIGHT CAMEO-SIM output subroutine. The data obtained from the user-defined input file can be output the same way.

For the ABCASE1H water model the determination of the concentration profile is accomplished using the relationships defined by Haltrin [36]. This method varies significantly from that employed in the ABCASE1 and ABCASE2 water models; the concentration profiles of the components in this model are determined as a function of the total chlorophyll concentration X_c with respect to a reference chlorophyll concentration X_c^0, which is defined to be 1 mg/m^3. HYDROLIGHT calculates these profiles according to the following relations:

$$X_l = 0.76284 X_c exp\left[0.03092 \left(\frac{X_c}{X_c^0}\right)\right], \tag{24}$$

$$X_f = 1.74098 X_c exp\left[0.12327 \left(\frac{X_c}{X_c^0}\right)\right], \tag{25}$$

$$X_h = 0.19334 X_c exp\left[0.12343 \left(\frac{X_c}{X_c^0}\right)\right] \tag{26}$$

and

$$X_s = 0.01739 X_c exp\left[0.11631 \left(\frac{X_c}{X_c^0}\right)\right], \tag{27}$$

where X_l, X_f, X_h and X_s are the concentration profiles of the large, fulvic, humic and small particles respectively. The results of these calculations are sent to file using the HYDROLIGHT CAMEO-SIM output subroutine for further processing using the DSTO software.

2.6.1.4 Scattering Phase Function Data

The scattering phase function $\tilde{\beta}(\psi)$ is implemented in HYDROLIGHT using a series of discretised functions that can be directly input into the RTE. It is performed this way as the RTE is solved numerically by partitioning the unit sphere into quadrilateral regions corresponding to directions with a constant value of θ and ϕ. This, for the most part, is achieved by a series of input files. Referring to Table 12 in Section 2.4.2, CAMEO-SIM requires the scattering density or more precisely the scattering phase function with respect to angle. Therefore a method must be devised to obtain the data in the correct format. Two methods have been employed for this purpose:

- input of the phase function from a user-defined file
- calculation of the phase function

Which of these methods is used depends on whether the phase function data is found in the literature.

Pure Water Scattering Phase Function

In all of the HYDROLIGHT water models discussed, the phase function employed for the pure water component is the same. It is the Morel Phase function which is commonly referred to as the Rayleigh scattering function which has the functional form [9]:

$$\tilde{\beta}_w(\psi) = 0.06225(1 + 0.835cos^2\psi), \tag{28}$$

where $\tilde{\beta}_w(\psi)$ is the scattering phase function of pure water and ψ is the angle in the range $0 \leq \psi \leq \pi$. Since this function is easily evaluated, the DSTO software performs the calculation across the range $0 \leq \psi \leq \pi$. It then outputs the data to the CAMEO-SIM input file.

Chlorophyll and Mineral Scattering Phase Functions

The chlorophyll and mineral scattering phase function can be defined in HYDROLIGHT using a number of relations. These are:

- the Petzold Average Particle phase function
- an Isotropic phase function
- the One-Term Henyey-Greenstein phase function
- the Fournier-Forand phase function
- the Kopelevich Large Particle phase function
- the Kopelevich Small Particle phase function

All of these are calculated by the DSTO software, except for the Petzold Average Particle phase function, which is input from file. The data corresponding to the Petzold Average Particle phase function can be found in *Light and Water Table 3.10* [9]. The Isotropic phase function $\tilde{\beta}^F(\psi)$ is calculated using the following relation [9]:

$$\tilde{\beta}^F(\psi) = \frac{1}{4\pi}, \tag{29}$$

where ψ is the scattering angle. The One-Term Henyey-Greenstein phase function $\tilde{\beta}_{HG}(g;\psi)$ is determined using [9]:

$$\tilde{\beta}_{HG}(g;\psi) = \frac{1}{4\pi}\frac{1-g^2}{(1+g^2-2gcos\psi)^{3/2}}, \tag{30}$$

where g is a user-defined parameter that adjusts the relative amount of forward and backward scattering. The Fournier-Forand phase function $\tilde{\beta}_{FF}(\psi)$ is defined by [48]:

$$\begin{aligned}\tilde{\beta}_{FF}(\psi) = C\pi\left(\frac{2\pi(n-1)}{\lambda}\right)^{\mu-3}\frac{1+cos^2\psi}{8sin(-\pi\nu)}\left[\frac{1}{(1-\delta^2)\delta^\nu}\right]\times \\ \left([\nu(1-\delta)-(1-\delta^\nu)]+\frac{4}{u^2}\left[(1-\delta^{\nu+1})-(\nu+1)(1-\delta)\right]\right),\end{aligned} \tag{31}$$

where C is a constant, μ is a user-defined parameter, n is the refractive index, and ν, δ and u are described by:

$$\nu = \frac{3-\mu}{2}, \tag{32}$$

$$\delta = \frac{u^2}{3(n-1)^2} \tag{33}$$

and

$$u = 2sin\left(\frac{\psi}{2}\right). \tag{34}$$

Finally, the Kopelevich Large and Small Particle scattering phase functions can be expressed as regressions of the following form [36, 49]:

$$\tilde{\beta}_l(\psi) = 5.61746exp\left[\sum_{n=1}^{5} l_n\psi^{\frac{3n}{4}}\right] \tag{35}$$

and

$$\tilde{\beta}_s(\psi) = 188.381exp\left[\sum_{n=1}^{5} s_n\psi^{\frac{3n}{4}}\right], \tag{36}$$

where $\tilde{\beta}_l(\psi)$ and $\tilde{\beta}_s(\psi)$ are the phase functions of the large and small particles, and l_n and s_n are their corresponding coefficients. The values for these coefficients can be found elsewhere [36].

Some of the above models of the phase function possess user-defined parameters. These parameters must be defined before the calculation of the phase function can proceed. As a consequence, once the phase function model is chosen the user is prompted to enter the appropriate input variables before the calculation proceeds. Following this, the phase function data is written to the CAMEO-SIM ocean component input file.

2.6.1.5 Examples

Figure 13 demonstrates imagery of oceans generated by CAMEO-SIM using HYDROLIGHT water models. This imagery was generated in the Cairns location in January (Section 3) and a viewing angle of 5°.

(i) HYDROLIGHT ABCASE1 Case 1 Water. (ii) HYDROLIGHT ABCASE1H Haltrin Water.

Figure 13: *Samples of oceans generated by CAMEO-SIM*

2.6.2 Converting CAMOGEN DP to CAMEO-SIM

It is not always necessary, or straightforward, to create an automated process for converting and transferring data from one code in the VST to another code. In this particular case, a procedure was devised and documented to achieve the desired result of converting a disruptive pattern (DP) from CAMOGEN into a texture in CAMEO-SIM. DPs generated in CAMOGEN can be used on objects in synthetic scene generation in CAMEO-SIM. This allows the CAMOGEN-created DP to be assessed in the complex scenarios which can be generated in CAMEO-SIM. However, the DP from CAMOGEN needs to be processed in a particular way to create a suitable texture for use in CAMEO-SIM.

1. **Generating output from CAMOGEN:** Various types of output can be generated from CAMOGEN (Section 2.3.3). The DP created in CAMOGEN is saved as a bitmap (bmp file) image. The same DP should also be saved using the separation files option. The separation bitmap images show where each colour is present in the DP and a file with spectral reflectance data for each colour is also produced. The bitmap image of the overall DP needs to be converted to a portable network graphics (png) format using a conversion program.
2. **Create materials for each colour:** Using the CAMEO-SIM materials editor, a material needs to be created for each colour in the DP. The reflectance data output

from CAMOGEN is used as input reflectance data in the CAMEO-SIM materials editor.

3. **Create a classified texture:** From the CAMEO-SIM main window, create a classified texture from the texture tools section. Choose file-open from the editor and select the PNG file containing the image of the DP. Save the texture using an appropriate name.

4. **Assign materials to texture pixels:** With the new texture opened in the classified texture editor, select window-image window to show the DP image. Select a pixel on this image (the colour selected will be shown on the bottom right of the classified texture editor window). Using surface-add material, select the material created above that corresponds to this pixel (the separation bitmap images can assist with identifying the correct material). Repeat this process until all colours are assigned a material.

The classified texture can be saved and applied to objects in CAMEO-SIM projects.

3 Applications

The VST can be applied to many situations to provide insight into the visible signature of naval platforms and help to determine strategies for improving the visible signature. Some limited work has been conducted to both assess the outcomes from the VST and provide examples of what type of work is possible with the VST. This work is presented in this section.

A Cairns location in January is used in some of the examples. This location was chosen as 16°40'48" S, 146°48' E on the 15th Janaury 2008. The MODTRAN parameters for the CAMEO-SIM spectral atmosphere are shown in Table 22. Atmospheric CO_2 was set at 381 ppm. The CAMEO-SIM thermal atmosphere was set at 10 hrs ahead of GMT with OCEAN.water_vis as the ground material.

Table 22: *Cairns location in January MODTRAN inputs for CAMEO-SIM Spectral Atmosphere.*

Season	Summer
Model	Tropical
Surface material	OCEAN.water_vis
Cloud type and rain rate	No cloud or rain
Haze type	Navy maritime
Air Mass Characteristic	7
Visibility	Default for haze model (i.e. set to 0)
Wind speed	0
Volcanic extinction model and distribution	Background/Moderate
Scattering type	Mie with Isaac multiple scattering

3.1 Submarines

ORACLE and CAMEO-SIM can be used to assess the visible signatures of submarines. That is, ORACLE can report the POD and CAMEO-SIM can produce synthetic imagery of a given scenario. In this section a number of examples will be presented.

Figures 14 and 15 show a sample of the ORACLE input spectra generated using the HYDROLIGHT ABCASE1 and ABCASE1H water models respectively. These spectra were generated by varying the depth and type of bottom surface. The background spectra were defined to have an infinite depth whose reflectance was homogeneous below the maximum depth of 30 m. The target spectra were defined to have a finite depth with a reflectance of $R = 4\%$ at the maximum depth. The full details of the HYDROLIGHT input parameters are summarised in Tables 23 and 24. The two solar zenith angles were chosen to approximate midday and either the early morning or late afternoon sun. The wind speed is the method employed by HYDROLIGHT to include capillary waves on the surface. A wind speed of 10 m/s corresponds to sea state 4. The figures clearly show that the sun position has a significant effect on the radiance distribution just above the sea surface. This demonstrates that the environmental conditions have a large bearing on visible signatures.

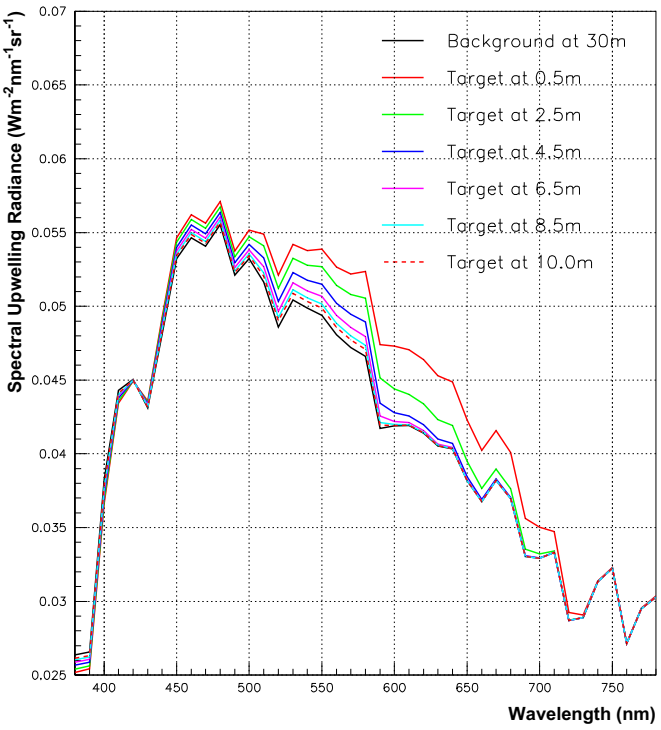

(i) Solar zenith angle of 0°.

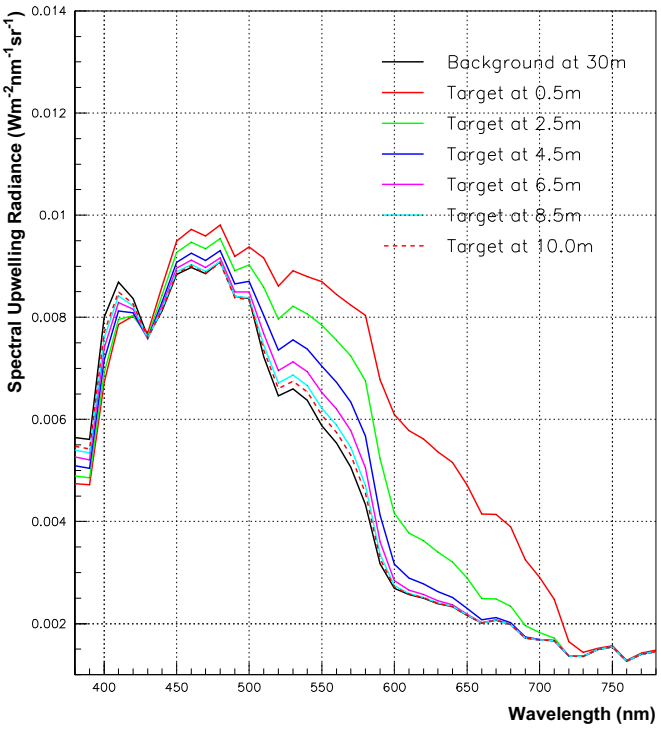

(ii) Solar zenith angle of 45°.

Figure 14: *The spectral upwelling radiance for the ABCASE1 water model at various depths.*

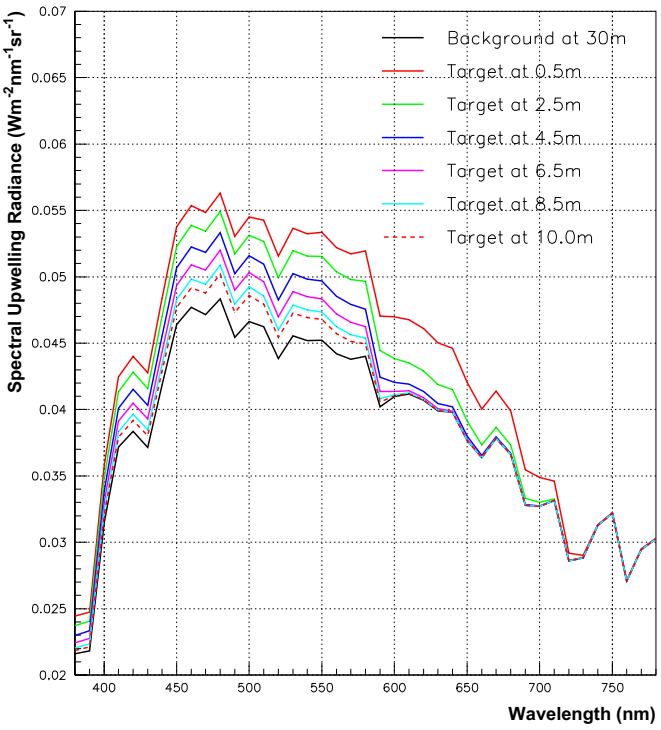

(i) Solar zenith of 0°.

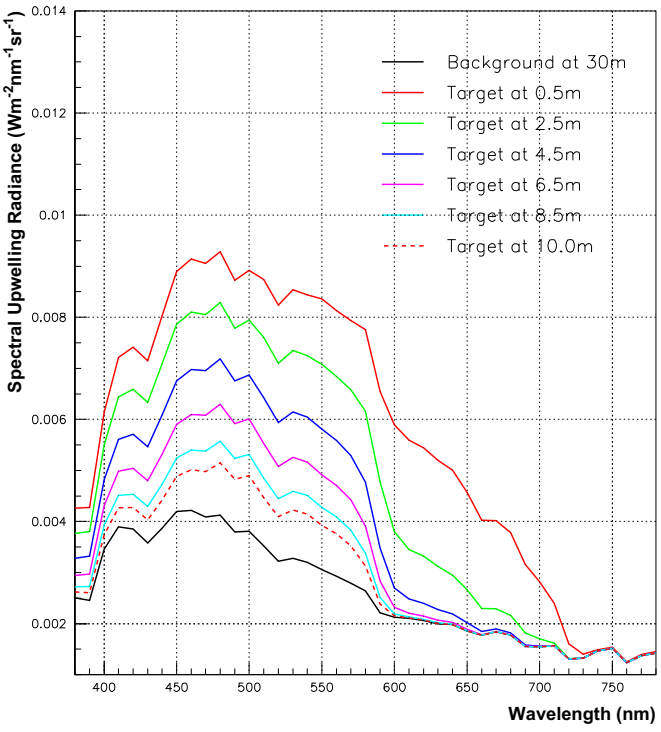

(ii) Solar zenith angle of 45°.

Figure 15: *The spectral upwelling radiance for the ABCASE1H water model for various depths.*

Table 23: *Ocean parameters for the HYDROLIGHT ABCASE1 Water Model.*

Water Component	**Absorption coefficient**	Pope & Fry [19]
	Scattering coefficient	Smith & Baker [20]
Chlorophyll Component	**Concentration profile**	HYDROLIGHT sample profile
	Absorption coefficient	Prieur-Sathyendranath-Morel [34]
	Scattering coefficient	Gordon & Morel [35, 37]
	Scattering phase function	Petzold average particle [21]
CDOM Component	**Concentration profile**	Same as Chlorophyll Concentration Profile
	Absorption coefficient	Prieur-Saythendranath-Morel [34, 42]
	Scattering coefficient	Assumed non scattering
Sun Position	**Solar Zenith Angle**	0° and 45°
Sky Model	**Semi-Empirical RADTRAN**	Gregg & Carder [12]
Sky Conditions	**Semi-Empirical normalised radiance pattern**	Harrision & Coombes [13]
Bottom Reflectance	**Background**	Infinitely deep at 30.0 m
	Targets	Finite Depth $R = 4.0\%$
Water Depth		$0.5 - 10.0$ m
Wind Speed		10 m/s
Cloud Cover		None

Table 24: *Ocean parameters for the HYDROLIGHT ABCASE1H Water Model.*

Water Component	**Absorption coefficient**	Pope & Fry [19]
	Scattering coefficient	Smith & Baker [20]
Chlorophyll Component	**Concentration profile**	HYDROLIGHT sample profile
	Absorption coefficient	Haltrin [36]
	Scattering coefficient	Haltrin [36]
	Scattering phase function	Kopelevich large particle [36, 49]
CDOM Fulvic Component	**Concentration profile**	Haltrin
	Absorption coefficient	Haltrin [36]
	Scattering coefficient	Assumed non scattering
CDOM Humic Component	**Concentration profile**	Haltrin [36]
	Absorption coefficient	Haltrin [36]
	Scattering coefficient	Assumed non scattering
Mineral Component	**Concentration profile**	Haltrin [36]
	Absorption coefficient	Assumed non absorbing
	Scattering coefficient	Haltrin [36]
	Scattering phase function	Kopelevich small particle [36, 49]
Sun Position	**Solar Zenith Angle**	0° and 45°
Sky Model	**Semi-Empirical RADTRAN**	Gregg & Carder [12]
Sky Conditions	**Semi-Empirical normalised radiance pattern**	Harrision & Coombes [13]
Bottom Reflectance	**Background**	Infinitely deep at 30.0 m
	Targets	Finite Depth $R = 4.0\%$
Water Depth		$0.5 - 10.0$ m
Wind Speed		10 m/s
Cloud Cover		None

From Figures 14 and 15 it can also be seen that the ABCASE1 and ABCASE1H water models exhibit distinctly different radiance distributions just above the sea surface. This is to be expected since the two water models not only contain different components, but also vary in their concentration profiles. In particular the ABCASE1H includes CDOM and mineral components, which are not present in the ABCASE1 water model. As a result there are differences in the absorption and scattering within the water body across the visible spectrum. Thus the magnitude of the radiance as a function of wavelength is quite different.

Figures 16 and 17 represent the corresponding PODs calculated by ORACLE using the HYDROLIGHT data shown in Figures 14 and 15. These plots are the culmination of 200 data runs in which the range and depth were varied. The full details of the ORACLE input parameters can be found in Table 25. The plots show an expected drop in the POD with increasing range. However, the relationship between the depth and the calculated POD is counter-intuitive. It would be expected that the POD should decrease with increasing depth. This, though, is not the case. When the solar zenith angle is 0° the POD remains relatively constant across the depth range and when the solar zenith angle is 45° the distribution first decreases and then increases as a function of depth for the ABCASE1 water model; and for the ABCASE1H water model it first increases then decreases. This situation is illustrated in the line plots given in Figure 18 for a range of 2.5 km.

Table 25: *Input Parameters for the ORACLE probability of detection analysis.*

Target Height (m)	3.59
Target Width (m)	38.9
Range (m)	500 - 5000
Crossing Velocity (m/s)	0.0
Closing Velocity (m/s)	0.00
Fractional Perimeter	1.00
Intrinsic Target Contrast	-0.100
Surrounding Luminance (cd/m^2)	10000.00
Meteorological Visibility (km)	15.0
Sky-to-Ground Luminance Ratio	4.0
Number of Glimpses	10
FOV Type	Circular
FOV Diameter (°)	20.0
Veiling Glare	0.00
Magnification	1.0
MTF Frequency Increments	0.05
Number of MTF Values	41
Background Spectra	HYDROLIGHT generated data file Infinitely deep water, homogeneous below 30 m
Target Spectra	HYDROLIGHT generated data files Finite depths from $0.5 - 10.0$ m $R = 4.0\%$
Airlight Spectrum	ORACLE example spectrum
Transmission Spectrum	ORACLE example spectrum

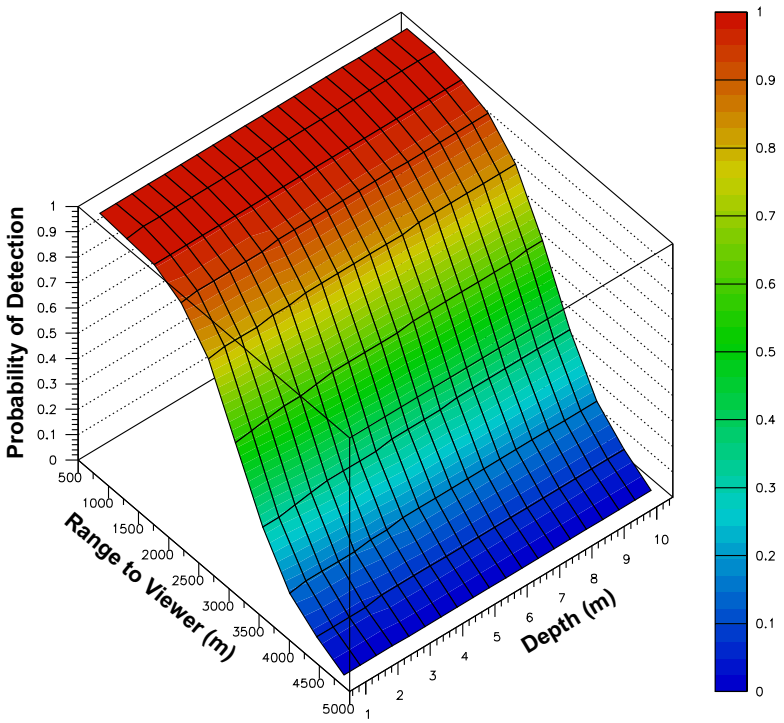

(i) Solar zenith of 0°.

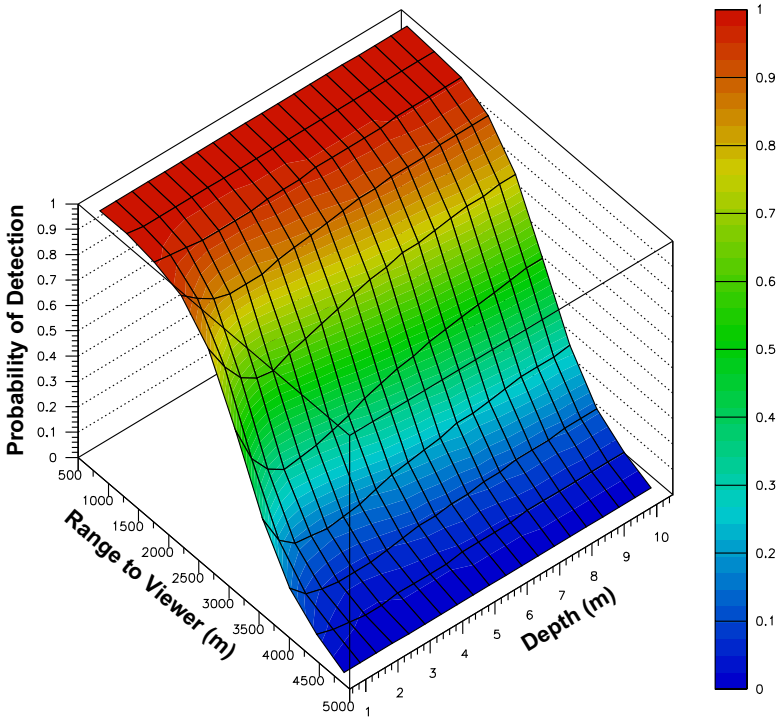

(ii) Solar zenith of 45°.

Figure 16: *The POD as a function of depth and range using the Foveal algorithm for the ABCASE1 water model and a retinal eccentricity of* 0°.

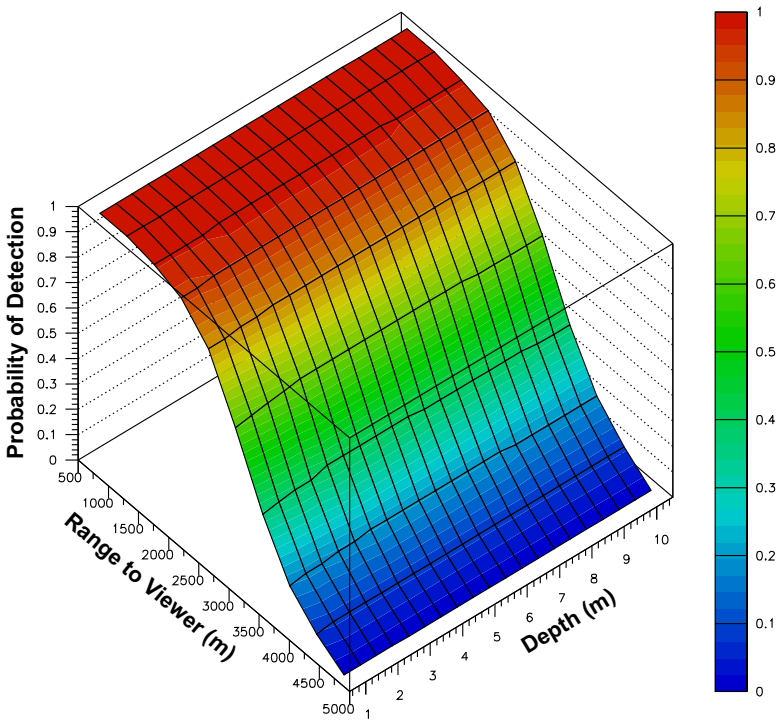

(i) Solar zenith of 0°.

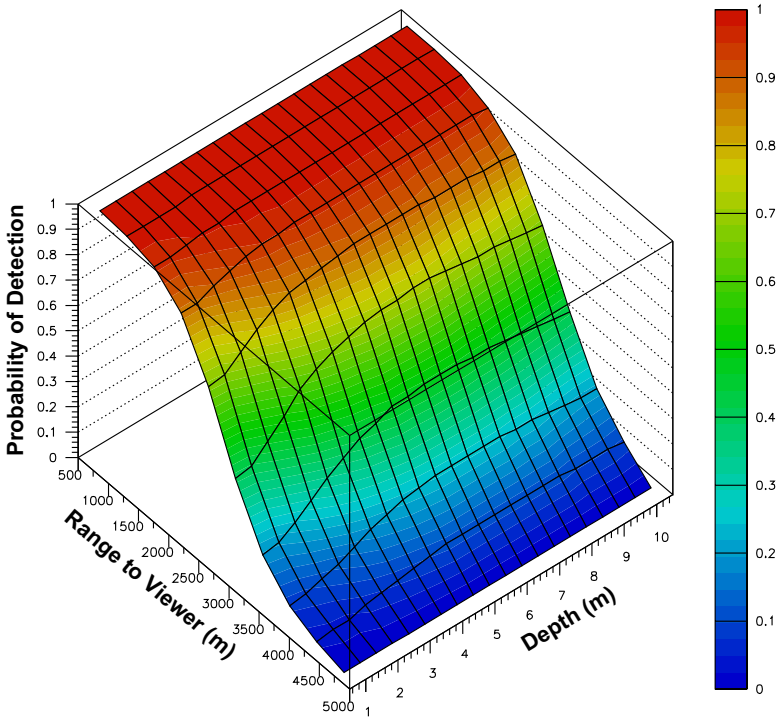

(ii) Solar zenith of 45°.

Figure 17: *The POD as a function of depth and range using the Foveal algorithm for the ABCASE1H water model and a retinal eccentricity of* 0°.

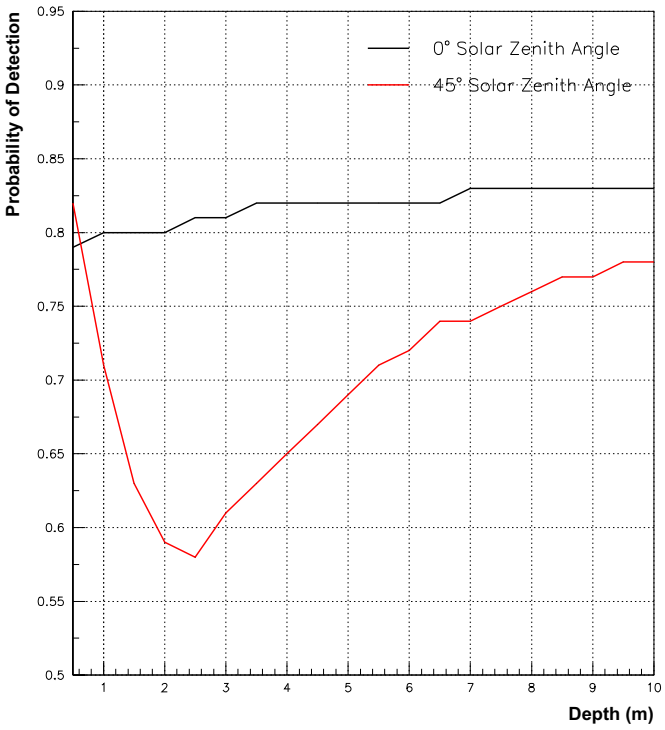

(i) The ABCASE1 water model.

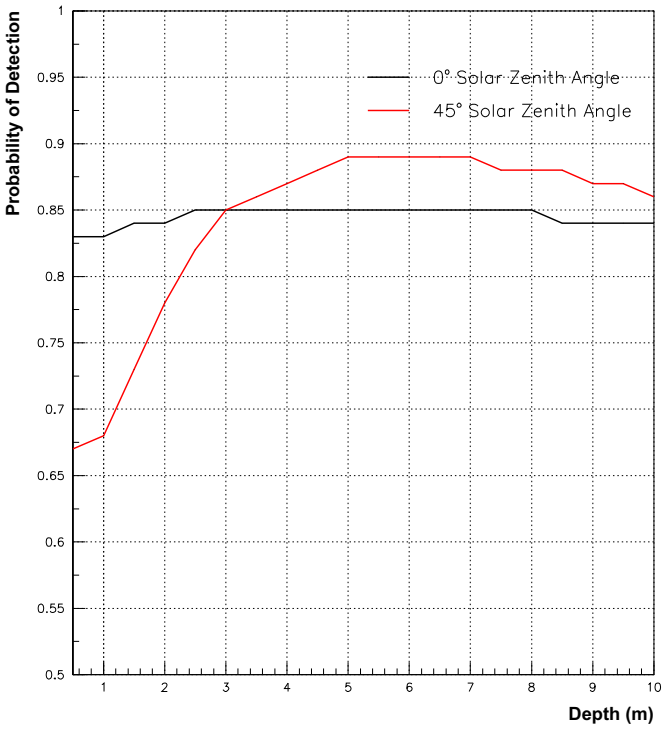

(ii) The ABCASE1H water model.

Figure 18: *The POD as a function of depth for glimpse 1 using the Foveal algorithm, a range of* 2.5 *km and a retinal eccentricity of* 0°.

The POD distributions as a function of depth for the solar zenith angle of 0° can be explained by referring to the HYDROLIGHT spectral radiance data shown in Figures 14(i) and 15(i). These show that as the depth decreases the radiance as a function of wavelength not only drops in magnitude, but also starts exhibiting similar shapes to that of the background. Since the fractional perimeter was set to 1.00 the visual task that ORACLE is performing is one of pure energy detection. As a result any difference between the target and the background spectra across the spectrum will lead to reasonably large PODs being calculated. However, it would still be expected for the POD to decrease somewhat with decreasing depth, as was the case in the example ORACLE data using the ABCASE1 water model presented in Figure 8 in Section 2.2.4. These two sets of data vary in both the HYDROLIGHT and ORACLE input parameters. The differences are summarised in Table 26.

Table 26: *Differences between the two ABCASE1 Data Sets.*

Parameter	**ABCASE1 Data Set 1**	**ABCASE1 Data Set 2**
Chlorophyll Fluorescence	Yes	No
Raman Scattering	Yes	No
Sun Position	Location: 37° 52′ S 145° 08′ E Date: 12th July 2006 Time: 2 : 00 *am* GMT	Solar Zenith Angles: 0° 45°
Wind Speed (m/s)	0	10
Airlight Spectrum	No	Yes
Transmission Spectrum	No	Yes

Shown in Figure 19 is the POD analysis for the ABCASE1 water model using the location of 37° 52′ S 145° 08′ E at 2 : 00 *am* GMT on the 12th July 2006 for the sun position. The addition of the sample airlight spectrum causes a small decrease in the POD at 7.0 m depth. The addition of the example transmission spectrum has the greatest effect on the POD distribution with respect to depth. It results in a decrease in the POD in the range $0.5 - 3.0$ m, a steady increase between 3.0 m and 6.5 m, a sharp increase from 6.5 m to 7.0 m, a sharp decrease from 7.0 m to 7.5 m and a steady increase from 7.5 m to 10.0 m.

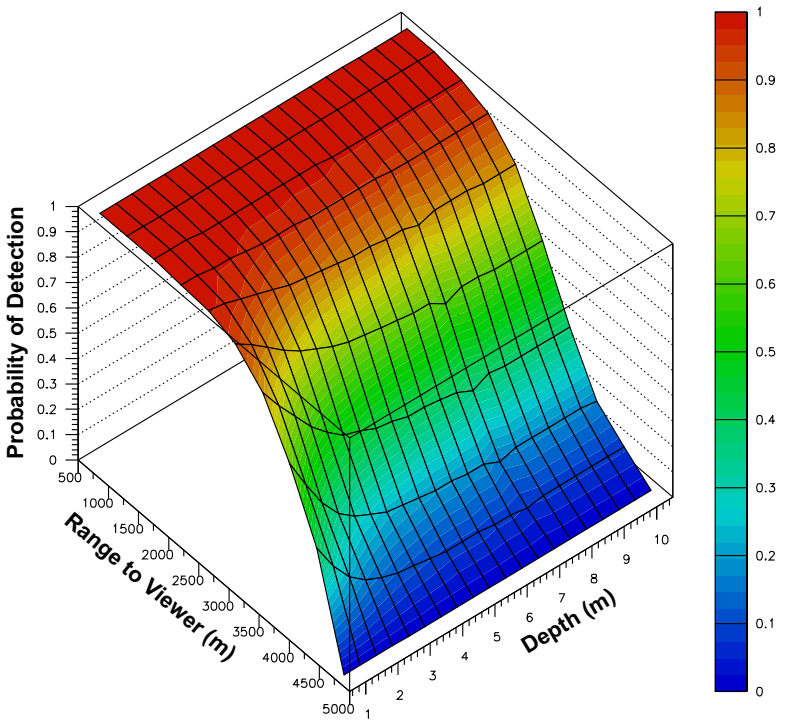

(i) ORACLE example airlight spectrum included.

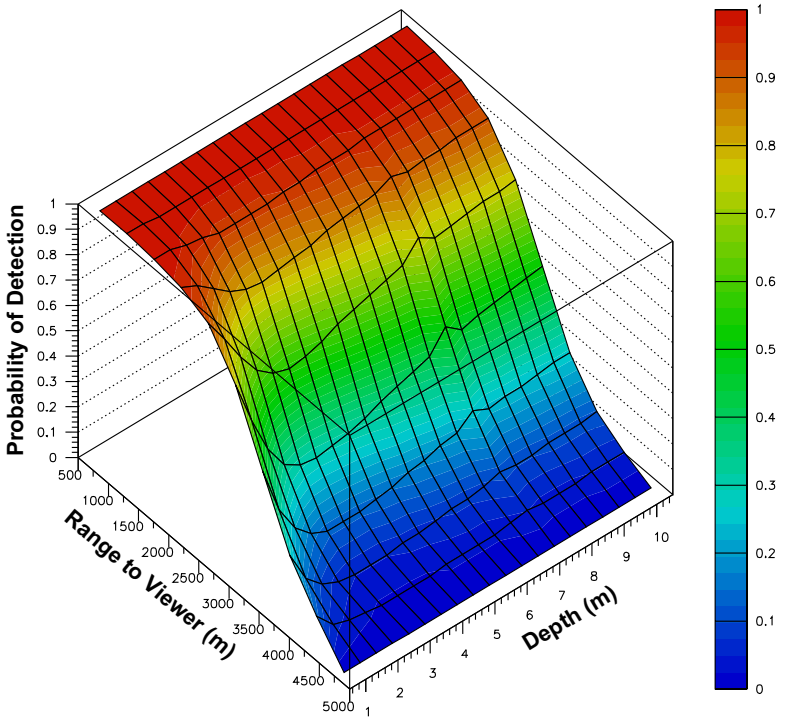

(ii) ORACLE example transmission spectrum included.

Figure 19: *The POD as a function of depth and range for the ABCASE1 water model on the 12th July 2006 at* $2:00$ *am GMT and a location of* $37^\circ\ 52'\ S\ 145^\circ\ 08'\ E$

The example airlight spectrum employed is shown in Figure 20(i). The airlight spectrum, in combination with the meteorological visibility, R_v, is responsible for the atmospheric attenuation. In ORACLE this is accomplished by calculating the reduction in contrast. This is found by determining the apparent contrast, C_R, using:

$$C_R = C_0 \left(\frac{B_0}{B_R} \right) exp\left[-\sigma_e R \right], \tag{37}$$

where C_0 is the intrinsic contrast of the target against its immediate background, σ_e is the atmospheric extinction coefficient, R is the distance between the observer and the target, B_0 is the intrinsic luminance of the background and B_R is the apparent luminance of the background. The ratio $\left(\frac{B_0}{B_R}\right)$ is the "so-called" sky-to-ground luminance or brightness ratio, and σ_e is defined in terms of the R_v using the following the relation:

$$\sigma_e = \frac{3.91}{R_v}. \tag{38}$$

The atmospheric attenuation is achieved in a two step process. First, the meteorological visibility is used to attenuate the inherent contrast of the target. Secondly, the amount of airlight required to achieve this attenuated contrast is added to the target and background spectra. That is, a weighting factor is determined for the contrast reduction and it is then applied to the airlight spectrum. This added airlight, depending on the value, will change the hue of the target and background. Therefore the sharp increase in the calculated POD at 7.0 m can be explained by a change in hue of both the target and the background. This change in hue results in the target standing out from the background more so following the hue changes in the 6.5 m and 7.5 m cases.

The transmission or filter spectrum used in the ORACLE POD analysis is shown in Figure 20(ii). This is applied after the contrast attenuation by the atmosphere is performed. The spectrum is assumed to be located at the observer and selectively reduces the target and background spectra. Whether this spectrum reduces the final calculated POD depends on whether it significantly reduces the ambient light level. This spectrum can also change the hue of the background and target spectra, depending on the amount of transmission across the visible spectrum. In Figure 20(ii) there is a small amount of transmission at the blue end, full transmission from green through to yellow and a sharp decrease at the red end of the spectrum. Hence the spectrum selectively filters out the blue and most of the red wavelengths. Since the background is most likely a blue colour it will have a greater effect on the background than on the target, depending on the hue of the target. This may explain the POD distribution shown in Figure 19(ii). The target, after the filter spectrum is applied, approaches the hue of the background between the depths of 0.5 m and 2.5 m, whereas for depths greater than 2.5 m the hue of the target diverges from that of the background. If this explanation is correct then generating images of the colour from the altered HYDROLIGHT radiance spectra should show that the colour of the target and background is similar in the region 0.5 m to 2.5 m. Another cross-check is to use CAMEO-SIM imagery. This method will not be as accurate as the above approach due to the atmospheric attenuation and transmission being modelled by MODTRAN in CAMEO-SIM instead of using the spectra utilised in the ORACLE POD analysis. However, it will yield an indication of the hue of the target and background.

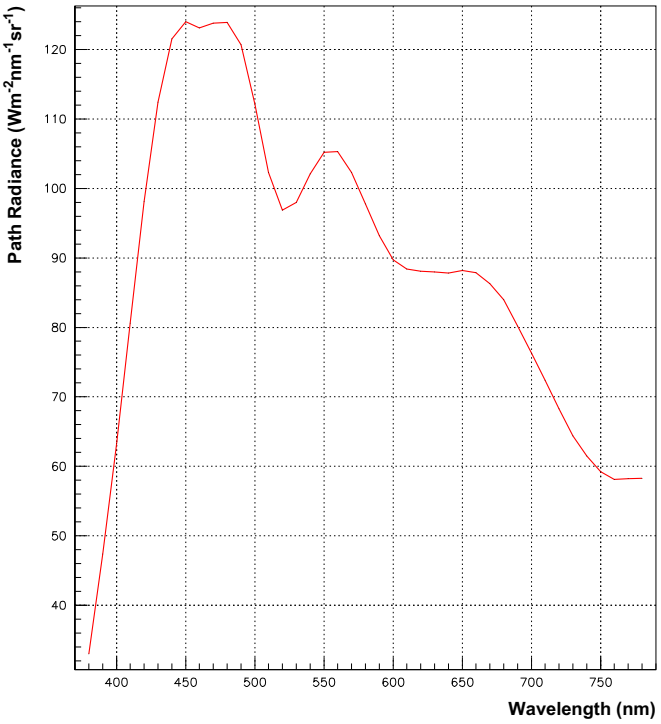

(i) Airlight.

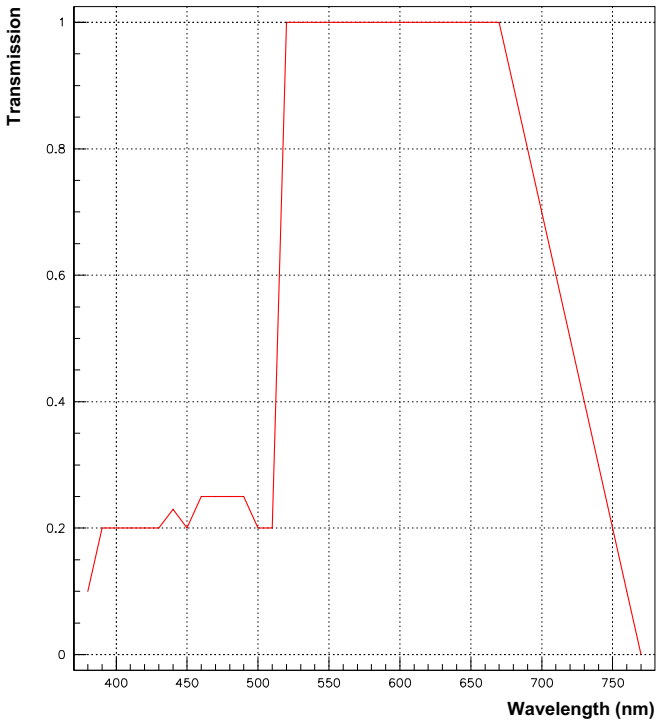

(ii) Transmission.

Figure 20: *The ORACLE example spectra.*

The variation of the POD as a function of depth for the ABCASE1H water model and a 45° solar zenith angle (Figure 17(ii)) is different to the ABCASE1 water model. For the ABCASE1H water model there is an increase from 0.5 m to approximately 6.5 m and then a slow decrease until 10.0 m, whereas in the ABCASE1 there is a decrease from 0.5 m to 2.5 m and a slow increase from 2.5 m to 10.0 m. The differences between the POD distributions of the two models can be explained by the differences in the constituents and therefore the absorption and scattering within the body. The variations between the two solar zenith angles is a consequence of the ambient light incident on the water surface. When the solar zenith is 45° the angle of incidence the sun makes with the water surface is significantly different to the 0° case. This change leads to differences in the amount of reflection and refraction at the air-water interface, which in turn changes the amount of spectral upwelling radiance that escapes the air-water interface. As a result the colour appearance of the water body changes, leading to different distributions in the ORACLE POD analysis.

The CAMEO-SIM imagery corresponding to the ORACLE POD analysis at 0.5 km are shown in Figures 21- 24. These images are of a black cuboid of dimensions $38.5 \times 3.6 \times 3.6$ m^3, a reflectance of 4% in the Cairns location given in Table 22 and the sea state 0 ocean as summarised in Table 27. This sea state was chosen as ORACLE at present does not model the noise introduced into a scene by the sea surface. Figure 21 demonstrates that the target is observable at all the sample depths, confirming the POD calculations of ORACLE (Figures 16 and 17). However, in Figures 22- 24 the generated images do not correspond to the calculated POD from ORACLE (Figures 16 and 17). The target is not observable at all depths. The discrepancy may be a result of ORACLE knowing *a priori* that the target exists in the scene, the type of visual task requested (pure energy detection) or a combination of both. As a consequence, although the human eye cannot see the target in the image if there is any difference in the contrast between the target and the background, ORACLE will report a large POD. If this second phenomenon is the major cause of the discrepancy then running edge detection software over the CAMEO-SIM generated images would be a useful cross-check. If there are edges in the imagery that the human eye cannot detect then edge detection software should find them. Another effect that may cause the discrepancy is the transmission and airlight spectra employed by ORACLE. At present these are example spectra included with the software distribution. However, CAMEO-SIM uses MODTRAN for modelling the atmosphere. Therefore for the two sets of data to be as consistent as possible it would be useful to use MODTRAN to generate the transmission and airlight spectra in ORACLE.

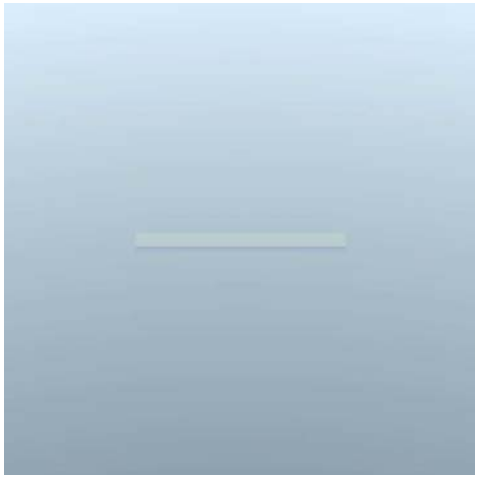

(i) 0.5 m below the surface.

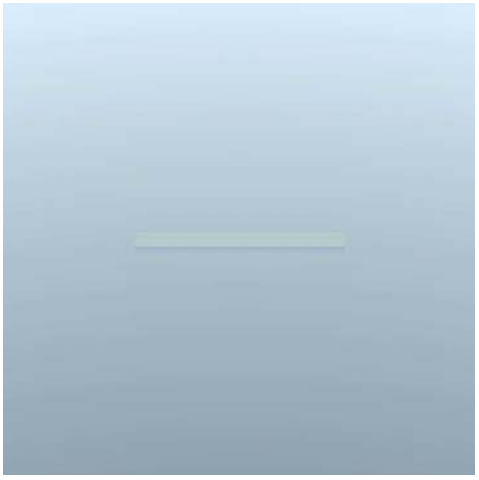

(ii) 2.0 m below the surface.

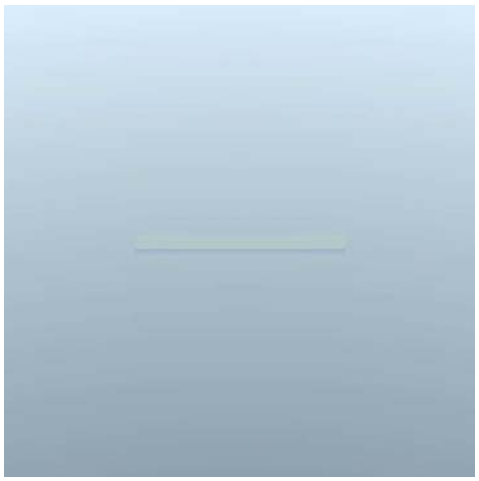

(iii) 4.0 m below the surface.

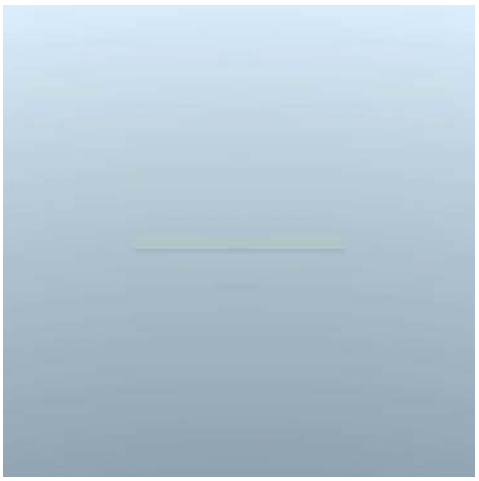

(iv) 5.5 m below the surface.

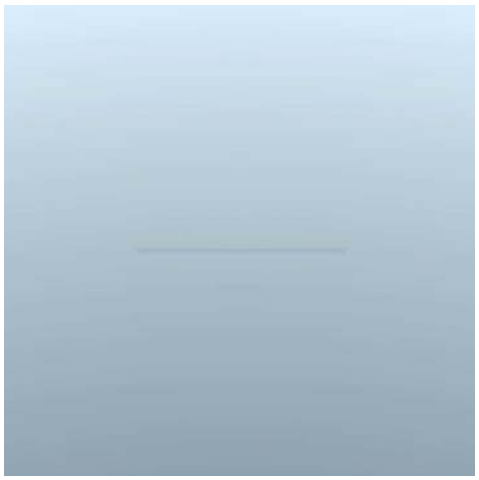

(v) 7.0 m below the surface.

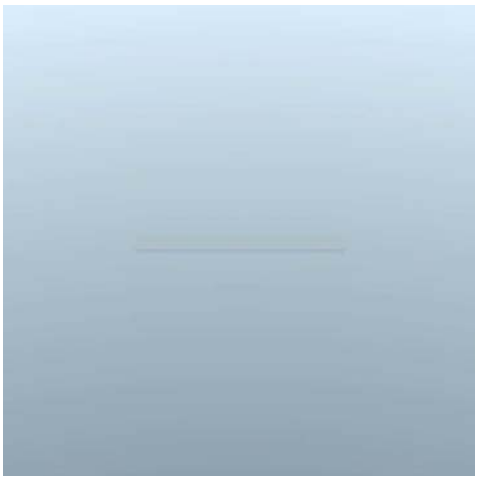

(vi) 9.0 m below the surface.

Figure 21: *A black cuboid in ABCASE1 water at a solar zenith of* 0°*, range of* 0.5 *km and an elevation of* 45°*.*

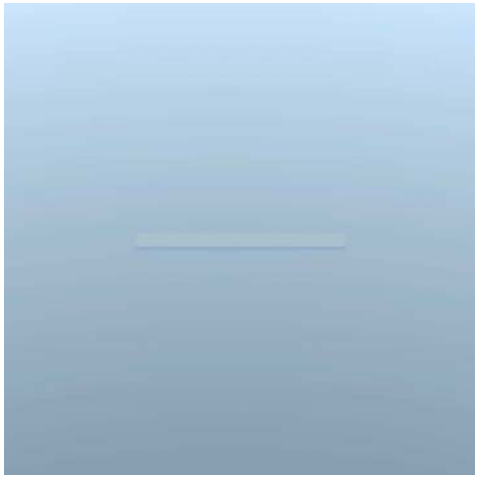

(i) 0.5 m below the surface.

(ii) 2.0 m below the surface.

(iii) 4.0 m below the surface.

(iv) 5.5 m below the surface.

(v) 7.0 m below the surface.

(vi) 9.0 m below the surface.

Figure 22: *A black cuboid in ABCASE1 water at a solar zenith of* 45°*, range of* 0.5 *km and an elevation of* 45°*.*

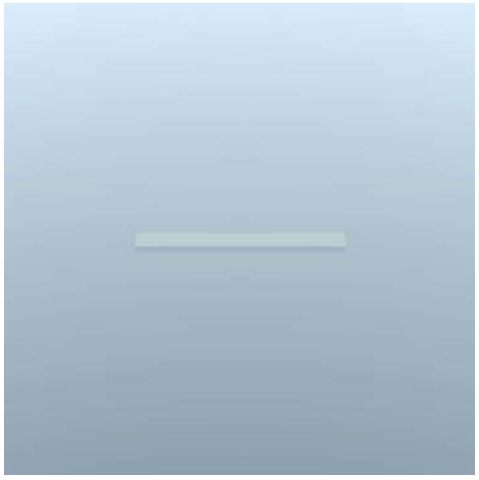

(i) 0.5 m below the surface.

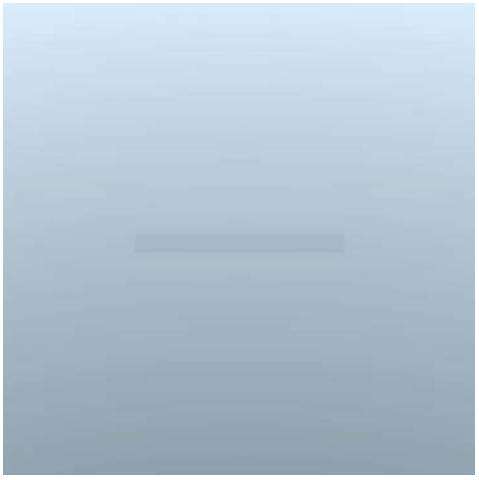

(ii) 2.0 m below the surface.

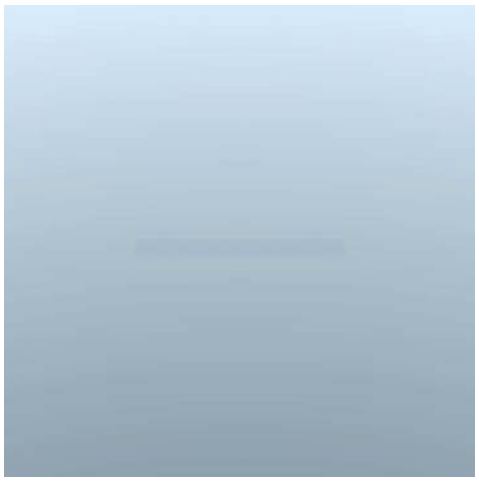

(iii) 4.0 m below the surface.

(iv) 5.5 m below the surface.

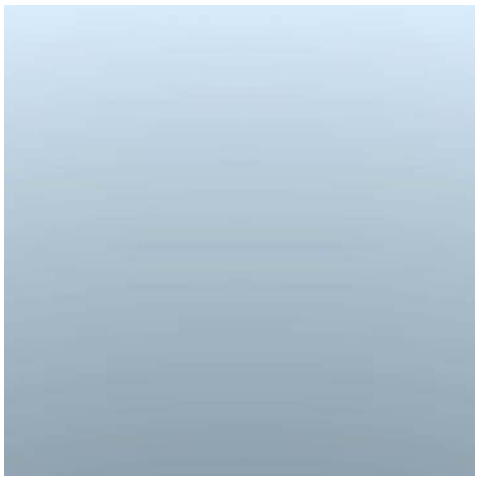

(v) 7.0 m below the surface.

(vi) 9.0 m below the surface.

Figure 23: *A black cuboid in ABCASE1H water at a solar zenith of* 0°*, range of* 0.5 *km and an elevation of* 45°*.*

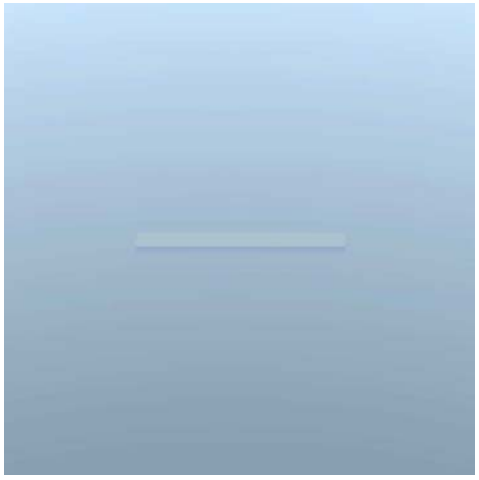

(i) 0.5 m below the surface.

(ii) 2.0 m below the surface.

(iii) 4.0 m below the surface.

(iv) 5.5 m below the surface.

(v) 7.0 m below the surface.

(vi) 9.0 m below the surface.

Figure 24: *A black cuboid in ABCASE1H water at a solar zenith of* 45°*, range of* 0.5 *km and an elevation of* 45°*.*

Table 27: *Ocean parameters employed in CAMEO-SIM for the ORACLE POD cross-check.*

Shape	Sea State 0 calculated power spectrum
Depth	1000 m
Tiling	Smooth and curved Earth
Tile size	500 m
Cells per tile	520
Repeat factor	100 in all directions
Materials	
Water	OCEAN.water_vis
Whitecaps	OCEAN.foam_ir
Ocean floor	SOIL.sea_water
Surface temperature	300 K
Surface roughness	0.01
Whitecaps	Off

Shown in Figure 25 is the CAMEO-SIM imagery of a black cuboid in ABCASE1 water at a range of 2.5 km and a solar zenith of 0°. These images are representative of the water models and solar zenith angles investigated and illustrate that it is much more difficult to isolate the target from the background than was the case at a range of 0.5 km. The target is not observable from a depth of 5.5 m[1]. This is contrary to the analogous ORACLE results of Figure 16, where the POD is approximately 0.8 across the depth range. Clearly ORACLE is over-estimating the POD. Again this could be a result of the pure energy detection task selected, in combination with ORACLE *a priori* knowing that a target exists. However, it may also be that ORACLE possesses a fundamental limitation as a result of the assumptions used to model human visual performance. In fact the Search algorithm has been investigated using land scenarios, and it has been reported that in ORACLE the predicted mean search time can be under-estimated by as much as 233% from the actual mean search time for an individual scene [50]. Since mean search time, τ, is defined by [50]:

$$\tau = \frac{t_g}{P_g}, \tag{39}$$

where t_g is the mean fixation time, and the POD is calculated using Equation 8 (Section 2.2.1), the POD is over-estimated. It has also been suggested by BAE SYSTEMS that the Search algorithm may not yield accurate results [51]. This is to be expected as human visual search is complex and difficult to model accurately. It is also why throughout this report the Foveal algorithm has been employed for the POD analysis, rather than the Search algorithm. If, however, the Foveal algorithm also over-estimates the POD, ORACLE can only be used to determine the visible signature for the worst case scenario.

[1]The target may not be observable at depths less than 5.5 m depending on the print quality. However, it is clearly observable on the screen in CAMEO-SIM.

More analysis is therefore required to validate ORACLE for use in the evaluation of submarine visible signatures.

Figures 26 and 27 show CAMEO-SIM generated imagery for a sea state 4 ocean (Table 28). These demonstrate that the addition of a realistic water surface decreases the visibility of the black cuboid at depth. It is evident to accurately model visible signatures of submarines using ORACLE a method of including the sea state is required. This could be achieved by modelling the capillary waves on the sea surface in the same manner as HYDROLIGHT. In other words, using a gaussian to model the wave slope [11]. The distribution could then be converted to a function that describes the optical system response following the introduction of the noise created by the water surface. This in turn could be entered into ORACLE through the MTF data file.

Table 28: *Moderate wave ocean parameters for CAMEO-SIM.*

Shape	Sea State 4 calculated power spectrum
Depth	1000 m
Tiling	Smooth and curved Earth
Tile size	360 m
Cells per tile	1024
Repeat factor	104 in all directions
Materials	
Water	OCEAN.water_vis
Whitecaps	OCEAN.foam_ir
Ocean floor	SOIL.sea_water
Surface temperature	300 K
Surface roughness	0.181
Whitecaps	Off
Interior (Section 3.1)	ABCASE1 water model parameters ABCASE1H water model parameters

(i) 0.5 m below the surface.

(ii) 2.0 m below the surface.

(iii) 4.0 m below the surface.

(iv) 5.5 m below the surface.

(v) 7.0 m below the surface.

(vi) 9.0 m below the surface.

Figure 25: *A black cuboid in ABCASE1 water at a solar zenith of* 0°*, range of* 2.5 *km and an elevation of* 45°*.*

(i) 0.5m below the surface.

(ii) 2.0m below the surface.

(iii) 4.0m below the surface.

(iv) 5.5m below the surface.

(v) 7.0m below the surface.

(vi) 9.0m below the surface.

Figure 26: *A black cuboid in ABCASE1H water at a solar zenith of* 0°*, a range of* 0.5 *km and downward viewing.*

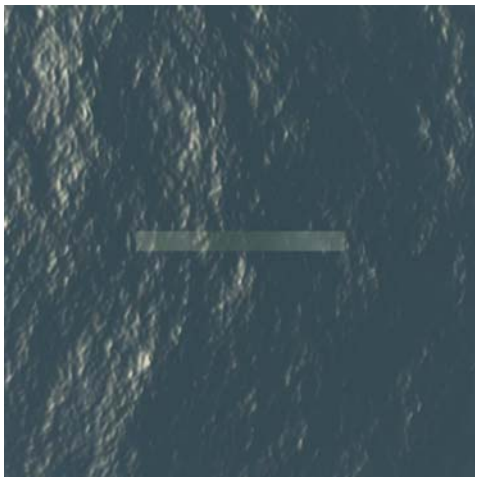

(i) 1.0m below the surface.

(ii) 2.0m below the surface.

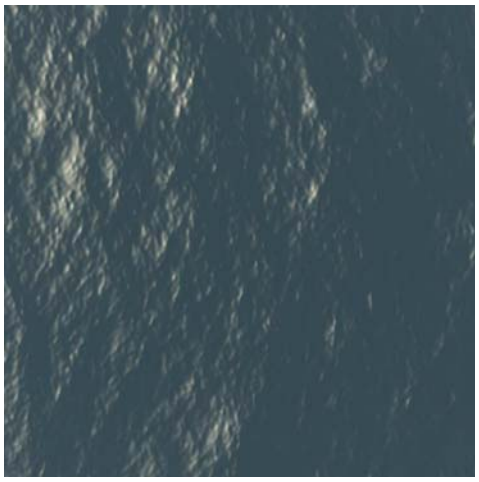

(iii) 4.0m below the surface.

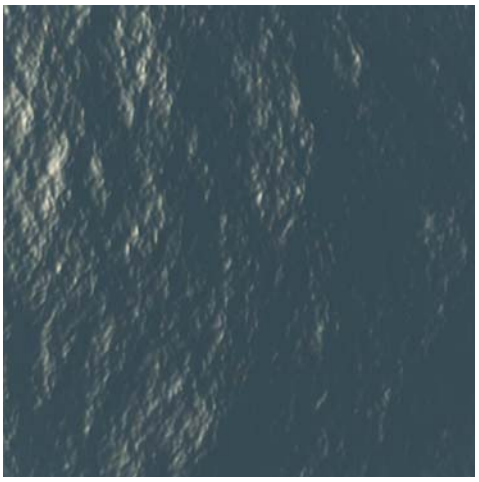

(iv) 5.5m below the surface.

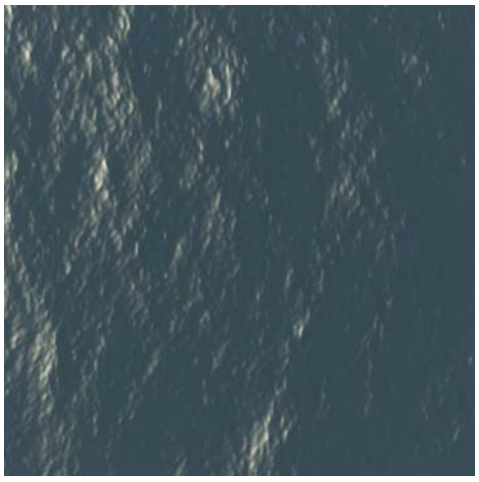

(v) 7.0m below the surface.

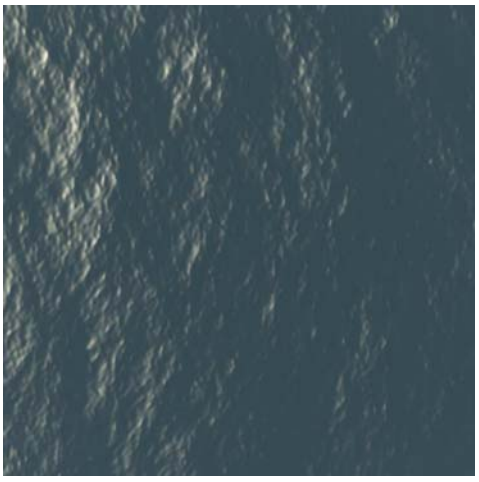

(vi) 9.0m below the surface.

Figure 27: *A black cuboid in ABCASE1H water at a solar zenith angle of* 45° *and downward viewing.*

Synthetic images of a generic submarine generated by CAMEO-SIM in the Cairns location in January and sea state 4 ocean (Table 28) are shown in Figure 28. In this example the depth refers to depth from the keel. The colour of the paint on the model was created by defining a 4% reflectivity across the spectral range. These images clearly illsutrate the change in visible signature with depth.

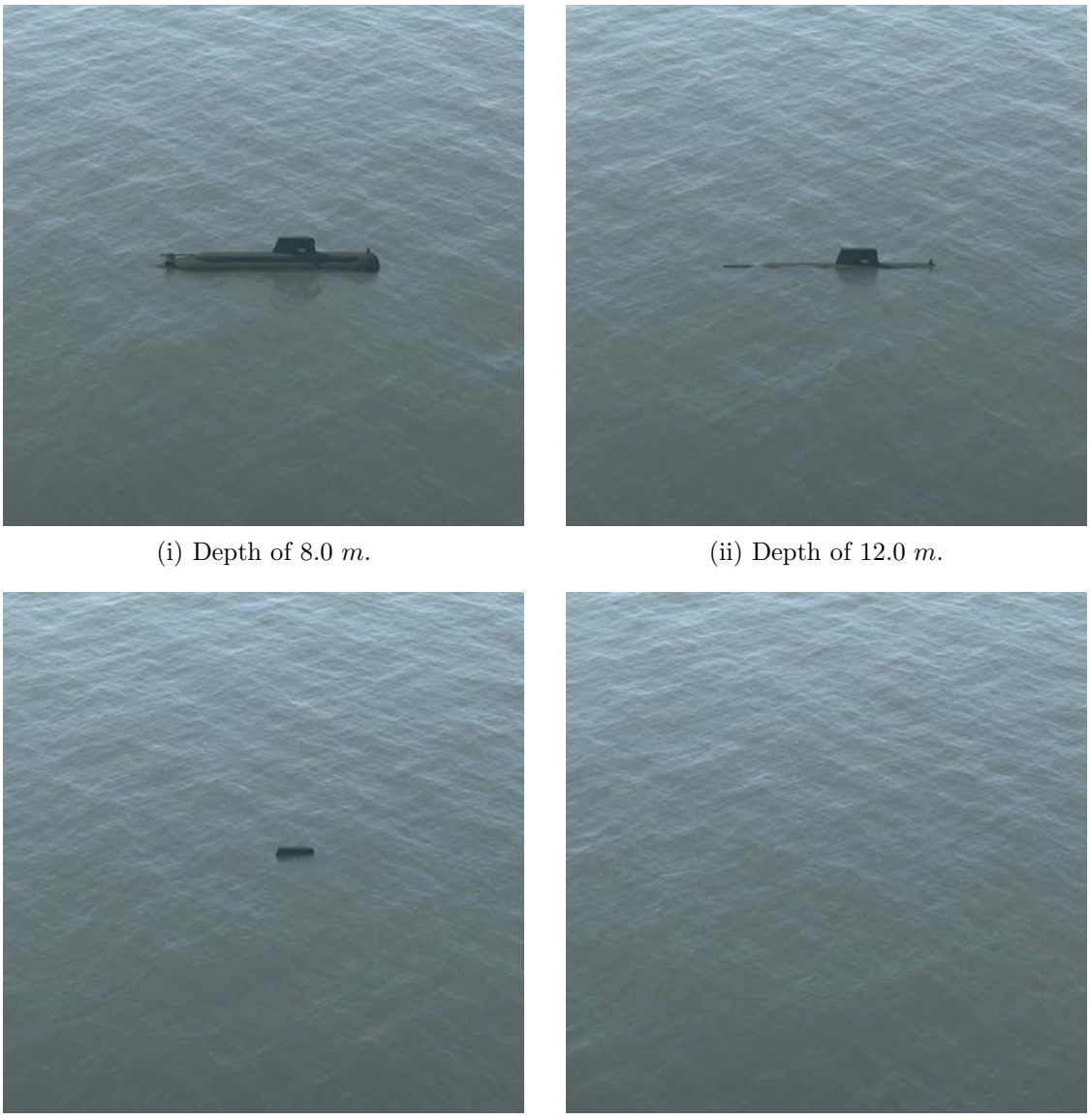

(i) Depth of 8.0 m.

(ii) Depth of 12.0 m.

(iii) Depth of 16.0 m.

(iv) Depth of 20.0 m.

Figure 28: *Generic submarine in ABCASE1H water, range of* 0.5 *km, a solar zenith of* 45°*, a reflectance of* 4% *and an elevation of* 22.5°*.*

3.2 Surface Ships

Synthetic images generated by CAMEO-SIM can also be used to qualitatively assess the visible signature of naval ships and some examples will be presented here. Figures 29 and 30 show synthetic images generated by CAMEO-SIM of an Anzac class frigate (FFH) heading north in the Cairns location in January using the Calm sea referred to in Table 29. The materials used for the paints in the model were created from spectroscopic data of the near-infrared (NIR) reflecting paints used on current RAN vessels. As would be expected, the time of day has a large effect on the visible signature; the change from midday to mid afternoon in Figure 29 provides a striking example of this effect. The contrast of the ship with respect to the background is a significant contributor to the visible signature.

Table 29: *Calm ocean parameters for CAMEO-SIM.*

Shape	Sea State 1 calculated power spectrum
Depth	1000 m
Tiling	Smooth and curved Earth
Tile size	500 m
Cells per tile	520
Repeat factor	100 in all directions
Materials	
Water	OCEAN.water_vis
Whitecaps	OCEAN.foam_ir
Ocean floor	SOIL.sea_water
Surface temperature	300 K
Surface roughness	0.01
Whitecaps	Off
Interior (see Section 3.1)	ABCASE1 water model parameters ABCASE1H water model parameters

(i) Early morning.

(ii) Mid morning.

(iii) Midday.

(iv) Mid afternoon.

(v) Late afternoon.

Figure 29: *FFH port side at 2 km at different times of day. Observer facing east.*

(i) Early morning.

(ii) Mid morning.

(iii) Midday.

(iv) Mid afternoon.

(v) Late afternoon.

Figure 30: *FFH starboard side at 2 km at different times of day. Observer facing west.*

Another example of the potential use of CAMEO-SIM generated synthetic imagery is shown in Figure 31. In this case, two images of the FFH in the Cairns location in January in the Calm sea are shown. The figures shows the FFH on the starboard side at mid-morning. The difference between the two images is the material used for the paint on the hull and superstructure. In the first figure, the standard RAN Storm Grey (NIR reflecting) is used and in the second figure a material that closely matches the colour of the sea is used. This particular example demonstrates how different colours perform in a particular scenario with the sea colour giving a reduced visible signature in this instance.

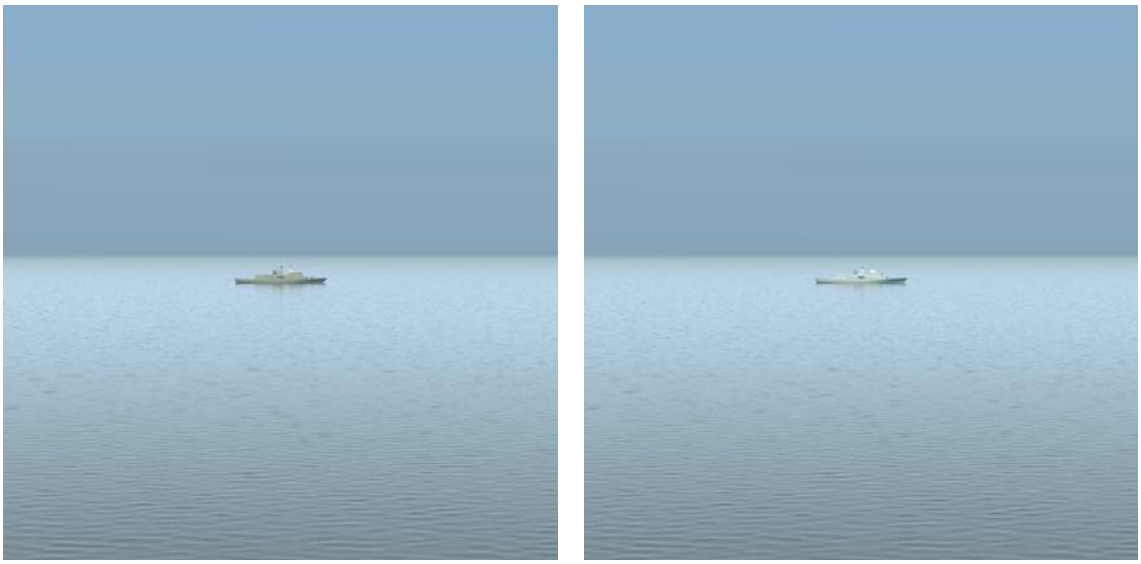

(i) Storm grey. (ii) Sea colour.

Figure 31: *Comparing paint colours. Observer facing west.*

The synthetic imagery generated from CAMEO-SIM can be used to quantitatively assess the visible signatures of naval platforms in a maritime environments using psychophysical trials involving human observers or using specialized image analysis software. The advantage of synthetic imagery is that a large number of options can be assessed rapidly and economically relative to the alternative of field trials. Another advantage is the ability to perform the assessment in a range of environmental conditions as opposed to being constrained by the limitations of actual field trials.

3.3 Developing Camouflage Disruptive Patterns with CAMOGEN

An example of developing camouflage patterns with a maritime flavour will be presented in this section. Since CAMOGEN requires imagery of scenes as input to the process of generating DPs, this section will be divided into two parts. The first part will describe the field trial conducted to acquire appropriate imagery and associated data. The second part will cover the processing of the images with CAMOGEN to produce various DP options and the initial assessment of the DPs produced.

3.3.1 Field Trial

3.3.1.1 Location

The location chosen was along a section of the Maribyrnong river near Avondale Heights at Canning Reserve in Melbourne, Australia (GPS co-ordinates 36° 46' S, 144° 52' E). The trial occurred on the 11th of December 2007 on a mainly fine day.

3.3.1.2 Equipment

All images were captured using a Sony DSC-F828 set to manual mode, manual focus, 8 megapixel image size, fine picture quality, tiff recording mode, picture effects off, real colour, normal sharpness and normal saturation. The panels used for colour calibration were a 24 patch GretagMacbeth ColorChecker® chart and a Spectralon® reference panel. The latter represents a near perfect reflecting diffuser. Spectral radiance of the Spectralon® reference panel and patches on the ColorChecker® chart were measured using an Analytical Spectral Devices Inc. (ASD Inc.) FieldSpec® Pro, Model number FSP 350-2500P, with a gun probe equipped with a 1° FOV foreoptic. A Magellan eXplorist 500 GPS unit was used to record the location, a laser range finder was used to measure the range of various objects in the scene and laptop computers were used for data acquisition and recording.

3.3.1.3 Results

An image of the basic scene chosen is shown in Figure 32. Data for colour calibration was obtained by taking an image of the same scene with calibration panels placed in the scene (Figure 33). Spectral radiance measurements of the panels were taken immediately prior to acquiring the image. These measurements were taken by holding the probe 20 to 30 *cm* away from the target and using a sight attached to the probe for alignment. Spectral radiance measurements were converted to tristimulus values (see Section 2.3.2 for details) in absolute luminance. The patches measured, as well as the calculated tristimulus values, are shown in Table 30.

3.3.2 DP Generation

The tristimulus values from Table 30 were used to create a CAMOGEN standards file. Using the image with the calibration panels (Figure 33), and the newly created standards file, a calibration matrix was calculated and applied to the basic scene image (Figure 32). The calibrated scene image can now be used to generate DPs in CAMOGEN.

Figure 32: *Image of Maribyrnong River at Canning Reserve.*

Figure 33: *Image of Maribyrnong River at Canning Reserve with calibration panels.*

Table 30: *Patches measured on ColorChecker® chart and Spectralon® panel.*

Number	Description	CIE Tristimulus values (cd/m^2)		
		X	**Y**	**Z**
1	Dark skin	1168.74	1068.54	766.79
4	Foliage	1352.11	1610.66	998.98
10	Purple	1178.08	968.58	1731.07
13	Blue	821.10	645.84	2641.26
15	Red	2133.77	1371.22	684.64
20	Neutral 8	5429.86	5667.1	6174.57
23	Neutral 3.5	1002.82	1051.84	1194.97
n/a	Spectralon®	5677.29	5900.18	6528.18

3.3.2.1 Selecting Patches

To generate a DP in CAMOGEN, areas of the image are selected to form the basis of the DP. These areas, or patches, are chosen by the user and should reflect regions of the image that are deemed to be important for creation of the DP. In this example a DP suitable for a watercraft on the river is desired so patches of the water are the main focus of attention. The patches chosen for this example are shown in Figure 34.

3.3.2.2 Weighting Schemes

Three categories were used to classify the patches; mix, shrub and sky. Shrub represents patches of water that mainly reflect greenery, sky represents water that mostly reflects sky and mix is somewhere in between shrub and sky categories, reflecting a mix of both shrub and sky. The patches placed in each category can be determined from the image and caption of Figure 34. In addition to placing patches in various categories, each category can be assigned a weighting. This weighting allows control over the amount of each category used in the DP synthesis. To show the effect of category weighting, two weighting schemes were employed. The first, labelled "a", is given weightings of 1,4 and 4 for the mix, shrub and sky categories respectively. The second, labelled "b", is given weightings of 1,1 and 2 for the mix, shrub and sky categories respectively. Weighting values are generally assigned arbitrarily based on which features are considered more or less important.

Figure 34: *Patches chosen for DP creation. From left to right, the patches are labelled shrub1, mix1, mix2, sky1, sky2 and shrub2.*

3.3.2.3 Generating Candidate DPs

All of the DPs generated were 2 m by 2 m physical size with 256 pixels along each side (resolution = 7.8 mm). The number of iterations was set to 3 and the random number seed was set to 1. Four DPs were generated for each of the weighting schemes. Histogram matching was used for colour quantisation and both 3 and 5 colour schemes were produced. For each colour scheme, two types of sub-band combination were chosen; simple and regional bias (level = 2). The DPs generated for weighting scheme "a" are shown in Figure 35 and those for weighting scheme "b" are shown in Figure 36.

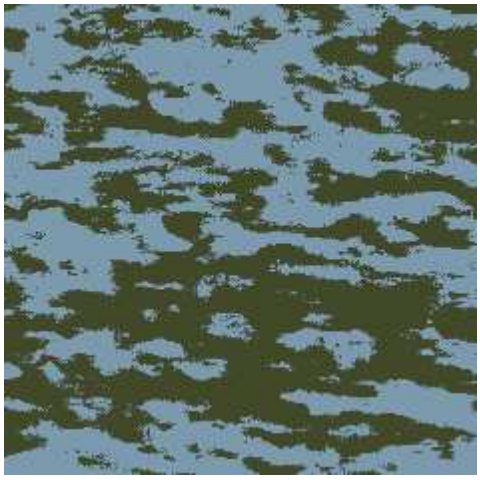

(i) Three colour, simple method sub-band combination.

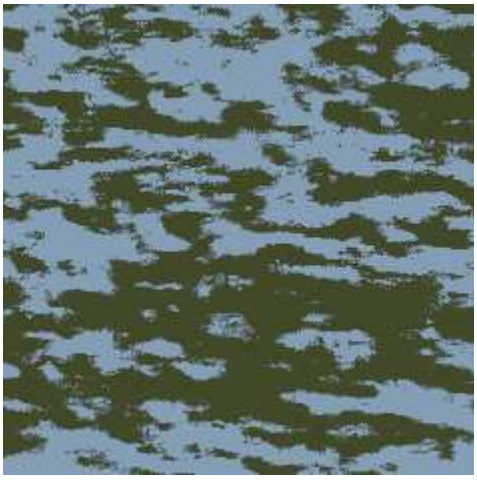

(ii) Five colour, simple method sub-band combination.

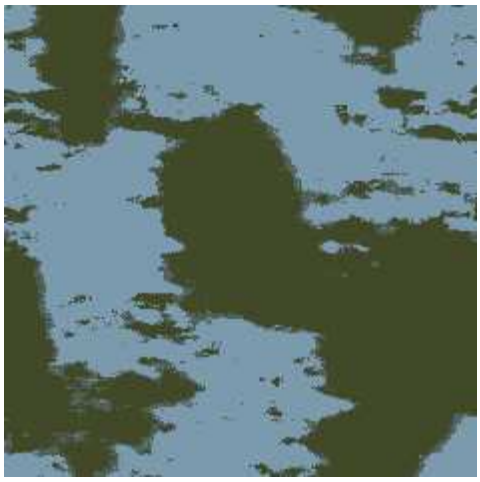

(iii) Three colour, regional bias method (level = 2) sub-band combination.

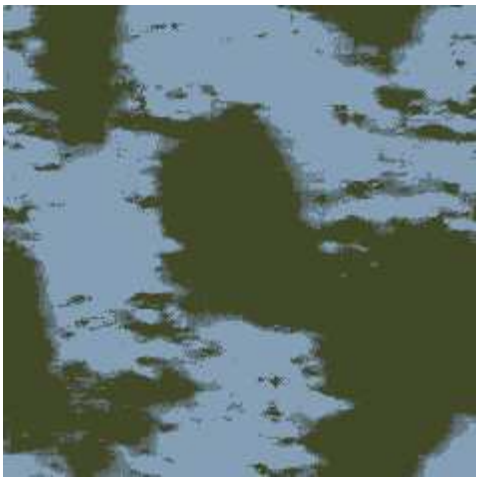

(iv) Five colour, regional bias method (level = 2) sub-band combination.

Figure 35: *DP generated using weighting scheme "a".*

The choice of sub-band combination method has a significant effect on the DP produced. In all cases the difference between the simple method and the regional bias method (level = 2) is pronounced. The regional bias method produces a coarser pattern where the spatial variation is of a larger scale compared with that produced by the simple method. The patterns produced by the simple method are finer with a more homogeneous spatial distribution of the colours. There is only minimal discernible difference between the three colour and five colour schemes for a given sub-band combination method. For weighting scheme "a" there is almost no difference between the 3 and 5 colour schemes for both the simple and regional bias methods. For weighting scheme "b" the difference between the 3 and 5 colour schemes is noticeable for the simple method and relatively obvious in the regional bias case. The weighting schemes also have an effect on the DPs produced by CAMOGEN in this example. Close inspection shows that weighting scheme "a" has a

(i) Three colour, simple method sub-band combination.

(ii) Five colour, simple method sub-band combination.

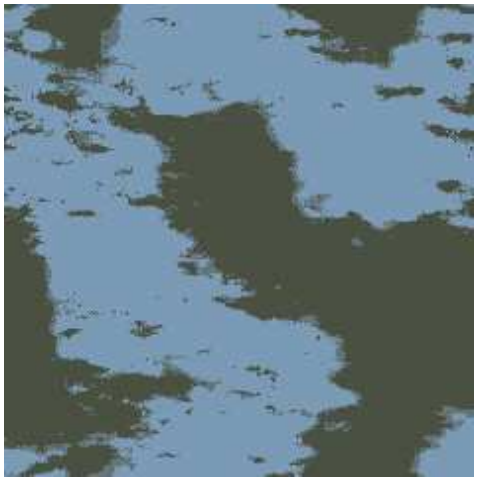

(iii) Three colour, regional bias method (level = 2) sub-band combination.

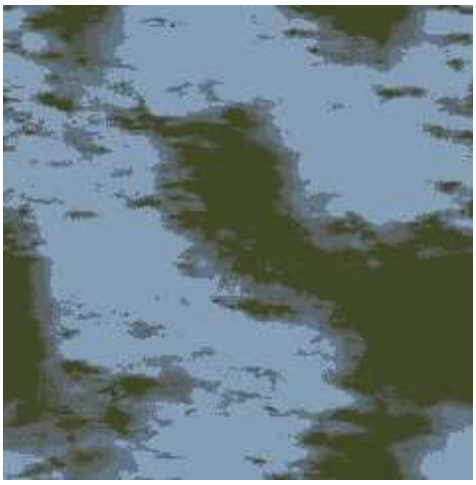

(iv) Five colour, regional bias method (level = 2) sub-band combination.

Figure 36: *DP generated using weighting scheme "b".*

stronger green colouration compared to weighting scheme "b"[1]. This effect is most noticeable when comparing the five colour, regional bias method DPs for weighting schemes "a" and "b"(Figure 35(iv) and Figure 36(iv)). This is not surprising since in weighting scheme "a" the shrub category has the same weighting as the sky category whereas in weighting scheme "b" the shrub category has half the weighting of the sky category.

[1]Although this may not be obvious in lower quality printed copy, it is readily seen on screen in CAMOGEN.

3.3.2.4 Assessing Candidate DPs

Initial assessment of the candidate DPs can be performed using CAMOGEN. In this example, a 2D bitmap representation of a rigid hull inflatable boat (RHIB) was created to facilitate the assessment. The 2D RHIB template is shown in Figure 37(v) placed in the river scene. The all-black template is clearly visible on the river. Also shown in Figure 37 are the 2D RHIB templates with various candidate DPs applied. Since there is little difference between the 3 and 5 colour schemes, only the 5 colour DPs are shown in Figure 37. In this example, the templates were placed in the same location to permit an equitable comparison. The location chosen was a region with predominantly sky reflection. Although all of the DPs afford some level of visual camouflage, it is difficult to decide which is best. Since this is only an example to demonstrate the capabilities of CAMOGEN, a determination of the best scheme will not be attempted here. In a real example, the images shown in Figure 37 would undergo further evaluation. One method would be to generate many images, such as those shown in Figure 37, and present them to human observers [52]. By using many observers, and perhaps a metric like time to detect the target, a statistical measure of POD can be estimated. An alternative approach is to use image processing to estimate POD using a code like VISEO (VISual and Electro-Optical) [53–55]. Nonetheless, the ability to place targets with DPs applied back into the original images using CAMOGEN is useful. It permits a first-cut of DPs generated and allows the user to limit subsequent evaluation to DPs that appear to be promising. It is relatively quick to place targets back into images using CAMOGEN and it is thus an efficient way to screen larger numbers of DPs.

3.3.3 Summary

To successfully create DPs using CAMOGEN, appropriate imagery must first be obtained. This imagery should be of the locations/regions in which the DP is destined to be deployed. The acquisition of the imagery also requires collection of data to permit colour calibration of the images. Creating DPs using CAMOGEN then requires selection of regions of interest within the images and weighting those regions based on largely subjective criteria. Choice of the colour quantisation method, the sub-band recombination method and the number of colours in the final DP will all influence the DP produced. Many DPs covering the choices described above can be generated and then placed back into the original imagery for initial assessment. Further refinement using CAMOGEN is possible but ultimately some quantitative assessment of POD is required to progress the assessment of the candidate DPs. Finally, physical realization of the most promising DPs and field assessments complete the process of camouflage pattern development.

(i) Five colour, simple method sub-band combination, weighting scheme “a”.

(ii) Five colour, simple method sub-band combination, weighting scheme “b”.

(iii) Five colour, regional bias method (level = 2) sub-band combination, weighting scheme “a”.

(iv) Five colour, regional bias method (level = 2) sub-band combination, weighting scheme “b”.

(v) 2D template of RHIB.

Figure 37: *DP assessment.*

4 Limitations and Known Issues

All of the software programs utilised in the VST for modelling and assessing visible signatures have limitations. They are limited by the assumptions they make. Since these are numerous, this section will focus on the limitations which contribute to the accuracy of modelling and evaluating visible signatures.

4.1 ORACLE

ORACLE has a number of limitations in modelling and evaluating visible signatures. These can be divided into limitations due to target characteristics, visual performance algorithms and environmental conditions.

The target characteristics that lead to fundamental limitations in ORACLE are that of geometry and appearance. In ORACLE the geometry of the target is defined by its height and width. As such not only is it a 2D object, but it can only ever be used to analyse rectangular or square targets. This presents a significant problem since, for example, submarines are in essence cylindrical objects with a conic section that houses the masts. The second characteristic, that of appearance, is even more limiting. In ORACLE the appearance of the target is achieved using its spectral radiance. Consequently, the target can only be defined in terms of a single colour. Therefore imagery generated by CAMEO-SIM cannot be input into ORACLE to assess the effectiveness of DPs on submarine masts. This in turn means that DPs developed for different operational environments cannot be assessed in terms of POD.

The limitations due to the visual performance algorithms have been alluded to earlier. These refer to the assumptions made in order to model human visual performance and therefore determine the POD. ORACLE is a purely statistical model, and as such does not possess the facility to input images, nor does it attempt to account for all the cognitive factors in human visual search [56]. Human visual search is a complex problem and it is almost impossible to account for all aspects of cognition in any model of vision. One such factor is the variability in the visual search process. For instance, once an observer has viewed a scene his/her search strategy changes to focus on areas of interest. Consequently, the area that is searched will, in most cases, be smaller than the search FOV. The GTV (Georgia Tech Vision) model attempts to address this issue by training the software to distinguish between targets and clutter in scenes using a number of input images before calculating the POD [55, 57].

There are a number of environmental conditions that may limit ORACLE and its ability to accurately predict PODs. However, the most significant for modelling visible signatures of naval platforms is its inability to model the noise introduced into a maritime scene by the sea surface. Without this capability any object put in a scene will possess a large POD and therefore a large visible signature.

4.2 CAMEO-SIM

CAMEO-SIM has two known limitations with respect to visible band synthetic image generation of maritime platforms. The first is the inability to include ship wakes and the second, which only applies to the generation of animations, is that ship motion cannot be coupled to the ocean model. The latter means that although ship motion can be incorporated into a CAMEO-SIM simulation, it is not currently possible to make the ship move in synchronisation with the ocean swell or wave motion.

5 Future Work and Extensions

Throughout this report an emphasis has been placed on the methods employed to turn the stand-alone software programs into a software suite for modelling and evaluating visible signatures. To enable more accurate cross-checks between the stand-alone software packages new DSTO developed software and procedures are required. In the following section a summary of proposed DSTO developed software procedures and future extensions that would make the VST a more complete package for modelling and assessing visible signatures is presented.

CAMEO-SIM uses MODTRAN for modelling the atmosphere, whereas HYDROLIGHT uses RADTRAN. This presents a problem when attempting to use CAMEO-SIM imagery to validate the ORACLE POD analysis as HYDROLIGHT is used to generate the target and background spectra. To obtain a more accurate representation of the CAMEO-SIM imagery HYDROLIGHT should use MODTRAN for atmospheric modelling. This could be accomplished by developing new HYDROLIGHT subroutines to permit the atmospheric modelling to be performed using MODTRAN.

The second part enabling CAMEO-SIM to more accurately represent the ORACLE POD data is to permit MODTRAN to generate the necessary airlight spectra for entry into ORACLE. This can be achieved by running MODTRAN with the appropriate input parameters. Following this, an output file can be produced containing the airlight data.

DSTO will also develop a procedure to calculate the RGB coordinates corresponding to the spectral radiance of the target and background calculated by HYDROLIGHT and entered into ORACLE. These coordinates could then be used to generate an image of the calculated colour. This will then be checked against the analogous CAMEO-SIM imagery of the target in its background. It would not be precise, but it would give an indication of whether CAMEO-SIM and HYDROLIGHT are producing similar colours. This could also be adapted to include the effects of the airlight and transmission spectra on the target and background in ORACLE.

To further validate the ORACLE POD analysis, DSTO will develop a technique to take the images generated by CAMEO-SIM of the black cuboid and determine whether their edges are within the image. This is easily accomplished using an edge detection algorithm. A procedure such as this would provide another method of validating the ORACLE POD analysis.

ORACLE, at present, does not have the capability to model the noise introduced into a scene from the sea surface. This limits the ability of ORACLE to accurately represent mar-

itime environments and therefore also the visible signature of maritime platforms. Since the interaction of submarines with the ocean and its surface play a critical role in determining its visible signature this is a severe limitation of the ORACLE software. Therefore a DSTO developed technique is required in order to incorporate the noise introduced into a scene from the sea surface into ORACLE through the MTF data file responsible for the response of the optical system.

In its current form the VST does not have the capability of determining the POD for the synthetic imagery generated by CAMEO-SIM. At present the only way to quantify the visible signature from these images is to conduct human observer trials. These trials are both time consuming and costly. A more complete software suite should include the ability to calculate POD from generated scene images. The VISEO detection analysis software provides such a capability [53, 54]. VISEO is an integrated software suite developed for the Army Aviation Troop Command, Applied Technology Directorate (ATCOMM/AATD) in the US. The key component of VISEO is the GTV model, which takes images of scenarios and returns a POD of detection. It would be advantageous to either acquire a developed software package such as GTV or for DSTO to develop a capability to perform POD analysis on synthetic imagery.

6 Conclusion

A software suite has been developed to model and assess visible signatures of naval platforms. This suite is known as the VST and consists of a number of connected software packages that result in either calculation of a POD or the generation of synthetic images of targets in scenes.

A variety of examples have been presented to demonstrate the capabilities of the VST. These included the POD analysis of submarines, synthetic image generation of a generic submarine and an Anzac Class Frigate, and pixellated camouflage schemes developed for a watercraft on a river. Some validation of ORACLE and CAMEO-SIM has been performed. However, more work will be undertaken to verify the models.

The major limitation of the VST at present is its inability to quantify the visual signatures of platforms from synthetic imagery without human observer trials. Therefore it would be beneficial to include the capability to calculate the POD from generated synthetic imagery. In this way the visible signature reduction strategies developed could be quantitatively determined in a timely and cost effective fashion.

References

1. Fraedrich, D., Stark, E., Heen, L. T. & Miller, C. (2003) ShipIR model validation using NATO SIMVEX experiment results, *in Targets and Backgrounds IX: Characterization and Representation*, Vol. 5075, SPIE, Orlando, FL, USA, pp. 49–59.

2. Vaitekunas, D. A. & Fraedrich, D. S. (1999) Validation of the NATO-standard ship signature model (SHIPIR), *in Targets and Backgrounds: Characterization and Representation V*, Vol. 3699, SPIE, Orlando, FL, USA, pp. 103–113.

3. Vaitekunas, D. A. & Lawrence, O. E. (1999) Infrared scene capabilities of SHIPIR, *in Targets and Backgrounds: Characterization and Representation V*, Vol. 3699, SPIE, Orlando, FL, USA, pp. 92–102.

4. Fearns, P., Dekker, A. & Lynch, M. (2001) Modelling water-leaving radiance, *in Geoscience and Remote Sensing Symposium IGARSS'01 IEEE International*, Vol. 6, IEEE, pp. 2701–2703.

5. Fearns, P. R. & Lynch, M. J. (2003) Modelling Ocean Colour, *in Ocean Remote Sensing and Imaging II*, Vol. 5155, SPIE, pp. 174–181.

6. Duarte, J., Velez-Reyes, M., Tarantola, S., Gilbes, F. & Armstrong, R. (2003) A probabilistic sensitivity analysis of water-leaving radiance to water constituents in coastal waters, *in Ocean Remote Sensing and Imaging II*, Vol. 5155, SPIE, pp. 162–173.

7. Albert, A. & Mobley, C. (2003) An analytical model for subsurface irradiance and remote sensing reflectance in deep and shallow case-2 waters, *Optics Express* **11**(22), 2873–2890.

8. Wang, J. & Cota, G. F. (2003) Remote-sensing reflectance in the Beaufort and Chukchi seas: observations and models, *Applied Optics* **42**(15), 2754–2765.

9. Mobley, C. D. (2004) *Light and Water Radiative Transfer in Natural Waters*, 2nd edn, US Office of Naval Research.

10. Mobley, C. D. & Sundman, L. K. (2005) *Hydrolight 4.2 Technical Documentation*, Sequoia Scientific Inc., USA, Third Printing.

11. Mobley, C. D. (1999) Estimation of remote-sensing reflectance from above-surface measurements, *Applied Optics* **38**(36), 7442–7455.

12. Gregg, W. W. & Carder, K. L. (1990) A simple spectral solar irradiance model for cloudless maritime atmospheres, *Limnology and Oceanography* **35**(8), 1657–1675.

13. Harrison, A. W. & Coombes, C. A. (1988) An Opaque Cloud Cover Model of Sky Short Wavelength Radiance, *Solar Energy* **41**(4), 387–392.

14. Mobley, C. D. & Sundman, L. K. (2005) *Hydrolight 4.2 Users' Guide*, Sequoia Scientific Inc., USA, Third Printing.

15. Cooke, K. J., Stanley, P. A. & Hinton, J. L. (1995) The ORACLE approach to target acquisition and search modelling, *in Vision models for target detection and recognition*, Vol. 1, World Scientific, New Jersey, pp. 135–171.

16. Cooke, K. J. (2005) *ORACLE Web*, BAE SYSTEMS Advanced Technology Centre Ltd., Bristol, UK.

17. Human Factors Department Advanced Technology Centre BAE SYSTEMS Ltd. (2005) ORACLE suite version 1.7. Bristol, UK.

18. Morel, A. & Maritorena, S. (2001) Bio-optical properties of oceanic waters: a reappraisal, *Journal of Geophysics Research* **106**(C4), 7163–7180.

19. Pope, R. M. & Fry, E. S. (1997) Absorption Spectrum (380 nm - 700 nm) of Pure Water II. Integrating Cavity Measurements, *Applied Optics* **36**(33), 8710–8723.

20. Smith, R. C. & Baker, K. S. (1981) Optical properties of the clearest natural waters (200-800 nm), *Applied Optics* **20**(2), 177–184.

21. Petzold, T. J. (1972) *Volume scattering functions for selected ocean waters*, Technical Report SIO 72-78, Scripps Institution of Oceanography, San Diego, CA, USA.

22. CERN - The European Organization for Nuclear Research, Geneva, Switzerland (2005) *PAW - Physics Analysis Workstation*.

23. Stroud, C. A., Sutherland, R., Wilson, M. & Filbee, D. R. (2005) CAMOGEN - a method for generating optimized camouflage schemes, *UK Journal of Defence Science* **10**(1), 10–17.

24. *Standard practice for computing the colors of objects by using the CIE system* (2006) Designation: E 308 - 06, ASTM International, West Conshohocken, PA, USA.

25. Gilmore, M. A., Moorhead, I. R., Oxford, D. E., Liddicoat, T. J., Filbee, D. R., Stroud, C. A., Hutchings, G. & Kirk, A. (1999) CAMEO-SIM: A broadband scene generation system that is fit for purpose, *in Targets and Backgrounds : Characterization and Representation V*, Vol. 3699, SPIE, Orlando, FL, USA, pp. 217–228.

26. Houlbrook, A. W., Gilmore, M. A., Moorhead, I. R., Filbee, D. R., Stroud, C. A., Hutchings, G. & Albert, K. (2000) Scene simulation for camouflage assessment, *in Targets and Backgrounds VI: Characterization, Visualization, and the Detection Process*, Vol. 4029, SPIE, Orlando, FL, USA, pp. 247–255.

27. Moorhead, I. R., Gilmore, M. A., Houlbrook, A. W., Oxford, D. E., Filbee, D. R., Stroud, C. A., Hutchings, G. & Kirk, A. (2001) CAMEO-SIM: A physics-based broadband scene simulation tool for assessment of camouflage, concealment, and deception methodologies, *Optical Engineering* **40**(9), 1896–1905.

28. Filbee, D. R., Kirk, A., Stroud, C. A., Hutchings, G., Ward, T. & Brunnen, D. (2002) Modeling of high-fidelity synthetic imagery for defense applications, *in Targets and Backgrounds VIII: Characterization and Representation*, Vol. 4718, SPIE, Orlando, FL, USA, pp. 12–22.

29. Kirk, A., Cowan, M. & Allen, R. D. (2004) CAMEO-SIM: An ocean model extension to the physically accurate broadband EO scene generation system for the assessment of target vehicles within their natural environments, *in Targets and Backgrounds X: Characterization and Representation*, Vol. 5431, SPIE, Orlando, FL, USA, pp. 288–299.

30. Gilmore, M. A., Newman, S., Haynes, A., Jones, C., Allen, R. D., Richardson, D. & Stroud, C. A. (2005) Camouflage effectiveness assessment using synthetic imagery, *UK Journal of Defence Science* **10**(1), 1–9.

31. Hutchings, G. (2006) *CAMEO SIM Rendering Guide*, Lockheed Martin UK INSYS Ltd., INS/336/DOC/002.

32. Hutchings, G. (2006) *CAMEO SIM Scene Generation Guide*, Lockheed Martin UK INSYS Ltd., INS/336/DOC/001.

33. Berk, A., Anderson, G., Acharya, P., Chetwynd, J., Bernstein, L., Shettle, E., Matthew, M. & Adler-Golden, S. (2000) *MODTRAN4 Version 2 User's Manual*, Air Force Research Laboratory, Space Vehicles Directorate, Hanscom AFB, MA 01731-3010, USA.

34. Prieur, L. & Sathyendranath, S. (1981) An optical classification of coastal and oceanic waters based on the specific spectral absorption curves of phytoplankton pigments, dissolved organic matter, and other particulate materials, *Limnology and Oceanography* **26**(4), 671–689.

35. Morel, A. (1991) Light and marine photosynthesis: a spectral model with geochemical and climatological implications, *Progress in Oceanography* **26**, 263–306.

36. Haltrin, V. I. (1999) Chlorophyll-based model of seawater optical properties, *Applied Optics* **38**(33), 6826–6832.

37. Gordon, H. R. & Morel, A. (1983) Remote Assessment of Ocean Color for Interpretation of Satellite Visible Imagery A Review, *in Lecture Notes on Coastal and Estuarine Studies*, Vol. 4, Springer-Verlag.

38. Bricaud, A., Morel, A. & Prieur, L. (1981) Abosrption by dissolved organic matter of the sea (yellow substance) in the UV and visible domains, *Limnology and Ocenaography* **26**(1), 43–53.

39. Cunningham, A., Boyle, J. C. & Wood, P. (2002) Radiative transfer modelling of the relationship between seawater composition and remote sensing reflectance in sea lochs and fjords, *International Journal of Remote Sensing* **23**(18), 3713–3724.

40. Carder, K. L., Steward, R. G., Harvey, G. R. & Ortner, P. B. (1989) Marine humic and fulvic acids: Their effects on remote sensing of ocean chlorophyll, *Limnology and Oceanography* **34**(1), 68–81.

41. Volynsky, V. A., Marra, J. & Knudson, C. (1996) Estimation of some characteristics of ocean waters using optical data (Case I), *in International Geoscience and Remote Sensing Symposium IGARSS*, Vol. 1, IEEE, pp. 296–298.

42. Bricaud, A., Morel, A., Babin, M., Allali, K. & Claustre, H. (1998) Variations of light absorption by suspended particles with chlorophyll a concentration in oceanic (case 1) waters: Analysis and implications for bio-optical models, *Journal of Geophysical Research* **103**(C13), 31033–31044.

43. Berwald, J., Stramski, D., Mobley, C. D. & Kiefer, D. A. (1995) Influences of absorption and scattering on vertical changes in the average cosine of the underwater light field, *Limnology and Oceanography* **40**(8), 1347–1357.

44. Lui, C.-C. & Miller, R. L. (2003) A spectrum matching method for estimating the inherent optical properties from remote sensing of ocean color, *in Ocean Remote Sensing and Imaging II*, Vol. 5155, SPIE, pp. 141–152.

45. Morel, A. (1988) Optical Modeling of the Upper Ocean in Relation to Its Biogenous Matter Content (Case I Waters), *Journal of Geophysical Research* **93**(C9), 10749–10768.

46. Gould Jr, R. W., Arnone, R. A. & Martinolich, P. M. (1999) Spectral dependence of the scattering coefficient in case 1 and case 1 waters, *Applied Optics* **38**(12), 2377–2397.

47. Lewis, M. R., Cullen, J. J. & Platt, T. (1988) Phytoplankton and Thermal Structure in the Upper Ocean: Consequences of Nonuniformity in Chlorophyll Profile, *Journal of Geophysical Research* **88**(C4), 2565–2570.

48. Fournier, G. R. & Forand, J. L. (1994) Analytic phase function for ocean water, *in Ocean Optics XII*, Vol. 2258, SPIE, pp. 194–201.

49. Haltrin, V. I. (1997) Theoretical and empirical phase functions for Monte Carlo calculations of light scattering in seawater, *in Fourth International Conference Remote Sensing for Marine and Coastal Environments*, pp. 509–518.

50. Toet, A., Bijl, P. & Valeton, J. (2000) Test of three visual search and detection models, *Opt. Eng.* **39**(5), 1344–1353.

51. Cooke, K. (2007) *Personal Communication.* 31st July.

52. Copeland, A. C., Trivedi, M. M. & McManamey, J. R. (1995) Psychophysical experiments for evaluating target distinctness in images, *in Targets and Backgrounds: Characterization and Representation*, Vol. 2469, SPIE, Orlando, FL, USA, pp. 452–461.

53. Doll, T. J., Home, R., Cooke, K. J., Wasilewski, A. A., Sheerin, D. T. & Hetzler, M. C. (2003) Human vision simulation for evaluation of enhanced and synthetic vision systems, *in Enhanced and Synthetic Vision 2003*, Vol. 5081, SPIE, Orlando, FL, USA, pp. 77–89.

54. Doll, T., McWhorter, S. W., Schmieder, D. E., Hetzler, M. C., Stewart, J. M., Wasilewski, A. A., Owens, W. R., Sheffer, A. D., Galloway, G. l. & Harbert, S. D. (1997) Biologically-based vision simulation for target-background discrimination and camouflage/LO design, *in Targets and Backgrounds : Characterization and Representation III*, Vol. 3062, SPIE, Orlando, Florida, pp. 231–242.

55. Doll, T. J., McWhorter, S. W., Schmieder, D. E. & Wasilewski, A. A. (1995) Simulation of selective attention and training effects in visual search and detection, *in Vision models for target detection and recognition*, Vol. 1, World Scientific, New Jersey, pp. 396–418.

56. Cooke, K. (2000) The Sources of Variability in the Search Process, *in NATO RTO Meeting Proc. No. 45, Search and Target Acquisition*, NATO Research and Technology Organization, Neuilly-Sur-Seine Cedex, France.

57. Daley, W. D., Doll, T. J., McWhorter, S. W. & Wasilewski, A. A. (1998) Machine Vision Algorithm Generation Using Human Visual Models, *in Precision Agriculture and Biological Quality*, Vol. 3543, SPIE, pp. 65–72.

DEFENCE SCIENCE AND TECHNOLOGY ORGANISATION DOCUMENT CONTROL DATA	1. CAVEAT/PRIVACY MARKING

2. TITLE	3. SECURITY CLASSIFICATION
The Visible Signature Modelling and Evaluation ToolBox	Document (U) Title (U) Abstract (U)
4. AUTHORS	5. CORPORATE AUTHOR
Joanne B. Culpepper and Rodney A.J. Borg	Defence Science and Technology Organisation 506 Lorimer St, Fishermans Bend, Victoria 3207, Australia

6a. DSTO NUMBER	6b. AR NUMBER	6c. TYPE OF REPORT	7. DOCUMENT DATE
DSTO–TR–2212	AR–014–321	Technical Report	December, 2008

8. FILE NUMBER	9. TASK NUMBER	10. SPONSOR	11. No OF PAGES	12. No OF REFS
2008/1067589/1	NAV 07/070	CCSG	90	57

13. URL OF ELECTRONIC VERSION	14. RELEASE AUTHORITY
http://www.dsto.defence.gov.au/corporate/reports/DSTO–TR–2212.pdf	Chief, Maritime Platforms Division

15. SECONDARY RELEASE STATEMENT OF THIS DOCUMENT

Approved For Public Release

OVERSEAS ENQUIRIES OUTSIDE STATED LIMITATIONS SHOULD BE REFERRED THROUGH DOCUMENT EXCHANGE, PO BOX 1500, EDINBURGH, SOUTH AUSTRALIA 5111

16. DELIBERATE ANNOUNCEMENT

No Limitations

17. CITATION IN OTHER DOCUMENTS

No Limitations

18. DSTO RESEARCH LIBRARY THESAURUS

Target Signatures	Modelling
Visual detection	Camouflage

19. ABSTRACT

A new software suite, the Visible Signature ToolBox (VST), has been developed to model and evaluate the visible signatures of maritime platforms. The VST is a collection of commercial, off-the-shelf software and DSTO developed programs and procedures. The software can logically be divided into image generation and probability of detection (POD) modelling codes. CAMOGEN (CAMOuflage GENeration) and CAMEO-SIM (CAMouflage Electro-Optic SIMulation) provide the image generation, whereas ORACLE provides the POD analysis capability. The ocean modelling is supplied by HYDROLIGHT. All of these stand-alone programs are integrated through DSTO developed software and procedures, to produce a software suite. The VST can be utilised to model and assess visible signatures of maritime platforms. A number of examples are presented to demonstrate the capabilities of the VST. In one example, the visible signature of a submarine is examined under various conditions. In another example, visible imagery of a ship is presented for different times of day and various observer perspectives. A demonstration of how a change in surface colour affects the visible signature of the ship is also shown. The final example is the creation and initial assessement of a disruptive pattern for a watercraft on a river.